Characterising a Novel Role for LBP in Angiogenesis

Jay Stone

October 2011

Department of Cell Biology
UCL Institute of Ophthalmology
11 – 43 Bath Street
City of London
EC1V 9EL

This thesis is submitted to the University College of London
for the degree of Doctor of Philosophy

Abstract

Vascular remodelling and angiogenesis are commonly associated with sight threatening diseases such as age related macular degeneration (AMD) and diabetic retinopathy. Current treatments for retinal vascular pathology are limited to inhibitors of potent growth factors such as vascular endothelial growth factor (VEGF), which despite preventing any further vascular growth cannot mend the damage already done. Vascular abnormalities are associated with late stages of disease, meaning we are treating patients too late. We must identify new, earlier therapeutic tagets to preserve vision.

Gene expression profiling was performed on retinal vessels isolated from three mutant mouse strains (Curlytail, VLDLR-/- and RD1) that display retinal vascular abnormalities. Sixty-two genes were found to change in all three models. One gene which was significantly up-regulated was LBP (lipopolysaccharide binding protein). This is an acute-phase response glycoprotein, which through its binding to LPS and activation of TLR4 is involved in inflammatory signalling.

We have tested the hypothesis that LBP has a novel function separate from its characterised LPS recognition. qPCR analysis of VLDLR-/- mice has shown LBP to be expressed in the neuroretina and isolated vessels. qPCR data has shown LBP to be up-regulated in VLDLR-/- mice just prior to an increase in VEGF expression and the vascular abnormalities being observed. Testing LBP affects in Matrigel, Aortic ring and Metatarsal assays revealed an increase in vessel sprouts and branching. Western blot analysis has suggested LBP can induce phosphotyrosine and phophoERK responses in a variety of cell lines and immnocytochemistry data provides evidence that this is not occuring through the well-established LBP-LPS NfkB pathway. PCR analysis of older passage HUVEC which are unresponsive to LBP has given us a candidate receptor.

In conclusion, we have revealed a potential role for LBP in contributing to angiogenesis.

Declaration

I, Jay Stone, confirm that the work presented in this thesis is my own. Where information has been derived from other sources, I confirm that this has been indicated in the thesis.

London, October 2011

Acknowledgements

This project would not have been possible had it not been for the encouragement I had from my friends and family, and the guidance I received from two great supervisors, Steve Moss and John Greenwood.

I would like to thank the MRC for the funding and the LMCB PhD programme, with special mention to Dan Cutler, Karl Matter and Giovanni Lesa who formed my PhD committee.

I consider myself very lucky to have had the opportunity to discuss my work within the institute with Alan Bird, Patric Turowski and Marcus Fruttiger, whose vast knowledge and probing questions have been incredibly beneficial to this project. I also wish to thank Xiaomeng Wang and Jennifer McKenzie, who have been two of the best post docs I could've wished for, teaching me all the laboratory techniques I have needed and never (noticeably) tiring of 'reminding' me where the reagents were stored.

There are too many things I need to thank Jennifer Williams, Emily Steed and Natalie Hudson for, I cannot list them all. The three of you have been instrumental to my happiness over the past four years and I know in the future, when I look back on this time, it will be the memories I have of you that will make me smile.

There have been many people over the years who I need to thank for making the institute such a great place to work – Claire, Charmie, and Aida for ensuring the department ran smoothly, the BRU staff for all animal related questions (there were many), Matt Hayes for his imaginative insights, Adam Grieve for being such an enjoyable distraction, Shalini Jadeja for her tips on dissection, Michael Powner for countless antibodies, Matthew Pearson for helping me to overcome my fear of microscopes, Lux, Ah-Lai, Mark and Rebecca who were great to share an office with when I started my PhD, and their replacements, Ingrid, James, Rachel, Vineeta, Tom, Apostolos and Hui who have been equally fantastic. I also want to thank Natasha Jeffs and Matthew Swire who may not have shared an office with me but have still had to endure many of my lab presentations and trips to the local.

Table of Contents

List of Figures

List of Tables

Abbreviations

A2a	Adaptor Related Protein Complex 2a
A2aR	Adenosine A2a Receptor
AGEs	Advanced Glycation Endproducts
AMD	Age Related Macular Degeneration
Ang	Angiopoietin
BBB	Blood Brain Barrier
BMP	Bone Morphogenetic Proteins
BPI	Bactericidal Permeability-Increasing Protein
BRVO	Branch Retinal Vein Occlusion
BSA	Bovine Serum Albumin
CETP	Plasma Cholesteryl Ester Transfer Protein
CFH	Complement Factor H
CNV	Choroidal Neovascularisation
CRP	C-Reactive Protein
CRVO	Central Retinal Vein Occlusion
CT	*Grhl3*^{CT}/J Curlytail mouse
DAB	Diaminobenzidine
DAG	Diacylglycerol
DMSO	Dimethyl Sulfoxide
DNA	Deoxyribonucleic Acid
ECL	Enhanced Chemiluminescence

ERK	Extracellular Signal Regulated Kinases
FDA	Food and Drug Administration
FGF2	Fibroblast Growth Factor-2
GPC	Glypican
HDL	High Density Lipoproteins
HRP	Horse Radish Peroxidase
HRVO	Hemiretinal Vein Occlusion
HSPGs	Heparan Sulfate Proteoglycans
HUVEC	Human Umbilical Vein Endothelial Cells
IAR	Intussusceptive Arborisation
IBR	Intussusceptive Branching
IDDM	Insulin Dependent Diabetes Mellitus
IL	Interleukin
IMG	Intussusceptive Microvascular Growth
INL	Inner Nuclear Layer
JAK	Janus Kinase
LAL	Limulus Amebocyte Lysate
LBP	Lipopolysaccharide Binding Protein
LDL	Low-Density Lipoprotein
LPS	Lipopolysaccharide
MacTel	Macular Telangiectasia
mCD14	Membrane Bound CD14
mDC14	Membrane Bound CD14 Antigen
MEMa	Minimal Essential Medium Alpha
MMPs	Metalloproteinases

NDP	Norrie disease protein
NF-kß	Nuclear Factor Kappa ß
NICE	National Institute of Health and Clinical Excellence
NIDDM	Non Insulin Dependent Diabetes Mellitus
Np-1	Neuropilin-1
OCT	Optimal Cutting Temperature Compound
OIR	Oxygen Induced Retinopathy
PCR	Polymerase Chain Reaction
PDGF	Platelet-Derived Growth Factor
PDK	Phosphoinositide-Dependent Protein Kinase
PI3K	Phosphoinositide 3-Kinase
PIP2	Phosphoinositide (3,4)-Bisphosphate
PKB	Protein Kinase B
PKC	Protein Kinase C
PlGF	Placental Growth Factor
PLTP	Phospholipid Transfer Protein
qPCR	Quantitative Polymerase Chain Reaction
RAP	Retinal Angiomatous Proliferation
RAS	Renin-Angiotensin System
RBE4	Rat Brain Endothelial 4
RD1	Retinal Dystrophic-1
RNA	Ribonucleic Acid
ROS	Reactive Oxygen Species
RPCs	Radial Peripapillary Capillaries
RPE	Retinal Pigment Epithelium

RVEC	Retinal Vascular Endothelial Cells
sCD14	Secretory CD14 Antigen
sCD14	Soluble CD14
SFK	Src Tyrosine Family Kinases
SH2	Src Homology 2
SRF	Serum Response Factor
STAT	Signal Transducers and Activators of Transcription
TAMs	Tumour Associated Macrophages
TGFß	Transforming Growth Factor-ß
Th	Helper T Cells
TICAM1 / TRAF	Toll-Like Receptor Adaptor Molecule 1
TIR	Toll-IL-1 Resistance
TLR	Toll Like Receptors
Tm	Melting Temperature
t-PA	Tissue Plasminogen Activator
VEGF	Vascular Endothelial Growth Factor
VEGFR2	VEGF receptor
VLDLR	Very-Low Density Lipoprotein Receptor

Introduction

Introduction

1. The Eye

1.1 Function and Anatomy

Our eyes detect light and help us to interpret the world in which we live. The white light surrounding us contains a blend of coloured wavelengths. When light hits an object some of the coloured wavelengths are absorbed whilst others are reflected. This reflected light then effectively carries information about the object it has touched. When light reaches our eyes it is defracted by the cornea, passes through the pupil, is defracted once more by the lens, passes through the vitreous humour and then reaches the retina, a layer of cells lining the back of the eye, approx 42mm in diameter and 0.1-0.3mm thick (depending on where in the tissue the measurement is made, fovea 0.1mm, foveal rim 0.23-0.32mm) [1].

The retina contains endothelial cells, neuronal cells, glial cells, retinal pigment epithelium (RPE) and two specialised photoreceptors called rods and cones, which detect light via the visual pigment retinal embedded in their bilipid membranes (figure 1). Rod cells function at low light intensity to give us vision in darker conditions as well as shadow perception. Cone cells are responsible for our colour vision, they can be sub-divided into three types able to detect different light wavelengths of red, blue and green colour. The ability of cone cells to detect different wavelengths depending on what form of opsin protein combines with the retinal pigment [1]. The placement of rods and cones throughout the retina is highly variable depends on species, but in primates cone cells are more prevalent in the central regions with a greater proportion of rods in the periphery [2].

There is a structure in the primate retina, adjacent to the optic nerve head called the macula. The macula has a central region known as the fovea, which contains the highest percentage of cone cells in the retina. This results in the fovea being a vitally

important region for central vision and acuity, a retinal characteristic unique to humans and other primates [1-3]. The macula also has a high concentration of xanthophyll pigments called lutein and zeaxanthin [4]. Xanthophylls cannot be synthesised by the body and so have to be obtained through a diet rich in certain vegetables such as leafy green vegetables and yellow/orange peppers. The exact function of macular pigment is still not fully understood, but being enriched in the Henle fibre layer adjacent to the foveal photoreceptors, it is thought to have a photo-protective role [5]. The eye is susceptible to oxidative damage due to its frequent light exposure and the high concentration of polyunsaturated fats in receptor membranes [6]. The macular pigment is thought to help filter out damaging wavelengths (especially blue light) thus preventing oxidation and reactive oxygen species (ROS) such as hydrogen peroxide from forming in the photoreceptor layers [7]. When the photoreceptors capture light, they translate the information into an electrical signal, which can then be transmitted by the neuronal cells within the retina to the optic nerve and then onto the brain for processing [3]. The output information is what we define as vision. Sight is incredibly important to us. It enables us to observe and assess the world around us so we can interact accordingly. When there is a problem with our sight it can be seriously disabling, demand huge adaptations of our behaviour and force us to develop coping mechanisms that rely on our other senses.

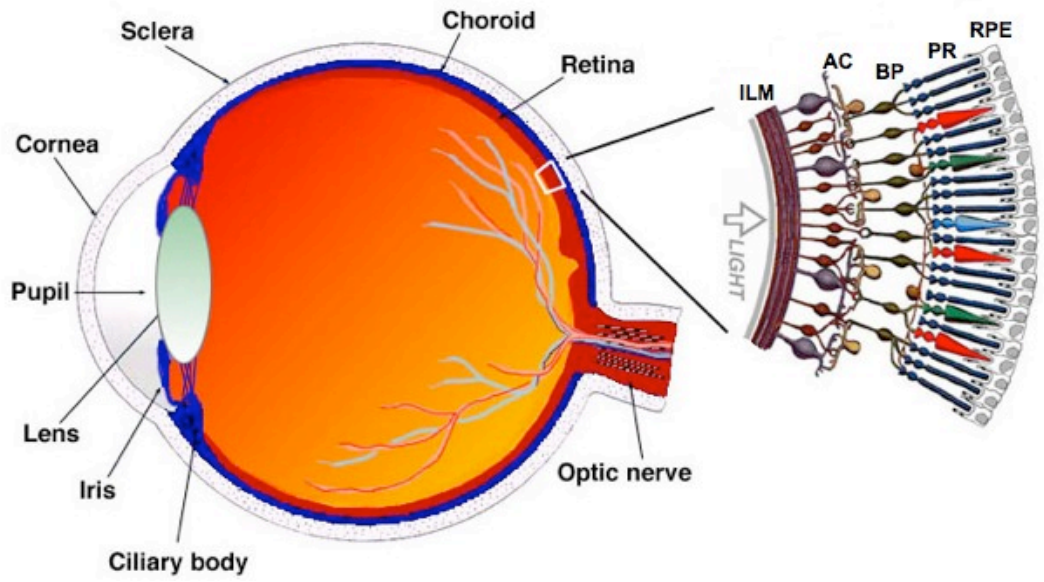

Kolb, H. et al. 2013. Webvision: The Organization of the Retina and Visual System. Copyright ©2013 Webvision: Attribution, Noncommercial, No Derivative Works Creative Commons license.

Figure 1: Schematic of a Human Eye. Drawing of a sagittal slice through an eye with magnification of the retinal cells. Inner limiting membrane (ILM), Amacrine cells (AC), Bipolar cells (BP), Photoreceptor (PR), Retinal pigment epithelium (RPE). Taken from WebVision resource http://webvision.med.utah.edu/book/part-i-foundations/simple-anatomy-of-the-retina/

1.2 Blood Supply

The retina receives blood from two sources. The majority (65-85%) comes from the choroidal blood vessels of the choriocapillaris behind the eye. This supply is particularly important for supporting the outer retina. The remaining 20-30% comes from the central artery, which originates through the optic disc, fans out across the retina and splits into three capillary networks (figure 2). This splitting enables blood and nutrients to reach and sustain all of the inner retinal layers. The vessel distribution within the retina has resulted in the three layers being termed 'superficial vessels', 'intermediate vessels' and the 'deeper vessel plexus'. The radial peripapillary capillaries (RPCs) make up the superficial layer as they share the pathways of the major vessels found 4-5mm from the optic disk. The deeper layer of capillaries runs parallel to the RPCs in the ganglion cell layer and connects to the RPCs through anastomosis [8]. The macula and fovea receive a limited blood supply from the superior and inferotemporal arteries, but have no vessel network within, in order to enable high acuity central vision [3].

Figure 2: Blood Supply to the Eye. Drawing shows the two blood supplies to the eye displaying the choroidal perfused layers and the three inner retinal vessel layers. Taken from the NHS Scottish diabetic screening services handbook http://www.ndrs.scot.nhs.uk/Train/Handbook/drh-06.htm

2. Angiogenesis

Angiogenesis is the generation of new blood vessels from a pre-existing vessel bed or network. It occurs as a normal process important in the body for development and wound healing, however pathogenic angiogenesis is a major contributing factor to diseases [9] such as growth or metastatic dissemination of solid tumours, and also proliferative diabetic retinopathy and the neovascular 'wet' form of age related macular degeneration (AMD) [10]. Angiogenesis can be divided into different sub-types depending on the mechanism of vessel generation [11].

1. Vasculogenesis occurs in early embryonic development and refers to do novo vessel development via differentiation of endothelial precursor cells. It can be divided into extraembryonic and intraembryonic blood vessel formation, which are spatially and temporally distinct processes. Growth factors such as fibroblast growth factor-2 (FGF2), bone morphogenetic proteins (BMPs), downstream SMAD targets have been identified as having key in vasculogenesis and vascular endothelial growth factor (VEGF)[12].

VEGF is a potent promoter of both vessel growth and vessel permeability, which is another problem in eye disease [13-15]. Five isoforms of the growth factor are produced through alternate splicing of its eight exons and seven introns, namely VEGF-A, VEGF-B, VEGF-C, VEGF-D and VEGF-E. VEGF-A is the major isoform and the one of interest concerning angiogenesis [16]; it exists in three splice variants, these being VEGF 121, 165 and 189 (figure 3), each of which can be alternatively spliced into antiangiogenic 'XXXb' variants [16]. All VEGF-A variants have been found to contain exons one to five but vary in their six to eight content. Exons six and seven encode for the C terminus and regulate the affinity of VEGF isoforms for heparan sulfate proteoglycans (HSPGs). $VEGF_{121}$ lacks the binding motifs in its C-terminus, meaning it does not bind to HSPGs on the extracellular matrix or cell surface, which makes it readily diffusible. $VEGF_{165}$ has partial binding so is weakly sequestered by HSPGs, and $VEGF_{189}$ has high affinity for HSPGs so remains sequestered until cleaved [17]. As well as HSPGs, VEGF-A isoforms have been shown to bind to Neuropilin-1 (Np-1) and two high affinity VEGF receptors, VEGFR1 (also known as Flt-1) and VEGFR2 (Flk-1). VEGFR1+2 share 44%

sequence homology and are both transmembrane tyrosine kinase receptors [18]. VEGF is an important growth factor in vascular development and restructuring of blood vessel networks under hypoxic conditions [18, 19]. VEGFR2 mediates most of the biological activities of VEGF-A [20], this VEGF binding to VEGFR2 induces receptor dimerisation and autophosphorylation to generate sites for Src homology 2 (SH2) domain containing protein (e.g. Grb2) recruitment. After docking on SH2 sites these proteins are phosphorylated to induce further signal transduction of proliferative pathways like the Raf1/MEK/ERK cascade [21]. VEGFR2 deficient mice have been reported to die at embryonic age 8.5-9.5 as a consequence of a lack of vascularisation demonstrating the critical role of VEGFR2 in VEGF angiogenic signalling [22]. VEGFR1 also has high affinity for VEGF-A but appears to behave as a decoy receptor, inhibiting the signalling effects of VEGF. It can however have angiogenic effects through binding and signalling of placental growth factor (PlGF)[103]. Mice deficient in VEGFR1 also die at E8.5-9.5 but show a hyperactivity of VEGF signalling, consistant with the idea that the receptor is required for negative regulation of VEGF [13, 18].

Figure 3: Vascular Endothelial Growth Factor (VEGF) Signalling. Schematic to show the activity of the different isoforms of VEGF, their receptor interactions and physiological effects. Neuropilin 1 and 2 (Nrp-1 and Nrp-2), Placental growth factor (PlGF). Taken from Paul Scherrer Institut Prota lab page http://sb.web.psi.ch/projects/neuropilin.html

2. Sprouting angiogenesis (figure 4) occurs throughout adulthood and refers to the generation of new blood vessels from pre-existing capillary networks. The process is vital for supporting expansion of new tissue and wound healing, but if not well controlled can contribute to diseases such as cancer and rheumatoid arthritis [23]. Sprouting angiogenesis is initiated by growth factor (FGF, VEGF, PlGF and angiopoietin 1) stimulation of neighbouring vascular support cells (e.g. pericytes, smooth muscle cells) and endothelial cell surface receptors. This leads to production of matrix metalloproteinases (MMPs) that break down the surrounding extracellular matrix and basement membrane thus allowing the endothelial cells to proliferate and invade the surrounding tissue, with cell polarity establishing a vessel lumen [23, 24]. VEGF is thought to be the key regulator of sprouting angiogenesis, acting as a guidance factor for the specialised tip endothelial cells, and as a proliferative inducer for the endothelial stalk cells within the vessel [11, 23, 25].

Figure 4: A Schematic of Sprouting Angiogenesis. Chronological representation of the events thought to drive sprouting angiogenesis. a) Angiogenesis is regulated with a tight balance between pro-angiogenic and anti-angiogenic factors. Some endothelial cells will respond (green) whereas some will not (grey). b) The growing cell sprout is guided by a VEGF gradient with tip cells releasing platelet-derived growth factor (PDGF) recruiting pericytes (yellow). c) When tip cells contact there are either attractive or repulsive cues present to regulate fusion. d) Tip cell fusion establishes a luminal space, allows blood flow and thereby removes hypoxic initiation of further angiogenesis. [11]

3. Intussusceptive angiogenesis (also known as splitting angiogenesis) is a specialised remodelling process which follows four growth steps (figure 5) – 1) Opposing walls of the vessel lumen protrude, generating a contact point for the endothelial cells. 2) Intracellular junction proteins reorganise to join the contacted cells together. 3) Supporting cells (e.g. pericytes and myofibroblasts) deposit matrix proteins for the cellular network. 4) The generated vessel pillar increases in size to create a thicker vascular pillar [25, 26].

Three different variants of intussusceptive angiogenesis have been reported, which vary in the angle of their pillar generation. Intussusceptive microvascular growth expands the capillary plexus via production of transluminal pillars. Intussusceptive arborisation splits the plexus with vertical pillars to generate 'feeding' vessel networks. Intussusceptive branching does not generate new vascular tissue but by inserting vertical pillars at vascular branch points it enables remodelling of the vessel network. The underlying mechanism for intussusceptive angiogenesis is not understood but studies in mice have shown Ang1, VEGF, transforming growth factor ß (TGFß) and Notch4 signalling to be required for vascular remodelling similar to the variants of intussusceptive angiogenesis [25, 26].

Figure 5: A Schematic of Intussusceptive Angiogenesis. Diagram to show the nature of splitting angiogenesis. The generation of tissue pillars enables the vessel to branch, the molecular mechanisms involved are not currently known but thought to involve cell proliferation, migration, degradation of extracellular matrix (ECM) and deposition of new ECM. [11]

3. Diseases of the Retinal Vasculature

It is estimated that every 15 seconds someone, somewhere in the world loses their vision [27]. This is an alarming statistic and one which needs addressing. The variety of cell types within the eye means that a complex functional interplay needs to be

maintained in order to sustain a healthy retina. If one cell type becomes dysfunctional or diseased it can have a knock-on effect for the entire visual system ultimately resulting in a threat to vision. There are numerous examples of retinal diseases that have their origins in photoreceptor death (e.g. retinitis pigmentosa) or elevated ocular pressure (glaucoma), however the focus of this thesis is retinal vascular disease so I will concentrate on conditions where vascular abnormalities are a major contributor to clinical symptoms and disease progression.

3.1 Age related Macular Degeneration (AMD)

AMD is one of the most common eye diseases, causing degenerative blindness in patients over 50 years of age. AMD can be divided broadly into two types; atrophic ('dry') and neovascular ('wet'). Atrophic AMD is far more common (approximately 90% of patients) than neovascular (10%). Generally patients with atrophic AMD experience less visual disturbance then patients with neovascular disease, however this is not always the case as it depends on the severity and geography of drusen formation. Drusen are fatty deposits, which form at the interface of Bruch's membrane and the RPE and are the first clinically detectable sign of AMD (figure 6). It is thought that increased oxidative damage to the photoreceptor layer produces waste products, which the RPE are unable to digest [28, 29]. This causes accumulation of waste in the RPE, altering their metabolism and stimulating them to secrete products basally, which collect and contribute to the formation of drusen [28, 30]. It is known that there are different types of drusen; hard drusen appear as small discrete deposits containing tube-like vesicle structures and collagen, soft drusen tend to be larger with ill-defined boundaries containing membranous debris, semisolid drusen are a mixture of the two types, and calcified drusen appear to glisten upon examination [31, 32]. It is estimated that over 50% of the population >70yrs of age have drusen but report no visual disturbances [32]. Thus, drusen formation is not causative of disease itself, and may be considered part of normal healthy aging. However, the severity of vision loss appears to correlate with the number of drusen deposits and where they form. A high number of central drusen correlates with central vision impairment, and in general soft drusen are more detrimental than the other types [32, 33].

Atrophic AMD can develop into neovascular AMD upon the growth of new blood vessels from the choroidal plexus. The new vessel sprouts push through the Bruch's membrane and invade the RPE layer where they leak and cause damage, promoting cell death. [34].

Retinal angiomatous proliferation (RAP) is a distinct form of choroidal neovascularization that has been found to correlate to a poor disease prognosis. The exact cause remains unknown but research has shown it to have a higher prevalence in women and the elderly [35] and that its development is thought to occur over three stages: 1) intraretinal neovascularization where the deeper plexus intraretinal capillaries proliferate. 2) subretinal neovascularization where the growing vessels invade the subretinal space and 3) clinical manifestation where the RAP / CNV could be determined clinically [36].

There are two processes thought to provide the triggers for AMD onset, hypoxia and chronic inflammation. Bruch's membrane naturally thickens with age, which is thought to gradually diminish diffusion of the nutrients from the blood supply into the retina, resulting in oxygen deprivation. This then promotes VEGF induction and blood vessel growth [37, 38]. Crucially AMD has been found to have a higher prevalence in patients with specific genetic variations in certain complement proteins [37, 38, 39].

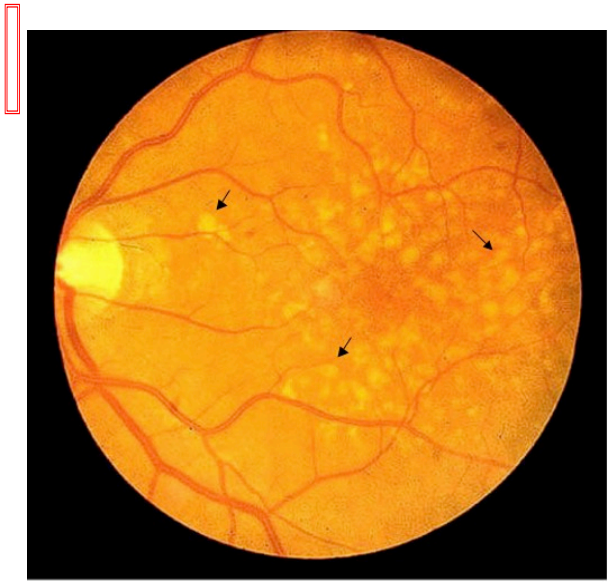

Figure 6: Fundus Photograph of a Patient with AMD. Shows soft drusen (arrowed) formation within the retina. Taken from WebVision resource http://webvision.med.utah.edu/book/part-i-foundations/simple-anatomy-of-the-retina/

Kolb, H. et al. 2013. Webvision: The Organization of the Retina and Visual System.

The complement system is part of the innate immune system. It consists of over 25 circulating inactive proteins, receptors and proteases, which are activated upon infection to have cell killing affects. Complement factor H (CFH) is an important regulator of the complement cascade [40]. The Y402H polymorphism in CFH has been linked to an increase in the chances of developing AMD [40-43]. Thus, 50% of AMD patients are believed to have the Y402H polymorphism, in which a tyrosine residue is replaced with a histidine residue. The change occurs in the heparin and C-reactive protein (CRP) binding sites, decreasing the affinity of CFH for its substrates [44]. This is thought to diminish or inhibit CFH function, thus sending complement into overdrive [32, 40]. It remains unclear exactly how this chronic signal activation is thought to drive disease pathogenesis but polymorphisms in other complement proteins such as factor B, C2 and C3 are also associated with AMD, confirming a causative link between immunity and the disease [39, 47]. The CFH Y402H variant is also thought to be linked to soft drusen formation as Japanese and Chinese AMD patients have decreased soft drusen formation as well as a lower prevalence of Y402H (<5%) whereas white Caucasian AMD patients have a higher soft drusen occurrence along with higher prevalence of Y402H (>35%). This observation suggests that ethnicity as well as the CFH polymorphism contribute to susceptibility to AMD [48]. Histopathology studies have demonstrated an increased presence of fibroblasts, macrophages and lymphocytes within Bruch's membrane of AMD patient eyes, further supporting a link between immunity and the disease [49].

Other genetic alterations are also associated with AMD. Mutations affecting the activity of ABCA4, an ATP-binding cassette transporter of retinaldehyde, expressed in the photoreceptors have been linked to AMD [50-52] suggesting faulty photoreceptor function as a contributing factor. In addition, functional disruption to proteins involved in extracellular matrix remodelling (e.g. TIMP3, fibulins 5 and 6) have also been implicated [53]. As previously mentioned, due to its frequent light exposure the retina has high levels of oxidative stress. The generation of ROS through oxidative stress can be pathogenic if unbalanced as ROS damage all major cellular components, including DNA [54]. Faulty mitochondrial function and polymorphisms in deoxyribonucleic acid (DNA) base excision repair genes hOGG1 and MUTYH, which repair ROS-induced damage to nucleic acids, have been identified in AMD patients, supporting increased oxidative damage as a contributing

factor to the progression of the disease [6]. There is still much debate over what causes the disease to progress from atrophic to neovascular; some work has suggested that a polymorphism in the promoter for the heat shock serine protease HTRA1 is required [55, 56]. The genetic alteration appears to increase the transcriptional affinity for the adaptor related protein complex 2a (A2a) and serum response factor (SRF), which is suggested to promote vascular growth. Interestingly expression of HTRA1 is up-regulated under oxidative stress, again supporting a link between this process and AMD [56].

Lifestyle choices, such as poor diet and smoking have also been shown to increase the chances of developing AMD. Smoking can harden the blood vessels so they become fragile or blocked. This fragility can lead to breakages and leakage of fluid into surrounding tissue. Moreover, venal obstruction may result in growth of new blood vessels to compensate for the oxygen deprivation caused by inadequately supported tissue. Studies have shown that smoking also increases ROS generation and the levels of CRP in circulating plasma, thus mimicking an immune response and inducing complement activation [6, 38]. It has been reported that neovascular AMD progresses four times faster in smokers than in non-smokers [6, 57].

A healthy diet is thus important for preventing disease. A decrease in the amount of macular pigment has been indicated as being associated with an elevated risk of AMD progression [5]. Adipose tissue has been found to sequester the pigments, implying that obesity may compromise the delivery of the protective pigments to the retina [57, 58].

3.2 Diabetic Retinopathy

Diabetes mellitus is a common disease affecting over 2.8 million people in the UK alone [59]. There are two types of the disease, insulin dependent (IDDM) where the patient is unable to make any or enough insulin to metabolise glucose, and non-insulin dependent (NIDDM) where the patient often makes enough insulin but their cells have become unresponsive to the hormone. A range of health complications accompanies diabetes, among which retinopathy is the most common. Thus, 80% of patients who have had IDDM for 10yrs will have retinopathy, and 20yrs of the

disease increases the likelihood to 95% [60-62]. Diabetic retinopathy is the leading cause of blindness in developed countries, affecting the working age population (20-74yrs) and estimated to generate 12% of the annual cases of blindness [63].

Diabetic retinopathy can affect many cell types within the retina but it is characterised as a disease of the intraretinal blood vessels. There are two types of the disease, non-proliferative and proliferative (figure 7). The non-proliferative form is the most common and is characterised by increased capillary permeability and basement membrane thickening [64]. Patients with non-proliferative diabetic retinopathy will sometimes remain asymptomatic depending on the severity and positioning of capillary leakage [64]. Diabetic patients show increased number and activation of leukocytes (leukostasis) [63]. Leukocytes are able to adhere to the endothelium via ICAM-1 interactions and have a capacity to secrete proteolytic enzymes [63], therefore leukostasis poses problems for the retinal microvasculature. *In vivo* observations have reported that vascular non-perfusion and leakage are temporally and spatially associated with intravascular leukocyte aggregation [65]. Proliferative diabetic retinopathy occurs as a result of the microvascular blockages threatening nutrient supply, inducing hypoxic conditions thus triggering neovascularisation into the surrounding tissue which causes damage, cell death and vision loss [64, 65].

Figure 7: Fundus Photography Representation of Diabetic Retinopathy. Shows the non-proliferative stage and the proliferative disease with marked neovascularisation. Taken from the DPLEI Certified Hospital webpage patient resource http://www.drpattnaik.com/vitreo.html

The molecular aetiology of diabetic retinopathy is not completely understood but studies have shown that hyperlipidemia and hypertension contribute to the pathogenesis and that hyperglycaemia is the principle cause of disease in both IDDM and NIDDM [62-64]. It was suggested that better glucose control could offer some protection from disease onset, but studies using diabetic dogs and rats with long-term regulated glucose levels followed by a short period of poor glucose control, demonstrated that long-term glucose management offered little protection [65, 66]. It is thought that the disease stems from a series of long term metabolic alterations in the retinal cells. Free amine groups found on proteins, nucleic acids and lipids undergo reversible non-enzymatic reactions to generate intermediate products known as Schiff bases and Amadori products. When glucose is low these products can be broken down to re-establish sugar groups and maintain an energy balance in the cell. When there is a high glucose concentration the products can be stored or undergo further modification to keep the sugars sequestered, however after a series of modifications the products will form AGEs [66]. This reaction balance means that diabetic patients will tend to have a higher concentration of AGEs, which in turn may covalently crosslink proteins, lipids and DNA altering their structure and behaviour [64, 67-69].

Generation of advanced glycation end-products (AGEs) and de novo synthesis of diacylglycerol (DAG) leading to overactivation of various protein kinase C (PKC) isoforms and the renin-angiotensin system (RAS) could contribute to retinal vascular pathogenesis [64, 73, 74]. Some receptors for AGEs have been identified with the most well characterised existing as a triple complex (R1, R2 and R3) called RAGE [66, 74]. The signalling capacity of AGEs is not well defined but has been suggested to induce PKC, Janus Kinase (JAK), signal transducers and activators of transcription (STAT), nuclear factor kappa ß (NF-kß) and AP1 [76].

The role of AGEs in retinopathy remains unclear but there has been insight into their contribution to renal disease as they have been found to induce transforming growth factor-ß (TGFß) [75, 77] and diabetic mice that do not express galectin-3 (the R3 component of RAGE) are protected against diabetic nephropathy [64, 79]. *In vitro* experiments have shown that treatment of endothelial cells with preformed AGEs induces proliferation, caused by an induction of VEGF [80]. This has also been

shown to occur *in vivo* with acute elevation of AGEs, however long term exposure to AGEs appears to inhibit vessel proliferation [64]. Four polymorphic alterations in the RAGE promoter have been identified, altering the transcription and expression of the receptor complex [81]. One of these alterations has been shown to have a higher prevalence in a small subset of NIDDM patients [81]. It could be that as AGEs appear to have a role to play in exacerbating diabetic retinopathy, polymorphic alterations in the AGEs receptor(s) could predispose diabetic patients to advanced retinopathy, or moderate tolerance to poor glucose management [64, 73, 78, 83].

3.3 Other Retinal Vascular Diseases

Idiopathic Macular Telangiectasia (MacTel) is a relatively rare disease (Beaver Dam Eye Study reported the disease prevalence is 0.1%, which although small still results in approximately 70,000 people in the US being affected [84] of the eye, first described in 1982. There are currently considered to be two variants of MacTel, aneurismal telangiectasia and perifoveal telangiectasia (figure 8). Most research has focused on the latter, as this is the most common form. Perifoveal MacTel occurs in two phases; the first being a non-proliferative stage in which there is loss of macular pigment and the retinal capillaries appear to dilate and leak. The second phase is an advanced stage where the capillaries proliferate into the foveal region and become tortuous displaying the characteristic telangiectasia phenotype. As the disease progresses further the vessels dive downwards through the retinal layers and make contact with the RPE. This contact appears to induce RPE proliferation up the vessel and causes vessel-RPE plaques to form. Foveal invasion leads to a progressive loss of central vision, which can eventually result in complete central blindness [85, 88]. Little is known about the causes of the disease, however recent studies have revealed a significant reduction in macular pigment in patients with MacTel [87, 88] suggesting that central loss of cone photoreceptors may be linked to increased oxidative stress. Furthermore, it was research into the basic cell biology of MacTel, undertaken as a part of the MacTel project [89] which led to the discoveries that paved the way for the work in this thesis.

Retinal vein occlusion can be sub-divided into three types; central retinal vein occlusion (CRVO), hemiretinal vein occlusion (HRVO) and branch retinal vein occlusion (BRVO). The leading cause of retinal vein occlusion is thrombus formation

thickening the neighbouring artery and therefore compressing the vein [90]. As with AMD, retinal occlusion is most common in people over 50yrs of age. Patients often have a history of atherosclerotic disease, hypertension and possibly diabetes. Vein occlusions are sometimes found in younger patients with a family history of vascular disease, or diseases where there is thickening of the blood making it more prone to forming a thrombus [90]. Most patients will report a sudden loss of vision, with CRVO patients found to also have iris neovascularisation upon clinical examination. Treatment is often laser ablation or surgical intervention to widen the vein and / or remove the thrombus. Tissue plasminogen activator (t-PA), a clot selective, recombinant fibrinolytic protein has shown some success in treatment of occlusion caused by thrombosis [90]. However targeted delivery of the protein is problematic with a chance of severe complications, which could prove fatal [90].

Figure 8: Fluorescein Angiogram Displaying Macular Telangiectasia. A) Arrow shows perifoveal leakage B) Arrow shows exudative scarring of the foveal region. Images taken from the vitreous-retina-macula consultants of New York webpage resource http://www.vrmny.com/pe/ipt.html

Coats' disease (also known as exudative retinitis) is a rare eye disease, which usually affects males in the first decade of life. It is a developmental disease where the choroidal capillary bed fails to form properly so the vessels leak causing structural and functional break-down of the retinal barrier as well as macular odema, generation of lipid deposits within the tissue and retinal detachment [90-92]. The disease can be divided into five stages; 1) Telangiectasia only – if caught early this stage of the disease can sometimes be successfully treated with laser coagulation therapy to remove the excessive vessels. 2) Telangiectasia and exudate – this stage can be

further subdivided into 2a, where the fovea is unaffected by the leakage or 2b, where the fovea is affected. Visual impairment can sometimes be successfully treated with laser coagulation or cryotherapy depending on the extent of leakage. 3) Subretinal or retinal detachment – this stage can also be further subdivided into 3a, where the retinal detachment is incomplete or 3b, where there is total retinal detachment. This stage of the disease may require surgery to repair the detachment. 4) Total retinal detachment and glaucoma – by this stage of the disease there is a dramatic loss of vision and limited treatment options. There can be severe pain in the eye due to increased ocular pressure, when this occurs enucleation is recommended. 5) Total blindness – this is the final stage of Coats' disease when the patient experiences total blindness. There is no treatment for the condition at this stage.

The cause of Coats' disease is unclear, it has been suggested that hypercholesterolaemia could contribute to adult Coats' but there is little experimental evidence for this [89]. A link has been found between Coats' and a somatic mutation in the Norrie disease protein (NDP), suggesting that a deficiency in the Norrin protein during development could lead to retinal vascular abnormalities [93]. Mice lacking Norrin appear to exhibit retinal disorganisation, and under development of the capillary bed supported a requirement for Norrin in the developing eye [93].

Eales' disease is an idiopathic inflammatory venous occlusion, which commonly affects males aged 14-29. Symptoms of the disease include vitreous haemorrhage and vascular proliferation. The exact causes of Eales' disease is not known, however, inflammation is commonly documented in the first stages of clinical presentation. Therefore suggesting a link between enhanced inflammation and the vascular disease progression [94].

Uveitis is an inflammatory disease of the uveal tract of the eye, made up of the iris, choroid and ciliary body. Any and all of these sections of the uvea can be affected thus giving rise to location specific types of uveitis. As overactive inflammation is the driving force behind the disease it is unsurprising that there is a high association between infection and uveitis. Anterior uveitis affects the iris and so can also be known as Iritis. It is the most common form of the disease accounting for 75% of patients and can occur suddenly, persisting for weeks even with treatment. It is also

found to be associated with autoimmune disorders such as rheumatoid arthritis. Intermediate uveitus, as the name suggests, affects the middle portion of the uveal tract and can disrupt the function of the muscles used to focus the lens. This form can also occur suddenly and persist for weeks or months even with treatment. Posterior uveitis affects the retina or choroid (or both) and can prove to be rapidly progressive, involving neovascularisation making it difficult to treat. Uveitis can be slow to respond to medication and threatens vision meaning it needs to be diagnosed and treated quickly. Antibiotics are used to fight the underlying infection and steroids can be prescribed to help with swelling [95].

4. Current Treatment for Retinal Vascular Diseases

Current treatment options can offer some symptomatic relief to patients but as yet there is no complete cure for retinal vascular disease. Frequently in diseases, such as those described in the previous sections, the severity of vision loss is caused by uncontrolled retinal or choroidal vessel proliferation and / or leakage. This means that treatments which target blood vessel behaviour can be of value.

Photodynamic therapy is an essentially destructive modality, but is one of the longest standing treatments for eye disease caused by abnormal vascular growth. This treatment utlises the photosensitivity of verteporfin. Normally verteporfin is stable but when it comes into contact with light it reacts with oxygen to become cytotoxic. By giving patients systemic injections of a drug that contains verteporfin the doctor can then wait for the drug to reach the abnormal retinal vessels, activate the drug with a laser and produce the cytotoxic reaction to kill the blood vessels [96]. The disadvantage of this treatment is that whilst it blocks or removes unwanted blood vessels, it doesn't eliminate the signals responsible for vascular growth, so it may have to be used in conjunction with other treatments [96]. Another problem is that after injection the patient remains light sensitive for up to 48h and so will need to be advised about what levels of light they can tolerate. There can also be some temporary visual disturbance or in rarer cases patients can experience a dramatic reduction in their vision for longer periods of time [96, 97].

Angiogenic factors make attractive therapeutic targets for retinal vascular disease, as well as other vessel pathologies. In some circumstances, such as stroke where limited

blood supply is a problem, promoting angiogenesis could be beneficial. In other cases such as in ophthalmic disease or cancer, where it has been calculated that a tumour cannot grow beyond $2mm^3$ if it fails to establish a blood supply, inhibiting angiogenesis could prevent disease progression [23].

As VEGF-A has been shown to increase endothelial migration and proliferation it is not surprising that deregulated expression and activity is often seen in disease [16, 98]. As a result some of the most effective current treatments for AMD work by inhibiting the effects of VEGF, either by blocking the VEGF receptor (VEGFR2) or by sequestering free VEGF[57]. The main VEGF inhibitor commonly used for the treatment of AMD is Ranibizumab (Lucentis). Lucentis was developed on a Fab fragment of a full length humanized monoclonal antibody, Bevacizumab (Avastin). Avastin was originally developed for the treatment of bowel cancer, but Lucentis has a much higher affinity for VEGF [98]. In 2006 the Food and Drug Administration (FDA) in the USA, and in 2008 the National Institute of Health and Clinical Excellence (NICE) in the UK approved Lucentis for use in the treatment of neovascular AMD. Patients given monthly intravitreal injections of Lucentis were compared to patients who received a sham injection. The results showed that 95% of the Lucentis patients reported stabilisation of their symptoms and that 40% experienced an improvement in their vision, as assessed by a gain of 15 or more readable letters in their central acuity [98, 102].

Because Avastin was originally marketed as a treatment for metastatic colorectal cancer it has not officially been approved as a treatment option for retinal vascular diseases, however it has a much longer half life than Lucentis (taking 100 times longer to clear from the circulation) meaning patients do not require as many injections, and it is substantially cheaper. It is estimated that there are approximately 25,000 new cases of AMD every year in the UK and that if all patients received Lucentis it would cost the National Health Service £300 million, whereas Avastin treatment would reduce this bill by £292 million [101]. A potential disadvantage of using Avastin instead of Lucentis is that whereas Lucentis is retained in the eye upon intraocular injection, Avastin may enter the systemic circulation, in fact it has been detected in blood of treated rabbits three weeks post-injection [102]. This could potentially lead to adverse side effects by inhibiting VEGF signalling elsewhere in

the body. Other general drawbacks to treating eye disease with VEGF inhibitors such as Avastin and Lucentis are that VEGF is also a key survival factor for neurons and Muller cells within the retina meaning its inhibition could still threaten vision [100]. Also, VEGF is often up-regulated in the later stages of disease, so by the time the drugs are prescribed it is not unusual for significant vision loss to have already occurred. Secondly, VEGF inhibitors may slow further disease but they cannot repair existing damage, and lastly the method of drug delivery is monthly intravitreal injection which is unappealing to patients and there is a small (<1%) risk of causing intraocular inflammation, retinal detachment or retinal tearing [102]. Despite the wide use of Lucentis it is reported that only 50% of patients respond to the drug, and as it is only used for treatment of neovascular 'wet' AMD, which accounts for only 10% of AMD cases, it is clear that although useful, Lucentis is not going to be 'cure-all' for retinal vascular disease [37, 57, 96].

Alongside these VEGF antibodies pharmaceutical companies have also developed 'VEGF traps' such as Aflibercept, which is a recombinant fusion protein of the VEGF receptor and the Fc domain of IgG1 [101]. Aflibercept differs from Avastin and Lucentis because it is not an antibody against VEGF, instead it utlises the VEGF receptor structure to capture the growth factor and prevent it from initiating its signalling effects [101].

VEGF is not the only growth factor that can promote vascular changes, and since patients receiving treatments such as Avastin frequently develop resistance to this therapy, other therapeutic modalities are required [99]. Thus, new therapeutic antibodies are being assessed in clinical trials, including a promising PlGF blocker, as well as small molecule inhibitors such as Sunitinib and Sorafenib (figure 9) [102, 104].

Sunitinib is a multi-tyrosine kinase inhibitor that has been shown to target all of the VEGFRs as well as the platelet-derived growth factor receptors (PDGF-Rs), which have been shown to promote angiogenesis [105]. Sorafenib (also known as Nexavar) is another multi-tyrosine kinase inhibitor also able to inhibit VEGFR and PDGF-Rs as well as the Raf serine threonine kinase, thereby preventing ERK activation and subsequent endothelial cell proliferation [[106, 107]. Both of these drugs have been

commissioned for use in cancer treatment. Sunitinib is considered the first drug choice for patients with advanced metastatic renal cell carcinoma, and Sorafenib is often used for treating hepatocellular carcinoma [101, 107]. The obvious disadvantage to using non-specific inhibitors is that they can have off target effects, thus causing adverse side effects in non-disease affected tissues [95].

Figure 9: Anti-angiogenic Drug Targets. Drawing to show where some of the current therapeutics target the angiogenic pathway. Examples A) Lucentis and Avastin B) Aflibercept C) Sunitinib and Sorafenib. [102]

One of the more promising targets for anti-angiogenic therapeutics is PlGF. PlGF belongs to the same cysteine knot superfamily of growth factors as VEGF and also shows affinity for the VEGF receptors. However, unlike VEGF-A, PlGF does not signal through VEGFR2, instead it has been found to initiate its effects through VEGFR1, Np-1 and Np-2. PlGF has been reported to enhance VEGF-A signalling in several ways – 1) Displacing VEGF-A from VEGFR1, thus making VEGF-A free and able to bind VEGFR2 to induce signalling activity [103]. 2) Binding of PlGF to VEGFR1 promotes cross-talk between VEGFR1+2 amplifying VEGFR2 signalling

[108, 109]. 3) PlGF signalling through VEGFR1 activates transcription of VEGF-A as well as other growth factors FGF2 and PDGF [107]. *In vivo* research has shown that PlGF is not required for vascular development but that it plays a role in pathogenic angiogenesis, inflammation and vascular leakage. Treatment with an anti-PlGF antibody has been shown to inhibit choroidal neovascularisation (CNV) in a mouse model of retinal vascular disease and promote regression of pre-existing tumour vasculature [102, 110]. PlGF is therefore a very attractive drug target for vascular disease due to it being involved only in pathogenic vasculogenesis. This means that targeting PlGF could permit treatment of the disease vasculature without affecting healthy blood vessels [102, 109].

Overall the available treatments for ocular vascular disease are limited and of variable efficacy. They can offer symptomatic relief but do not target the cause of disease and as they often target disease in its later stages they cannot repair damage already caused. In order to treat eye disease successfully a better understanding is needed of the driving forces behind abnormal vessel behaviour, and the molecular mechanisms that lead to increased VEGF production. In addition, greater insight into the earlier stages of disease and identification of novel markers for disease progression may permit diagnosis at earlier stages, and lead us to alternate drug targets suitable for earlier intervention.

5. A Genetic Screen to Identify Novel Drug Targets

To obtain new insight into the genetic changes responsible for pathogenic neovascularisation our lab carried out a microarray analysis of the genes expressed in isolated retinal vessels from three mouse mutants displaying varying degrees of vascular abnormality.

The mouse models chosen were the very-low density lipoprotein receptor knock out (*VLDLR*$^{-/-}$), the retinal dystrophic-1 (RD1) and the *Grhl3*^{CT}/J Curlytail mouse (CT). Neuroretinal tissue was dissected from the eyes of each mouse at an age at which vessel disease was established (16 weeks for *VLDLR*$^{-/-}$ and RD1, 12 weeks for CT). Vessel fragments were affinity purified from which ribonucleic acid (RNA) was then isolated, and global gene expression was compared to age-matched C57B6 wild-type mice. Bioinformatic analysis of the microarray data, using FDR and a P value of

<0.01, to define significance, led to the identification of sixty-two genes that commonly changed in all three mouse models when compared to controls. One of the most substantially up-regulated genes was *LBP*, which encodes the Lipopolysaccharide Binding Protein.

6. Lipopolysaccharide Binding Protein

6.1 Overview

The Lipopolysaccharide Binding Protein (LBP) is a 60kDa acute phase response glycoprotein that is primarily expressed and secreted by hepatocytes and macrophages. It belongs to the same protein family as bactericidal permeability-increasing protein (BPI), plasma cholesteryl ester transfer protein (CETP), and phospholipid transfer protein (PLTP), all members of which share a high degree of structural similarity and certain related functions [111, 112]. The LBP and BPI genes are both located on chromosome 20, and although they exhibit some marked differences in their bioactivity they have substantial sequence homology. Protein crystallography analysis of BPI has shown the protein to have a two domain 'hinge-like' structure. This structure is expected to be similar for LBP due to the fact that they share 45% amino acid sequence identity [113-115].

6.2 Immune Role

LBP functions, as its name suggests, to bind lipopolysaccharide (LPS), a cell wall component of gram-negative bacteria such as *E. coli.* The N-terminal domains of LBP and BPI appear to be responsible for the ability of the proteins to recognise and bind to LPS. However, whilst the antibacterial function of BPI is also dependent on a portion of the N-terminus [114]. LBP requires its C-terminus to either clear the endotoxin through transferring it to high density lipoproteins (HDL) or to elicit inflammatory signalling by presenting the endotoxin to soluble CD14 (sCD14) or membrane bound CD14 (mCD14) to activate cell signalling cascades (figure 10) [115]. LBP-LPS-CD14 activates pattern recognition receptors such as the toll like receptors (TLR), among which TLR4 is particularly important, which in turn leads to expression of key inflammatory agents such as TNFα and interleukins 1 and 6 (IL1, IL6) [116-118].

TLR4 was the first pattern recognition receptor identified, and following elucidation of its key role in mediating LPS-induced septic shock in the late 1990s it has been the focus of much research. As a result it is now one of the best characterised members of the TLR family [119]. Presentation of endotoxins such as LPS to TLR4 have been found to induce tyrosine phosphorylation of its Toll-IL-1 resistance (TIR) domain, which is then thought to recruit intracellular adaptor molecules and enable signalling cascades primarily through the NF-kß pathway [120-121]. TLR4 is currently the only known member of the TLR family which can recruit and activate two alternate TIR recognising adaptor proteins, namely MyD88 and the toll-like receptor adaptor molecule 1 (TICAM1 or TRAF). By signalling through these two adaptors TLR4 is able to mediate both an early phase of NF-kß transcription (through MyD88) as well as a later phase (through TRAF) [116-122].

Figure 10: A Schematic Showing the LBP + LPS Inflammatory Signalling Cascade in an Endothelial Cell. LBP binds to LPS and initiates docking the endotoxin at the cell surface either via membrane surface antigen CD14 or circulating CD14. This then induces TLR4 and MD-2 (a 25kDa protein required for TLR4 membrane localisation) heterodimers and activates receptor auto-phosphorylation. MYD-88 is then recruited and intracellular signalling through IRAK-1, TRAF 6, TAK1 and IKKαßγ, release of p65 and p50 and their nuclear localisation for NF-kß transcription activity. Image taken from MedScape news http://www.medscape.com/viewarticle/706510_4

Mammals express five NF-kß family members related by their Rel homology domains (RHD); p50, p52, p65 (also known as RelA), c-Rel and RelB. The RHDs enable these transcriptional elements to form any combination of homo and heterodimers which can then recognise kß binding sites present in specific gene promoters to modulate gene transcription. In the case of RelA, c-Rel and RelB, gene expression is activated, whereas p50 and p52 will only activate transcription as a heterodimer with RelA, c-Rel or RelB [122-124]. In contrast, when these molecules form homo or heterodimers with one another they inhibit gene transcription. All members of the NF-kß family are constitutively expressed and maintained in an inhibited sequestered form in the cell cytoplasm through their interactions with inhibitory Ikß proteins. There are currently seven known IkB inhibitory proteins; ikßα, Ikßb, Bcl-3, Ikße, Ikßg and the precursor proteins for p50 and p52, p100 and p105 [125].

There are two types of signalling that have been found to induce NF-kß activity, these being the canonical pathway which involves a ligand being presented to a membrane receptor (such as LPS-TLR4) leading to intracellular signalling through the recognition of phosphorylated sites, and the non-canonical pathway which is only generally observed during the development of lymphoid tissue. These two pathways are separated by the NF-kß elements through which they act, whereby the canonical pathway leads to the formation of dimers of RelA, c-Rel, RelB and p50, whilst the non-canonical pathway is reponsible for p52/RelB acitivity [122-124]. NF-kß activity has been shown to effect genes responsible for inflammatory responses, cell survival, cell differentiation and cell proliferation [122-125]. In view of these pleiotropic activities, it is unsurprising that poorly controlled NF-kß signalling is linked to disease, indeed up regulation of NF-kß activity has been linked to cancer, autoimmune disorders and chronic inflammatory conditions [124-127].

6.3 Immunity and Angiogenesis

Cancer progression is dependent on tumour cells receiving an adequate nutrient supply, which is achieved through successful angiogenesis. Angiogenic potential now appears to be determined by the tumour ‘microenvironment’, meaning the neighbouring cells and the factors they secrete [124]. Research has shown that these microenvironments are packed with immune cells and that prognosis for the patient

appears to be at least partly dependent on the balance between anti-tumour and pro-tumour immune responses [129].

T cells have been found to exert pro and anti-tumour effects depending on their cellular status. High levels of $CD4^+$ helper type-1 T cells (Th-1) in the tumour microenvironment appear to correlate with a better prognosis in colorectal cancer, whereas $CD8^+$ and $CD4^+$ helper T cells, activated by IFNγ appear to promote metastasis. T cells have also been found to educate tumour associated macrophages (TAMs), activating them to secrete proliferative factors, making them pro-angiogenic in breast cancer [130, 131]. When macrophages were first discovered they were considered to function only as scavenger cells. However, investigators soon noticed that macrophages secrete an array of functionally important proteins, and by 1976 the scavenger had emerged as a major player in angiogenesis [132-134]. TAMs are now known to be the principle source of cytokines and angiogenic factors in tumour development [132-134]. The macrophages effect appears to depend on its activation ligand – e.g. those that have been activated by a microbial ligand or IFNγ and expresses high levels of proinflammatory cytokines (e.g. TNFα, IL-1 and IL-6), have been linked to anti-tumour responses whereas macrophages that have been activated by IL-4, IL-10 or IL-13 and express high levels of anti-inflammatory cytokines (e.g. IL-10, arginase, scavenger receptor A) have been demonstrated as having tumour promoting abilities [49, 133]. It has been suggested that tumour inhibition or progression is solely dependent on the chemokine profile within the microenvironment and is not really reliant on the immune cell type producing the signals. IL-6, IL-17 and IL-23 have been shown to be pro-tumourigenic whilst IL-12, TRAIL and IFNγ are generally anti-tumourigenic [134, 135].

As previously discussed, LBP is secreted by macrophages and has a well characterised role in inducing inflammatory signalling through TLR4 and NF-kß activation [124]. However, in 2003 LBP was also suggested to be a key player in what is now being termed the ‘angiogenic switch’. Macrophages when stimulated with LBP-LPS were reported to increase their expression of inflammatory cytokines through activation of TLRs, however it was shown that if the macrophage was co-stimulated with an adenosine A2a receptor (A2aR) agonist the signalling cascade appeared to shift from inflammatory to anti-inflammatory, with an accompanying

increase in VEGF expression [136, 137]. This suggests that LBP could function in two different roles depending on the cell environment upon activation.

Macrophages, as previously mentioned, are increasingly associated with angiogenesis through the factors they secrete. LBP is secreted by macrophages but the possibility that LBP may have angiogenic activity has not been investigated. However, the identification of the angiogenic switch provides a rationale for LBP acting as a pro-angiogenic factor in certain conditions. Exactly how a macrophage is activated to produce certain cell surface antigens or secrete certain proteins is not yet fully understood, but it is thought that for a macrophage to become pro-angiogenic it requires more then just exposure to an infectious agent such as LPS [49]. This supports a model of angiogenesis being a multifactorial process that requires specific signal initiators alongside unique environmental cues.

6.4 LBP in the Retina and Signalling

Work from our laboratory that led up to this project identified LBP as a significantly up regulated gene in three mouse mutants of retinal vascular disease. The microarray analysis was performed on isolated retinal vessels, indicating that LBP is expressed by cells of the retinal vasculature, most likely a mixture of endothelial cells, pericytes and possibly Müller cells. As the mice used in this analysis were notionally free of LPS this suggests that LBP may have some other unknown function beyond its well characterised immunological role.

As discussed previously (see section 3.1) the protein with the highest homology to LBP is BPI [114]. BPI was once considered to function solely in an immune role to clear LPS, however in 2006 it was found to induce pericyte and RPE growth whilst suppressing VEGF-induced endothelial growth factor [138] and then in 2007 a paper by Geraldes *et al,* reported that BPI was able to signal through the Glypican 4 (GPC4) receptor to activate two serine and threonine kinases, namely extracellular signal regulated kinase (ERK1/2, also known as mitogen activated serine/threonine protein kinase, MAPK) and Akt (also known as protein kinase B, PKB) in RPE and pericytes [139].

It is intriguing that BPI, a structurally similar protein to LBP has been found to induce these kinases as both of these kinase families are implicated in angiogenesis [140].

There are three isoforms of Akt in humans, differing in their physiological functions and tissue expression profiles – Akt1 is a regulator of cell survival and is abundantly expressed in the heart, brain and liver. Akt2 is required for glucose metabolism and has been found to increase glucose uptake through incorporation of GLUT4 receptor into the plasma membrane, it is expressed in skeletal muscle. The function of Akt3 is less clear but it is expressed highly in the brain, and mice lacking Akt3 have been reported to have a decreased brain size [141]. Under normal cell conditions, Akt is found in the cytoplasm in a non-phosphorylated state. However, stimulation of certain cell surface receptors may induce activation of phosphoinositide 3-kinase (PI3K), which in turn generates phosphatidylinositol (3,4)-bisphosphate (PIP_2) in the cell membrane. This creates a binding site for Akt, thus anchoring it at the plasma membrane where it may be phosphorylated by two kinases, 3-phosphoinositide-dependent protein kinase 1+2 (PDK1+2) on threonine 308 and serine 473 [141]. This phosphorylation activates Akt enabling it to phosphorylate its downstream targets (e.g. Bad), leading to gene transcription promoting cell survival, proliferation and migration [141, 142]. Interestingly, mice lacking Akt1 have been found to have an inhibition in physiological angiogenesis but an enhancement in pathological vessel growth [142].

ERK1/2 are well characterised kinases known to be important regulators of a range of cellular processes including proliferation, survival and differentiation, with their dysregulation being reported in a wide variety of cancers [143]. There are believed to be over 160 ERK1/2 substrates all sharing the same modulation motif, X-Pro-Xaan-Ser/Thr-Pro-X. The best characterised signalling cascade featuring ERK is the Raf/MAPK pathway. Ligand interaction with a cell surface receptor induces Raf (MAP3K) activation, which then phosphorylates and activates MEK1/2 (MAP2K), which then phosphorylates and activates ERK1/2 (MAPK). Active ERK1/2 can then phosphorylate its downstream targets, which include a variety of transcription factors such as CREB, c-Fos, c-Jun and STAT, which in turn leads to modification of cellular behaviour [143, 144].

7. Hypothesis and Aims

These observations form the background to the work undertaken in this thesis. The aim of this project was to test the hypothesis that LBP has an as yet uncharacterized role in angiogenesis.

• Characterisation of LBP and growth factor expression in the VLDLR-/- mouse through the use of quantitative PCR analysis, retina flat mounting and tissue staining.

• Investigation of the angiogenic potential of LBP, both alone and in conjunction with other established growth factors such as VEGF through the use of *in vitro* and *ex vivo* growth assays and the oxygen induced retinopathy (OIR) mouse protocol.

• Investigation of LBP's ability to induce cell signalling independently of LPS in a range of available cell culture lines using molecular chemistry techniques such as Western blotting, immunocytochemistry, co-immunoprecipitation and genetic siRNA knock down.

Materials and Methods

Materials and Methods

1. Cell Culture

1.1 Cell Lines

Human Umbilical Vein Endothelial Cells (HUVEC), isolated from normal human umbilical veins were ordered from Lonza as a cryopreserved stock of ~7 x 10^5 cells in passage one. HUVEC were seeded onto 1% bovine skin gelatin (Sigma G9382) coated plastic tissue culture flasks and maintained in EGM2 (Lonza Clonetics CC-3162 containing growth supplements Hydrocortisone, hFGF-B, VEGF, R3-IGF-1, Ascorbic Acid, Heparin, FBS, hEGF, GA-1000) medium. Cultures were grown to confluency at 37^{o}C in 5% CO_2 with media replaced every 2-3 days.

The GPNT 24.6 cell line (Regina et al 1999) is a re-immortalised subclone of the Lewis rat brain endothelial cell line GP8 (Greenwood et al 1996). The cells were originally derived from primary cultures and immortalised by expression of the SV40 large T antigen. GPNT cells were seeded onto a 0.005% calf skin collagen I (Sigma C8919 containing 0.1M acetic acid) coated plastic tissue culture flask and maintained in a 1:1 mix of Ham's F-10 medium (containing L-glutamine) and a minimal essential medium alpha (MEMa) with Glutamax, supplemented with 10% FCS, 100U/ml penicillin and 100µg/ml streptomycin. Cultures were grown to confluency at 37^{o}C in 5% CO_2 with media replaced every 2-3 days.

The rat brain endothelial (RBE4) cell line is a well-characterised in vitro model for the blood brain barrier (BBB). RBE4 cells were seeded onto a 0.005% calf skin collagen I (Sigma C8919 containing 0.1M acetic acid) coated plastic tissue culture flask and maintained in a 1:1 mix of Ham's F-10 medium (containing L-glutamine) and minimal essential medium alpha (MEMa) with Glutamax, supplemented with 10% FCS, 100U/ml penicillin and 100µg/ml streptomycin. Cultures were grown to confluency at 37^{o}C in 5% CO_2 with media replaced every 2-3 days.

The MIO-M1 cell line was isolated from spontaneous immortalised Müller cells derived from eyes obtained from Moorfields Hospital Eye Bank [138]. MIO-M1 were seeded directly onto tissue culture plastics and maintained in DMEM (containing L-glutamine and 4.5g/l glucose, Lonza) supplemented with 10% FCS, 100U/ml penicillin and 100µg/ml streptomycin. Cultures were grown to confluency at 37^{o}C in 5% CO_2 with media replaced every 2-3 days.

1.2 Thawing Cells

Cryoamps of cell lines were defrosted rapidly in a 37^{o}C waterbath, appropriate cell line specific media were then added and the cells pipetted into a universal tube. The cells were then placed into a centrifuge and spun at 1100 rpm for 3 min. After pelleting, the supernatant was removed and the cells resuspended in their specific media before being transferred to a tissue culture flask containing ample cell media. Media were replaced after 24 h.

1.3 Collagen Coating

For GPNT and RBE4 cells the tissue culture flasks and dishes were coated with a 1:20 dilution of type I collagen (Sigma C8919 0.1% calf skin collagen containing 0.1M acetic acid) in HBSS (-Mg^{2+} and Ca^{2+}) overnight at 37^{o}C in 5% CO_2. The following day the collagen I was aspirated and the flask / dish washed twice in HBSS (-Mg^{2+} and Ca^{2+}) before cells were plated.

1.4 Splitting / Plating Cells

Cells were split routinely once confluent or when experiments required plating. The flask of cells was washed once in PBS (-Mg^{2+} and Ca^{2+}) before adding an appropriate volume (example 3ml for a T75 flask) of 1x trypsin and incubated at 37^{o}C until the a single cell suspension had formed. Media containing serum was then added to the flask to halt further proteolysis and the suspension transferred to a universal tube and spun at 1100 rpm for 3 min to pellet the cells. The supernatant was then aspirated and the cell pellet resuspended in the desired volume of medium. The cells were then plated at the desired density for experiments or re-seeded for continuing cell culture flasks. GPNT and RBE4 were seeded at a maximum dilution of 1:10 whilst MIO-MI and HUVEC were seeded at a maximum dilution of 1:6.

1.5 Cryopreserving Cells

A confluent flask of cells was trypsinised as described. The cell pellet was then resuspended in 1ml specific cell line media supplemented with 10% dimethyl sulfoxide (DMSO) and frozen in cryotubes. The cryotubes were cooled on ice for 10 min, frozen at -70^{o}C overnight and then placed into liquid nitrogen for long term storage.

2. Imaging

2.1 p65 Staining

MIO-MI cells were grown to confluency in 35mm^2 MatTek culture dishes before being treated with 10ng/ml recombinant human lipopolysaccharide binding protein, (LBP) (R&D Systems 870-LP lypophilized from 0.2µm filtered solution containing 20mM Tris, 100mM NaCl, 0.05mM EDTA, pH 8.0 containing 50µg bovine serum albumin per 1µg of cytokine) for 15 min +/- 50µg Lipopolysaccharide (LPS) (Sigma L8274 from *E.Coli* sterotype). The cells were then extensively washed with ice cold PBS and fixed by addition of 3.7% formaldehyde for 15 min followed by gentle washing with PBS. Cells were then permeabilised by addition of ice cold acetone to residual PBS for 30 s followed by rapid dilution in 0.1% BSA/PBS. The dishes were then blocked in 0.5% BSA/PBS for 15 min before a 90 min incubation in rabbit anti-p65 (Santa Cruz C-20, 0.2µg/ml) and DAPI bisbenzimide (1µg/ml). Cells were then washed extensively in PBS and incubated with fluorophore-conjugated anti-isotype specific pre-adsorbed secondary (Ig-FITC) antibody diluted in blocking solution for 45 min in the dark. Dishes were then washed extensively with PBS and mounted under Vectashield with glass coverslips.

2.1.1 Cell Imaging

To generate images, samples were observed for fluorescence using an inverted epifluorescent Leica microscope. DAPI images were taken using a 364nm wavelength light and FITC images with a RFP2 filter (594nm). Samples were viewed at 20x magnification and the exposure and gain settings were fixed across all treatment conditions to facilitate subsequent comparative analysis. Images were then saved as 2-channel 24-bit tiff files or as individual 8-bit grey tiff files.

2.2 Flat Mounts

2.2.1 Tissue Preparation

Whole mouse eyes were placed into 2x PBS / 2% PFA for 2 min. An incision around the eye was then made, below the aura striata and the cornea and lens disregarded. The neuroretina was then peeled away from the RPE/choroid and placed into fresh 2x PBS. Dissection scissors were then used to make cuts in four corners of the tissue and PBS aspirated to enable the neuroretina to lie flat. Ice-cold methanol (100%) was then added dropwise onto the tissue, turning it white and causing it to float. The sample was then placed at -20^{o}C for 20 min. The sample was then returned to room temperature and the methanol diluted out with PBS. The tissue was then transferred to a 96-well plate in fresh PBS, incubated at room temperature for a further 30 min and then placed into a blocking buffer containing 3% Triton X-100, 0.5% Tween-20, 1% BSA for another 30 min. The tissue was then incubated at room temperature overnight in 0.5mg/ml rat anti-mouse collagen IV antibody (BD Pharmingen) diluted 1:200 in blocking buffer. The following morning the primary antibody solution was removed and the tissue washed in fresh blocking buffer 3 x 10 min on a plate shaker. The sample was then incubated in AlexaFlour 594 (Invitrogen rabbit anti-rat IgG 2mg/ml) secondary antibody and isolectinB4 (Vector simplicifolia lectin 1 FL-1201) conjugated antibody, diluted 1/200 in blocking buffer for 1 h at room temperature. The wash step was repeated followed by the sample being mounted onto a microscope slide via Mowiol immersion.

2.2.2 Tissue Imaging

To generate images samples were observed for fluorescence using an inverted epifluorescent Leica microscope. Collagen IV-FITC was visualised with a RFP2 filter (594nm) at a 40x magnification focus adjustment used to observe the deeper plexus layer of the retinal vessels, with the exposure and gain settings being fixed across all tissue samples to permit comparative analysis. Images were then saved as monochannel 24-bit tiff files.

2.3 Tissue Sections

The eyes from 16-week-old wild type and VLDLR$^{-/-}$ mice were dissected, the lens removed and the ‘eye cup’ fixed in PFA and embedded in OCT. The eyes were then section sliced and mounted onto glass coverslips to be stored at -80^{o}C until required

for staining. When required the slide was removed from cold storage, residual OCT washed off with PBS before 3% H_2O_2 (in methanol) was added dropwise and left for 30_m. The slides were then washed briefly in PBS before being transferred to a humidified chamber and blocked in 100% goat serum at RT for 1 h. The LBP antibody (Santa Cruz rabbit polyclonal) was then diluted 1:200 in 100% goat serum and incubated on the slides in the chamber at RT for 2 h. The slides were then washed 6 times in PBS. Secondary anti-rabbit goat antibody (Vector Labs, ABC Kit) was then applied at RT for 1 h. Slides were washed 4 times in PBS and placed into final solution at RT for 30 m. They were then washed 3 times in PBS before Diaminobenzidine (DAB) (Sigma) added, with the slide being left at RT to develop (approx 20 m) before being washed thoroughly in H_2O and mounted in glycerol for imaging using a light microscope.

3. Molecular Biology

3.1 RNA Isolation

3.1.1 RNA Isolation from Cell Lines

The RNeasy Mini Kit 250 (Qiagen) was used for the isolation of RNA from confluent cells. The cells were washed once with D-PBS before being solubilised in lysis buffer RLT with β-mercaptoethanol (10µl/1ml of RLT) and then scraped. The homogenized lysate was directly added to the QIA shredder (Qiagen) and subjected to centrifugation for 2 min at room temperature at 50,000 x *g*. One volume of ethanol was added, mixed well and the sample was added to an RNeasy spin column. Centrifugation was carried out for 15 s and flowthrough was discarded. RNase-free Dnase set (Qiagen) was used to digest DNA as follows. RWI buffer (350µl) was added to the RNeasy spin column and spun for 15 s. DNase I stock solution (10µl) was added to 70µl buffer RDD, then added to the RNeasy spin column and left at room temperature for 15 min. A further 350µl of buffer RWI was added and the flowthrough discarded. Once the sample was DNase treated 500µl of buffer RPE was added and centrifuged for 15 s, followed by a further addition of 500µl buffer RPE. Centrifugation for 2 min at 50,000 x *g* followed with a further 1 min to ensure complete elimination of buffer RPE and the contaminating ethanol therein. RNA elution then occurred with the addition of 30-50µl of RNase free water and the concentration of RNA was measured using a Thermo Scientific Nano-drop machine.

3.1.2 RNA Isolation from Animal Tissue

3.1.2.1 RNA isolation from Neuroretina

The neuroretina was dissected from the mouse eye (see dissection description in 2.2.1 tissue preparation) and placed into 1ml Tri Reagent (Sigma T9424) and homogenised using a 23 & 26G needle. 200ul 1M Chloroform was added and the samples spun 12 x 10^3 rpm in a centrifuge at 4^{o}C for 10 min. The top aqueous layer was then carefully removed into a clean RNAse free Eppendorf tube and 500µl 1M isopropanol added to precipitate the genomic material. Sample tubes were then inverted for 15 s and samples left at RT for 15 min before being placed back into the centrifuge to repeat the spin as before. The isopropanol pellet is glassy so can be hard to observe, to overcome this problem glycogen can be added to visualise the pellet. The isopropanol supernatant was then decanted off and the tube blotted on RNAse zapped tissue. The pellet was then washed in 70% ethanol and again decanted and blotted as before. The pellet was then left to air dry for 30 seconds before being resuspended in 100µl RNAse free water and heat-treated at 50-60^{o}C to linearise the genomic strands. The sample is then passed through the QIAGEN RNAeasy clean up protocol as described.

3.1.2.2 RNA Isolation from Retinal Pigment Epithelium (RPE) and Choroid

Once the neuroretina had been dissected out of the eye sample, the remaining 'eye cup' was placed into 1ml Tri Reagent (Sigma T9424) and placed on an Eppendorf roller at 4^{o}C for 2 h. The tissue was then vortexed in the Tri Reagent to dissociate the RPE and the RNA isolation protocol carried out as for neuroretina.

3.1.2.3 RNA Isolation from Isolated Retinal Vessels

The neuroretina was dissected (see dissection description in 2.2.1 tissue preparation) and the tissue placed into 1ml collagenase/dispase digestion mix supplemented with 10µl RNAse free DNAseI (Ambion 20U/µl) in an RNAse free Eppendorf tube. Samples were then incubted at 37^{o}C for 1 h with pipetting up and down every 15 min. Samples centrifuged at 1400rpm for 5 min and the supernatant discarded. The pellet was resuspended in 1ml RNAse free PBS + 0.5% BSA + rat anti-mouse PECAM (BD Pharmingen) and placed on a rotator for 10 min. The sample was then spun again as before. Using a magnetic Eppendorf rack the anti-rat magnetic beads (Dynal BioTech Dynabeads anti-rat IgG, 4 x 10^8 beads/ml) were then washed 3 times in PBS and this bead mix was used to resuspend the tissue pellet. Sample and bead mix were then

placed back onto the rotator for 20 min, then back into the magnetic rack, whereupon the supernatant was removed and centrifuged at 1800rpm for 8 min, with pellet being resuspended in 1ml Tri reagent to use as a vessel-depleted sample. The magnetic beads were bound to the retinal vessels so these were placed in 1ml Tri reagent to generate a vessel-enriched sample. RNA was then isolated as described earlier for neuroretina and RPE.

3.2 Protein Isolation

3.2.1 Protein Isolation from Cell Culture

Cells were plated on 35mm^2 dishes to confluency and treated with desired treatments for desired time points. Cells were then washed in PBS before being lysed in 150µl of lysis buffer (125mM Tris pH 6.8, 4% SDS, 17.5% Glycerol, 5mg/ml bromophenol blue, 50mM DTT) and a cell scrapper used to dissociate cells. Samples were then pipetted into Eppendorf tubes and heat treated at 95^{o}C for 5 min.

3.2.2 Protein Isolation from Animal Tissue

3.2.2.1 Protein Isolation from Neuroretina

Neuroretinas were dissected as normal and placed in 250µl of lysis buffer before being placed on a rotator at 4^{o}C for 30 min with pipetting up and down at 15 min to break up the tissue. The sample was then pulled through a 23 and 26 gauge needle and placed back onto the rotator for 10 min. After being spun at max speed (>13000rpm) 4^{o}C for 10 min the supernatant was removed and stored at -20^{o}C whilst the pellet was resuspended in 250µl of fresh lysis buffer and also stored at -20^{o}C.

3.2.2.2 Protein Isolation from RPE and Choroid

RPE and choroid were isolated from mouse eyes as describe earlier, and the entire ‘eye cup’ was placed in 200µl lysis buffer. The sample was vortexed briefly before being placed on ice for 10 min, and then vortexed again and observed to see if the lysate had become a mirky brown (due to release of pigment). If the colour did not change the sample was placed back on ice and inspected again at 10 min intervals. The tissue was then spun at max speed (>13000rpm) 4^{o}C for 10 min and the supernatant removed and stored at -20^{o}C.

3.3 Gel Electrophoresis

3.3.1 Agarose RNA and DNA Gels

For RNA and DNA analysis, 1-2% agarose (supplemented with 1µg/µl EtBr to visualise sample) gels were used. For a 200ml gel approximately 25ng DNA was loaded, supplemented with bromophenol blue loading dye, the gel was run at 70 V for 1 h before being viewed under UV light. Bands were measured against a 1kb DNA ladder (Invitrogen).

3.3.2 Protein Analysis

3.3.2.1 Sodium dodecyl sulphate polyacrylamide gel electrophoresis (SDS-PAGE)

A stock of sample buffer containing 250mM Tris pH 6.8, 8% SDS, 35% Glycerol and bromophenol blue at a concentration of 10mg per ml was diluted 1:1 with PBS and 100mM DTT to make the lysis buffer used for the protein preparations. A stacking gel was used to pack the proteins after loading, and a separating gel was used to resolve the proteins in the sample according to their relative molecular weight (see Table 1).

Table 1: Gel mixes used for SDS-PAGE

Seperating gel (x2)			
	7.5%	10%	12.5%
Acrylamide (ml)	2.5	3.34	4
1.5M Tris pH 8.8 (ml)	2.5	2.5	2.5
Pure Water (ml)	4.85	4	3.35
10% SDS (µl)	100	100	100
10% APS (µl)	80	80	80
TEMED (µl)	4	4	4

Stacking gel (x2)	
Acrylamide (ml)	0.75
1M Tris pH 6.8 (ml)	0.63
Pure Water (ml)	3.4
10% SDS (µl)	50
10% APS(µl)	75
TEMED (µl)	10

The standard protocol for the Protean II mini-gel system (Bio-Rad) was used to set up, load and run the gels. 15µl-30µl of boiled cell lysate was added to each well, and 5µl

of Precision Plus Protein Standard ladder (Bio-Rad) was loaded into the wells next to the lysates. The gel tank chamber was filled with running buffer (250mM Tris, 192mM Glycine and 0.1% SDS) and the gel was run at a constant current of 30mA until the samples had passed through the stacking gel, then the current was increased to 60mA until the samples had passed through the separating gel, as judged by migration of the dye front.

3.3.2.2 Western Blotting

Following SDS-PAGE the gel was removed from the gel sets and equilibrated in transfer buffer (25mM Tris, 192mM glycine and 20% methanol) for 10-20 min. Five sheets of filter paper and one sheet of nitrocellulose membrane (Whatman Protran) were then soaked in transfer buffer and placed onto the Bio-Rad semi-dry transfer cell. The protein gel was then placed on top followed by a further five sheets of soaked filter paper. Air bubbles were removed from the sample stack using the roller pin exclusion technique in order to ensure successful protein transfer. Protein transfer as performed at 12 V for between 30 to 85 min depending on the molecular weight of the protein of interest. Once the transfer was complete the membrane was stained with ponceau red to ensure successful protein transfer.

3.3.2.3 Immunodetection

Prior to immunological detection, the nitrocellulose membrane was incubated in blocking solution containing 1% BSA (w/v), 1x TBS, 0.2% Triton X-100 and 0.1% Tween-20 at room temperature for 2 h in order to inhibit any non-specific antibody binding. The membrane was then incubated with the selected primary antibody overnight at 4^{o}C on a plate shaker. The following morning the membrane was washed twice in antibody-free blocking solution and then twice in PBS before being incubated with the appropriate secondary antibody for 1.5 h, diluted to 1:2000 in the secondary antibody solution containing 1% BSA (w/v), 1x PBS, 0.2% Triton X-100 and 0.1% Tween-20. The nitrocellulose membrane was then washed once in clean antibody wash and twice in TBS, 0.2% TritonX-100, 0.1% Tween-20 followed by one final wash in TBS.

Enhanced chemiluminescence (ECL) was used to detect the presence of the HRP-conjugated secondary antibody complexes. The membrane was placed in ECL mix

(lumi-light western blot substrate- Roche) for 5 min to ensure complete coverage. Excess solution was removed and the membrane placed in Saran wrap prior to exposure.

3.4 First strand cDNA synthesis

Total RNA was transcribed into cDNA using the QuantiTect (Qiagen) reverse transcription kit. Genomic DNA wipeout (2µl of 7x) was added to 1µg isolated RNA and the volume made up to 14µl with RNAse free water and the sample incubated at 42^{o}C for 15 min. Reverse transcriptase (1µl), Quantiscript RT buffer (4µl of 5x), and 1µl primer mix were then added, the sample was mixed and incubated at 42^{o}C for 15 min and then 95^{o}C for 3 min.

3.5 Polymerase chain reaction (PCR)

3.5.1 RT-PCR

For reverse transcriptase PCR we used the Phusion high fidelity DNA polymerase (Finnzymes) at the concentration and programme recommended by Finnzymes (see Tables 2 and 2a). 2µl of the first strand cDNA synthesis material was sufficient for a reaction, the products of which were examined on 1% agarose gels to normalise to ß-actin expression levels.

Table 2: Finnzymes Phusion Taq RT-PCR Recipe

Component	**50ul reaction**	**20ul reaction**	**Final Conc**
Water	16.5µl	5.4µl	
5x Phusion Buffer*	10µl	4µl	1x
10mM dNTPs	1µl	0.4µl	200µM each
Forward Primer	10µl	4µl	0.5µM
Reverser Primer	10µl	4µl	0.5µM
Template DNA	2µl	2µl	
Phusion Taq	0.5µl	0.2µl	0.02U/µl

* HF Buffer is default but can use GC Phusion Buffer if amplified sequence is GC rich

Table 2a: RT-PCR Programme

Suggested by Finnzymes for Phusion polymerase

2 – step protocol			3 – step protocol		
Cycle Step	**Temp**	**Time**	**Temp**	**Time**	**Cycles**
Denaturation	98°C	30 s	98°C	30 s	1
Denaturation Annealing Extension	98°C - 72°C	5-10 s - 15-30 s	98°C X°C 72°C	5-10 s 10-30 s 15-30 s	25-35
Extension	72°C 4°C	5-10 min HOLD	72°C 4°C	5-10 min HOLD	1
Our programme: 98°C 2 min / 98°C 30 s, 63°C 30 s, 72°C 30 s / 72°C 10 min					

3.5.2 qPCR

Quantitative PCR (qPCR) was performed using the Power Syber Green master mix (Applied Biosystems) containing the SYBR Green 1 Dye, AmpliTaq Gold® DNA Polymerase, dNTPs with dUTP and optimised buffer components at the suggested concentrations under the suggested qPCR programme (see Tables 3 and 3a). All reactions were set up in triplicate and read from a 96 well plate (see schematic 1).

Table 3: Applied Biosystems Syber Green Reaction Volumes			
	1x Reaction	**3x Reactions**	
Component	**Volume (µl)**	**Volume (µl)**	**Final Conc**
Water	Make up to 25	Make up to 85	
Syber Green	12.5	37.5	1x
Forward Primer*	X	X	
Reverse primer*	X	X	
DNA	0.5	1.5	
* Forward and reverse primer concentration determined by primer optimisation			

Table 3a: Applied Biosystems Syber Green Programme			
Cycle Step	**Temp**	**Time**	**Cycles**
Step1	95°C	10 min	1
Step 2	95°C 60°C	15 s 1 min	40
Step 3	95°C	15 s	1

	60°C 95°C	15 s 15 s	

Schematic 1: 96 well plate organisation for qPCR analysis

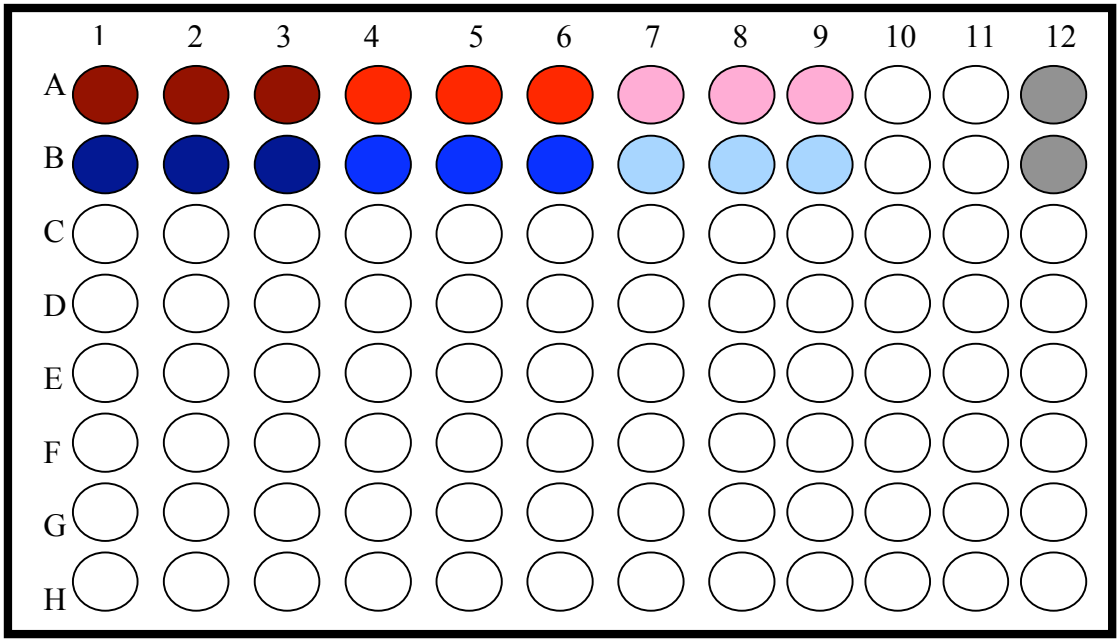

Key: A1-3 Sample 1, A4-6 Sample 2, A7-9 Sample 3 and A12 No template control.
B is a duplicate of A but with different primers to test a different gene

3.5.2.1 qPCR Analysis

Once the qPCR reaction was completed the Ct values (recording representing when the flourescence from double stranded DNA dye incorporation could be detected) were entered into a DART analysis programme, in order to calculate the relative fold changes in gene expression of target genes normalised to those of 'house keeping' genes such as ß-actin. The values were then transferred into an Excel spreadsheet for downstream analysis and graphical representation.

3.5.3 Primers

3.5.3.1 Primer Optimisation for qPCR

For optimum qPCR efficiency the primers used were subjected to reaction optimisation through the four set reactions recommended by Applied Biosystems (see

Table 4). The lowest Ct value indicates the most efficient reaction, therefore the primer sets chosen by their lowest Ct value.

Table 4: Primer optimisation reactions			
Reaction 1	**Reaction 2**	**Reaction 3**	**Reaction 4**
9µl Water	6µl Water	6µl Water	3µl Water
12.5µl Syber Green	12.5µl Syber Green	12.5µl Syber Green	12.5µl Syber Green
1.5µl PF	1.5µl PF	4.5µl PF	4.5µl PF
1.5µl PR	4.5µl PR	1.5µl PR	4.5µl PR
0.5µl DNA	0.5µl DNA	0.5µl DNA	0.5µl DNA

3.5.3.2 Primer Sequences

The mouse ß-actin primers were designed by Jennifer McKenzie, the human ß-actin by Amanda Carr and the human Toll-like receptors, Glypicans, Syndecans were taken from [139]. I designed the remaining primer sets, and checked them online using Primer3 for hairpins etc., and blasted them with the NCBI Blast software to ensure no significant similarity to alternate targets. Primers were ordered from MWG Operon and stored at -20^{o}C as a 100 pmol/µl stock.

Table 5: Primer Sequences		
Name	**Forward 5' → 3'**	**Reverse 5' → 3**
Mouse ß-actin	TCCAAGTATCCATGAAATAAGTG	GCAGTACATAATTTACACAGAAGC
Human ß-actin	TCCCTGGAGAAGAGCTACGA	AGGAGGGAAGGCTGGAGGAG
Mouse LBP	CCTTCTCAACAGCCTCTACC	GCACCCAAGTATAAGAAGTCC
Human LBP	GTCTCAGCATCTCCGACTCC	AAGTCTCCCGACATGTCCAC
Mouse ikBα	CAACCTGCAGCAGACTCCACTC	ACACGTGTGGCCATTGTAG
Human ikBα	CCAGGGCTATTCTCCCTACC	GCTCGTCCTCTGTGAACTCC
Mouse VEGFa	GACTTGTGTTGGGAGGAGGA	TCTGGAAGTGAGCCAATGTG
Human VEGFa	CTACCTCCACCATGCCAAGT	CACACAGGATGGCTTGAAGA
Mouse A2aR	TCAACAGCAACCTGCAGAAC	GGCTGAAGATGGAACTCTGC
Human A2aR	SAME AS MOUSE	GCCAGGAGACTGAAGATGGA
Mouse TGFß1	TTGCTTCAGCTCCACAGAGA	TGGTTGTAGAGGGCAAGGAC
Human TGFß1	GGGACTATCCACCTGCAAGA	CCTCCTTGGCGTAGTAGTCG
Human TLR1	GGTCTTGCTGGTCTTAGGAGAGA	CTGAAGTCCAGCTGACCCTG TAGCTTCACG

Human TLR2	GGCCAGCAAATTACCTGTGTG	CTGAGCCTCGTCCATGGGCCACTC
Human TLR3	CGGGCCAGCTTTCAGGAACCTG	GGCATGAATTATATATGCTGC
Human TLR4	TGCAATGGATCAAGGACCAGAGC	GTGCTGGGACACCACAACAATCACC
Human TLR5	CCTCATGACCATCCTCACAGTCAC	GGCTTCAAGGCACCAGCCATCTC
Human TLR6	CCAAGTGAACATATCAGTTAA ACTTTAGGGTGC	CTCAGAAAACACGGTGTACAAAG CTG
Human TLR7	CTCCCTGGATCTGTACACCTGTGA	CTCCCACAGAGCCTTTTCCGGAGCT
Human TLR8	GTCCTGGGGATCAAAGAGGGAAC	CTCTTACAGATCCGCTGCCGTAGCC
Human TLR9	GCGAGATGAGGATGCCCTGCCCT	TTCGGCCGTGGGTCCCTGGCAGAAG
Human TLR10	CAGAGGTCATGATGGTTGGATG	GACCTAGCATCCTGAGATACCAG GGCAG
Human GPC1	CGATGACCACTTCCAGCACC	CCGAGAGAGCTGCGCCTGCGG
Human GPC2	ACTGGGACACGACCTGGAC	GGGCTGAGAGGGAGAGAATG
Human GPC3	CCAAGAGGCCTTTGAAATTGT	TGACAGCCTGTTTCCAGTCA
Human GPC4	AGTGTGGTCAGCGAACAGTG	GGCGAGCCCAGAAGTCATTTA
Human GPC5	CACTTTTCTGCAGGCACTCA	GGCTTTGTGTGGGTGTTCTT
Human GPC6	CCAGGACCTCTTCACAGAGCTG	TGGGCAGTACAGCATCTTCA
Human SDC1	GCTCTGGCTCTGGCTGTGC	CTGTGTGGGGAGTGTGAAGG
Human SDC2	AAGACATGTACCTTGACAACAG	AACTCCACCAGCAATGACAG
Human SDC3	CAACCAGACACAGCCAATGAG	GACCAAGAAGGCAGCAAAGA
Human SDC4	ACGATGAGGATGTAGTGGGG	GGGTTTCTTGCCCAGGTC

3.6 Genetic knock down

3.6.1 siRNA preparation

Human syndecan-2 siRNA was purchased from Ambion (*silencer* siRNAs 12433, 12528 and 12618) and Santa Cruz (sc-41045) and made up to a 20μM stock in RNAse free water. Control siRNA-A (Santa Cruz) was used as the scrambled control and was made up to same stock concentration in RNAse free water.

3.6.2 Cell transfection optimisation

Day 1, Hela cells were split and plated into antibiotic free cell media (DMEM 10% FCS) in 12-well tissue culture plates at approx 40% confluence in the morning. After 6 h they were transfected with 100pmol of selected siRNA (Ambion supplied 3 separate

siRNAs, which were tested alone, in pairs and as the complete pool. Santa Cruz supplied 3 siRNAs already in a pool) using Oligofectamine (Invitrogen) transfection reagent. The cells were left at 37^{o}C, 5% CO_2 overnight. The following day (day 2) cells were split 1:2 and replated, and after 6 h the transfection was repeated as before. The following morning (day 3) the culture media were changed and cells left for the day at 37^{o}C in 5% CO_2. On day 4 the cells were placed into starvation serum with no FCS. After 48 h (day 6) the cells were treated with LBP, LBP+LPS or LPS at various concentrations for 30 min before being lysed in SDS-PAGE sample buffer and boiled at 95^{o}C for 5 min.

3.7 Analysis of signalling

Cell lysates were resolved by 10% SDS-PAGE and immunoblotted for phosphoERK and total ERK (Cell Signalling 1:2000) according to the western blotting protocol reported earlier. Scrambled control siRNA responses were compared to syndecan-2 knock-down to identify whether LBP responses had any dependence on syndecan-2 expression.

4. Angiogenesis Assays

4.1 Matrigel Tube Assay

To assess the angiogenic capability of LBP we decided to use the Matrigel assay. Fully confluent HUVEC were trypsinised and the cells pelleted and resuspended in 1ml EGM2 media before being counted using a 0.0025mm^2 Neubauer Haemacytometer. BD Matrigel (growth factor reduced, BD Biosciences) was thawed slowly on ice and 50 µl added to individual wells of a 96 well plate. The plate was then kept at room temperature for 15 min to allow the Matrigel to set. 10^5-10^6 HUVEC were then seeded on top of the Matrigel and EGM2 culture media was added to make the volume up to 100 µl. Gels were then divided into control PBS, and 10 ng LBP ± 50 µg LPS, with cells returned to culture overnight to be imaged after 12-16 h.

4.1.1 Matrigel Imaging and Analysis

To generate images the gels were photographed using a Leica epifluorescent microscope. 24-bit monochannel images were taken at 2x magnification under brightfield conditions. The image was then analysed by counting the number of

sprouts, branches and closed loops formed. An average of the gels for each treatment was then plotted and normalised to control conditions for statistical analysis.

4.2 Aortic Ring Assay

Thoracic aortas were dissected from wild type rats aged 2 weeks and placed into Optimem media (Gibco). The extraneous fat surrounding the vessel was carefully removed and any blood flushed out with a 25G needle and syringe. The tissue was then transversely sliced into aortic rings approximately 0.5 mm width. The rings were then mounted into wells of a 96 well plate in a Collagen I:E4 media mix at concentrations of 1.2 mg/ml (collagen I from rat tail, Sigma) and incubated at 37^{o}C, 5% CO_2 for 1 h. After this time the gel had fully polymerised and the ring was securely embedded. 150 µl of aortic ring media (E4 + 10% FCS) was gently added and the plate was placed back into the incubator. Two days later the ring was removed from the incubator and allowed to equilibrate to room temperature for 10 min. 120 µl of media were then removed and replaced with fresh ring media ± treatments as shown in figure legends. Ring samples were left for a further week with fresh medium (± treatments) applied every 2 days to stimulate sprouting.

4.2.1 Aortic Ring Staining

To assess vessel sprouting the samples were stained with isolectin-B4 (Vector). First the rings were fixed in 4% PFA/PBS for 20 min at room temperature before being permeabilised with 0.5% Triton X-100/PBS for 30 min and then immersed in a blocking solution (1% BSA, 0.5% Triton X-100/PBS) for a further 30 min. The samples were then incubated in fresh blocking solution supplemented with a 1:200 dilution of isolectin-B4 FITC on a plate shaker overnight at 4^{o}C. The following morning the samples were washed extensively in PBS and imaged immediately.

4.2.2 Aortic Ring Imaging and Analysis

To generate images the rings were photographed using an inverted Leica epifluorescent microscope. Isolectin-B4 FITC images were taken using a GFPA filter (488nm) with 5x magnification, which was usually sufficient for observing the entire ring and sprouts in one image. The image was then exported to ImageJ and inverted.

The ring and sprouts were sketched and a mean intensity value recorded. The ring was then isolated and its own intensity value recorded. The ring value was then subtracted from the ring + sprout value. This value was termed the sprout intensity. Treatments could then be compared for their sprout growth, and fold changes calculated by normalising to the control samples.

4.3 Metatarsal Assay

Metatarsal bones were dissected from wild type E16-18 age pups and placed onto 0.1% gelatin-coated 24 well plates. 180 µl of 10% DMEM media was gently pipetted into each well and the plates carefully transferred to an incubator at 37^{o}C, 5% CO_2 for 2 days. On the third day samples were assessed to ensure they had settled on the bottom of the dish, those that had not were not used. 120 µl of media was removed and 180 µl fresh media (with appropriate treatments) was added. The samples were left for 9 days with replenishment of media and agonists every 3 days.

4.3.1 Metatarsal staining

On the last day of the assay the media was carefully removed and the sample was gently washed twice in PBS. The tissue was then fixed in 4% PFA for 15 min at room temperature. The samples were then washed three times in PBS, after which the samples were placed into blocking buffer (10% BSA, 0.1% Triton in TBS) for 1 h. The blocking buffer was then removed and the samples put into fresh blocking buffer with PECAM-1 (1:200) antibody overnight at 4^{o}C. The next day the samples were washed three times in antibody-free blocking buffer and once in TBS. Anti-rabbit Alex 594 (1:200) in blocking buffer was then added to the samples for 1 h at room temperature. The samples were then washed three more times in antibody-free blocking buffer (each wash lasting 10 min) and then twice in TBS.

4.3.2 Metatarsal Imaging and Analysis

To generate images the samples were viewed using an upright stereoscope. PECAM-1 staining was observed using a RFP2 filter (594nm) and 24-bit monochannel images were taken at 2.5 x magnification to enable all of the tissue and sprouts to be seen. The images were then exported into the Imaris software where a set background level was

subtracted to minimise plastic autofluorescence, and the rendering programme was used to track the tissue sprouts. The data readouts (vessel area, volume, branch points etc) were then exported to Excel, and graphs constucted of the data to compare treated to control samples.

5. Statistics

All experiments were performed a minimum of three times and the data subjected to standard deviation, standard error of the mean and student TTest analysis where $P<0.05$ was taken as significant.

Results Chapter One

Characterisation of the *VLDLR*$^{-/-}$ Mouse Retinal Vasculature

Chapter One

Characterisation of the *VLDLR*$^{-/-}$ Mouse Retinal Vasculature

1.1 Background

The VLDLR is an 86kDa transmembrane protein belonging to the low-density lipoprotein (LDL) receptor family [147]. There is high interspecies cDNA conservation with human, mouse, rabbit and rat displaying >95% sequence similarity suggesting an important physiological role for this receptor [148]. Two isoforms of the VLDLR have been identified in humans, both of which display tissue-specific expression, with isoform one being expressed richly in the heart and skeletal muscle whilst isoform two appears more disperse in the cerebellum, adrenal glands and ovaries [147, 148]. Originally it was thought that the VLDLR simply functioned to aid triglyceride metabolism, however it has since been shown to behave as a receptor for many ligands including thrombospondin-1 and Reelin [149, 150]. Mutations in the VLDLR have recently been associated with cerebellum hypoplasia, mild cerebral gyral simplification and mental retardation [151].

The *VLDLR*$^{-/-}$ mouse exhibits angiogenic retinal vascular abnormalities with several groups reporting the pathogenic progression to mimic certain characteristics of human eye diseases such as MacTel and retinal angiomatous proliferation (RAP) [52]. Studies have shown the VLDLR protein to be expressed by the deeper plexus of the retina and the RPE with *in vitro* experiments demonstrating that *VLDLR*$^{-/-}$ retinal vascular endothelial cells (RVECs) form 3-11 times more capillaries in culture and have a 20-100% increase in proliferative rate [148-150, 152]. These studies and the knock out mouse phenotype suggest that the VLDLR is required for inhibition / regulation of angiogenesis in the retina. This is supported by one of the ligands for VLDLR, thrombospondin-1 being known to be anti-angiogenic and by genetic analysis identifying VLDLR polymorphisms as a contributing factor in the development of AMD [153-156].

1.1 Aim

The *VLDLR*$^{-/-}$ mouse displays abnormalities in its retinal vessels, so was chosen alongside the *Grhl3*^{CT}/J Curlytail mouse (CT) and Retinal-dystrophic-1 (RD1) mouse

to be one of the models used in a microarray screen to identify new genetic targets in retinal vascular disease. Genetic analysis showed there were sixty-two genes commonly altered in all three of the mouse models selected. The *VLDLR*$^{-/-}$ mouse is considered to be an angiogenic mouse model and was the model where LBP was most markedly up regulated. The first aim of this study was therefore to investigate the potential role of LBP in the *VLDLR*$^{-/-}$ mouse retinal vasculature.

2. Results

2.1 Gene validation

The vascular microarray identified 62 genes as commonly changing in all three of the mouse models. Genes were selected for validation and further investigation based upon their function and / or the level of change in their expression. We selected six genes for q-PCR validation (table 6).

GENE	NAME	FUNCTION
LBP	Lipopolysaccharide Binding Protein	Binds to LPS and presents it to CD14 & TLR4.
Atp8b1	ATPase 8b 1	Transporter for phosphatidylserine and phosphatidylethanolamine, shuttling them from one side of bilayer to other.
CRIM1	Cysteine rich transmembrane BMP regulator-1	Role in capillary formation and maintenance during angiogenesis
RSBN1	Round Spermatid basic protein-1	Spermatogenesis
GLCCI1	Glucocorticoid induced transcript-1	Uncertain
OAZ2	Ornithine decarboxylase antizyme-2	Regulates polyamine synthesis.

Table 6: Microarray Genes selected for q-PCR Validation

Neuroretina tissue was dissected from 16wk old *VLDLR*$^{-/-}$ and CT mice alongside 12wk old RD1 mice. RNA was isolated and the quality confirmed by the sample having a value of approximately 2 in the 260/280 absorbance recording using a

Thermo Scientific Nanodrop machine. Genomic DNA was then removed and first strand cDNA synthesis performed. Gene primers to six of the sixty-two genes identified in the microarray were designed, each containing >50% GC content and having a melting temperature (Tm) of 60°C. All primer pairs underwent q-PCR optimisation (Methods section 3.5.2) and were used at their optimal forward : reverse ratio to ensure minimal primer dimer formation (as indicated by a clean single peak in the dissociation curve, figure 11).

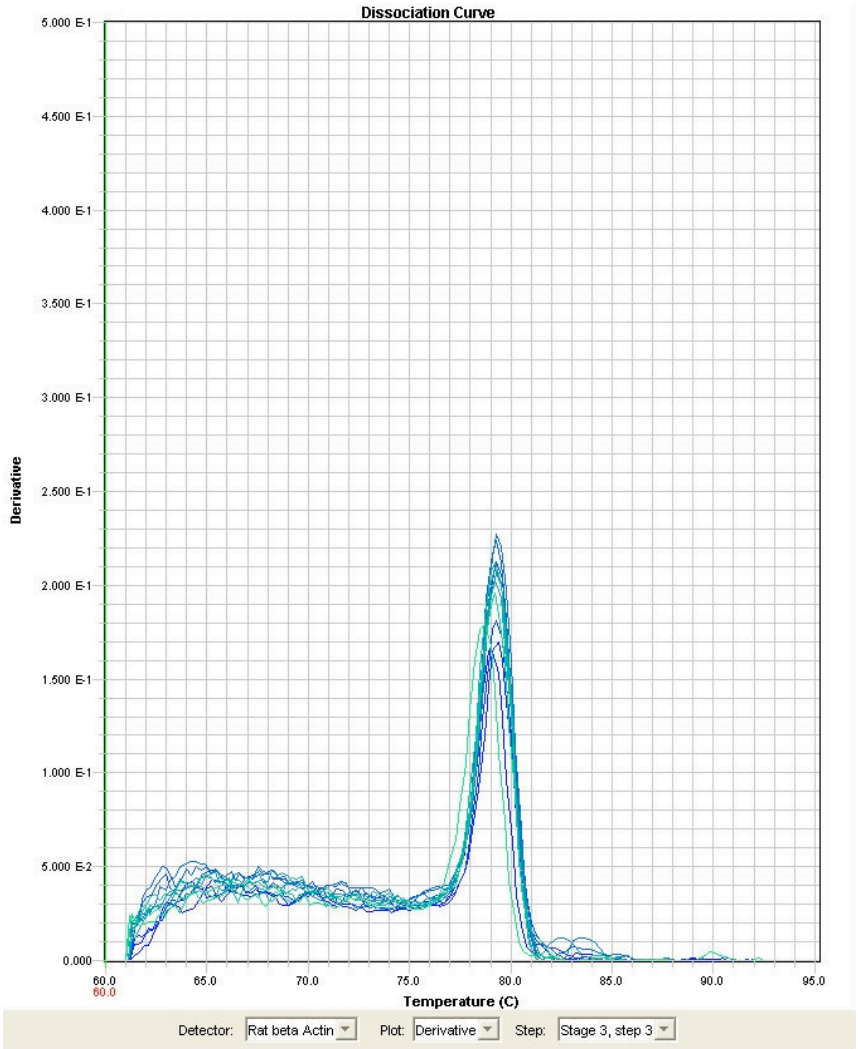

Figure 11: q-PCR Dissociation Curve. An example of a clean q-PCR primer dissociation curve. If there were primer dimer formation there would be a smaller peak visible between 70-75°C.

Two of the six genes analysed were found to confirm the microarray results, one of which was *LBP*, which demonstrated a much higher fold change in expression than the other validated gene *Oaz2*, 8-13 times increase compared to 2.5-3 (figure 12).

Curiously, LBP was only found to be elevated in the *VLDLR*$^{-/-}$ and CT mice, and not in the RD1 mouse. This is interesting because the *VLDLR*$^{-/-}$ and CT mice are considered to be models of retinal vascular angiogenesis [159] whereas the RD1 mouse does not appear to be angiogenic and is instead considered to be a model of retinal vascular remodelling [159]. As *LBP* was most markedly up-regulated ($P < 0.001$) in the *VLDLR*$^{-/-}$ mouse it was decided that further work investigating *LBP* expression in the retina would use this mouse model.

2.1 LBP and VEGF expression in the developing and adult mouse retina

The microarray was performed on 16wk old *VLDLR*$^{-/-}$ mice, when the vascular abnormalities were fully developed and the disease was established. Given that vascular abnormalities are evident in the *VLDLR*$^{-/-}$ mouse as early as P14 [157] we wanted to determine whether *LBP* was up-regulated earlier in the development of vascular pathogenesis. Changes in gene expression at a younger age could suggest a causative role for *LBP* in disease development. Due to the established role of *VEGF* in vascular disease we also decided to measure the changes in *VEGF-A* expression in the *VLDLR*$^{-/-}$ mouse, as any temporal similarities or differences in *LBP* and *VEGF-A* expression would be of potential interest. Neuroretina tissue was dissected from P0 – 16wk old C57B6 wild type and *VLDLR*$^{-/-}$ mice. RNA was isolated and the quality confirmed. Genomic DNA was then removed and first strand cDNA synthesis performed (P0-17 samples were prepared by Dr. Xiaomeng Wang, >P17 samples were prepared by myself). Primers were designed to detect all splice variants of *VEGF-A* and optimised as discussed previously (Methods section 3.5.2). *LBP* and *VEGF-A* expression were then quantified at the mRNA level using q-PCR. Gene expression was normalised to age-matched *ß-actin* levels, and then again normalised to model mouse matched P0 (e.g. C57B6 wild type P14 *LBP* expression was first normalised to C57B6 wild type P14 *ß-actin* and then normalised to C57B6 wild type P0 *LBP*) levels in order to reveal changes in gene expression during development of the retinal vasculature.

The results show (figure 13) that in C57B6 wild type mice *LBP* expression is very low at all time points, apart from during the development of the deeper vessel plexus (P10-14) when there is a 30-50 fold increase in its expression, due to the increased variation in expression levels at P14-21, this failed to reach significance. The *VLDLR*$^{-/-}$ mouse appeared to show

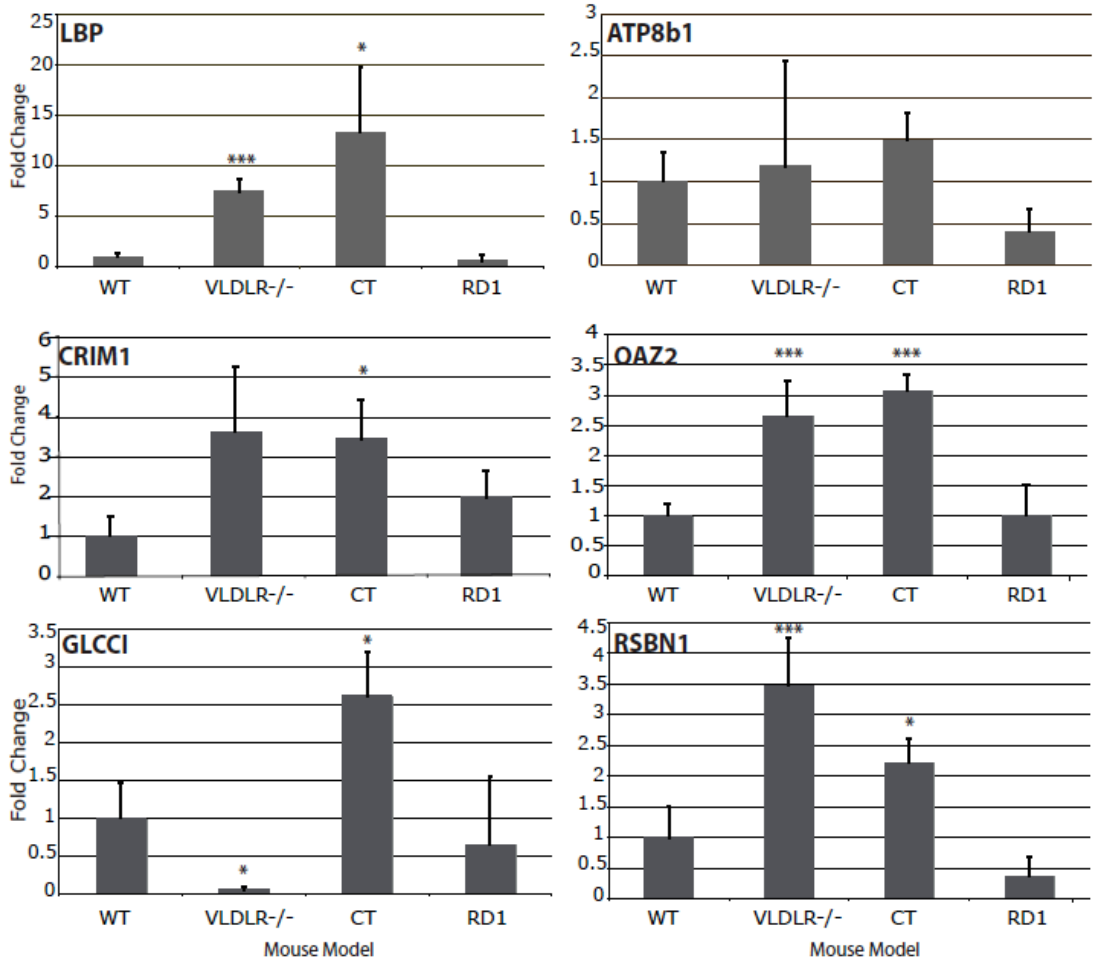

Figure 12: q-PCR Validation of Microarray Genes. Six genes were selected from the sixty-two genes identified in the vascular microarray analysis. Neuroretina tissue was dissected from 12wk old *Grhl3*$^{CT/J}$ Curlytail mice (CT), 16wk old Retinal Dystrophic-1 mice (RD1) and 16wk old very-low density lipoprotein receptor knock out (*VLDLR*$^{-/-}$) mice. RNA was isolated and cDNA synthesised from the tissue samples. Q-PCR analysis was then performed, comparing age-matched C57B5 wild type (WT) mice and normalising to internal *ß-actin* expression. (n=3). Standard error of the mean bars shown. p= <0.05* <0.01** <0.001***

increased *LBP* expression at all ages analysed, although the large increases (40-160 fold) in *LBP* expression from P14-P21, failed to reach statistical significance. Comparatively smaller (10-20 fold), but statistically relevant ($p = <0.05$) increases in *LBP* expression were observed at P4 and P8, prior to the formation of vascular abnormalities.

VEGF-A is expressed at much lower levels than *LBP* in the retina. *VEGF-A* expression appeared to remain approximately constant in the C57B6 wild type mouse during development and than decreased following maturation of the retinal vasculature at P21. Significantly increased levels of *VEGF-A* expression were observed in the *VLDLR*$^{-/-}$ mouse at all of the ages examined with the largest increase (2-4 fold) observed at P10-17, which, as previously mentioned, is when the deeper vessel plexus forms and when the onset of vascular abnormalities is known to occur. It is interesting to note that the increase in *LBP* expression occurs at approximately the same time as the increase in *VEGF-A*, this could suggest interplay between the two genes.

2.2 Vascular abnormality development in the *VLDLR*$^{-/-}$ mouse

It is known that the *VLDLR*$^{-/-}$ mouse begins to develop vascular abnormalities from P14 [145], the time of peak expression of both LBP and VEGF-A. We next investigated the generation of diseased vasculature within these mouse retinas in order to determine whether the vascular abnormalities could be detected at younger ages. Neuroretina tissue from C57B6 wild type and *VLDLR*$^{-/-}$ mice aged 3wks, 6wks and 9wks was dissected and flatmounts prepared. To visualise the vasculature the tissue was fluorescently immunostained with antibodies against collagen-IV and imaged by epi-fluorescence. The results show (figure 14) that in the *VLDLR*$^{-/-}$ mice, the vascular abnormalities were present at all ages analysed, with the number of vascular abnormalities increasing with age, consistent with previous reports [159].

2.3 LBP expression in the retina

LBP is a secreted glycoprotein primarily expressed by hepatocytes and macrophages [158]. However our microarray analysis, which detected an up regulation in LBP, was performed on isolated retinal vessels suggesting endothelial (or associated cell) expression of LBP.

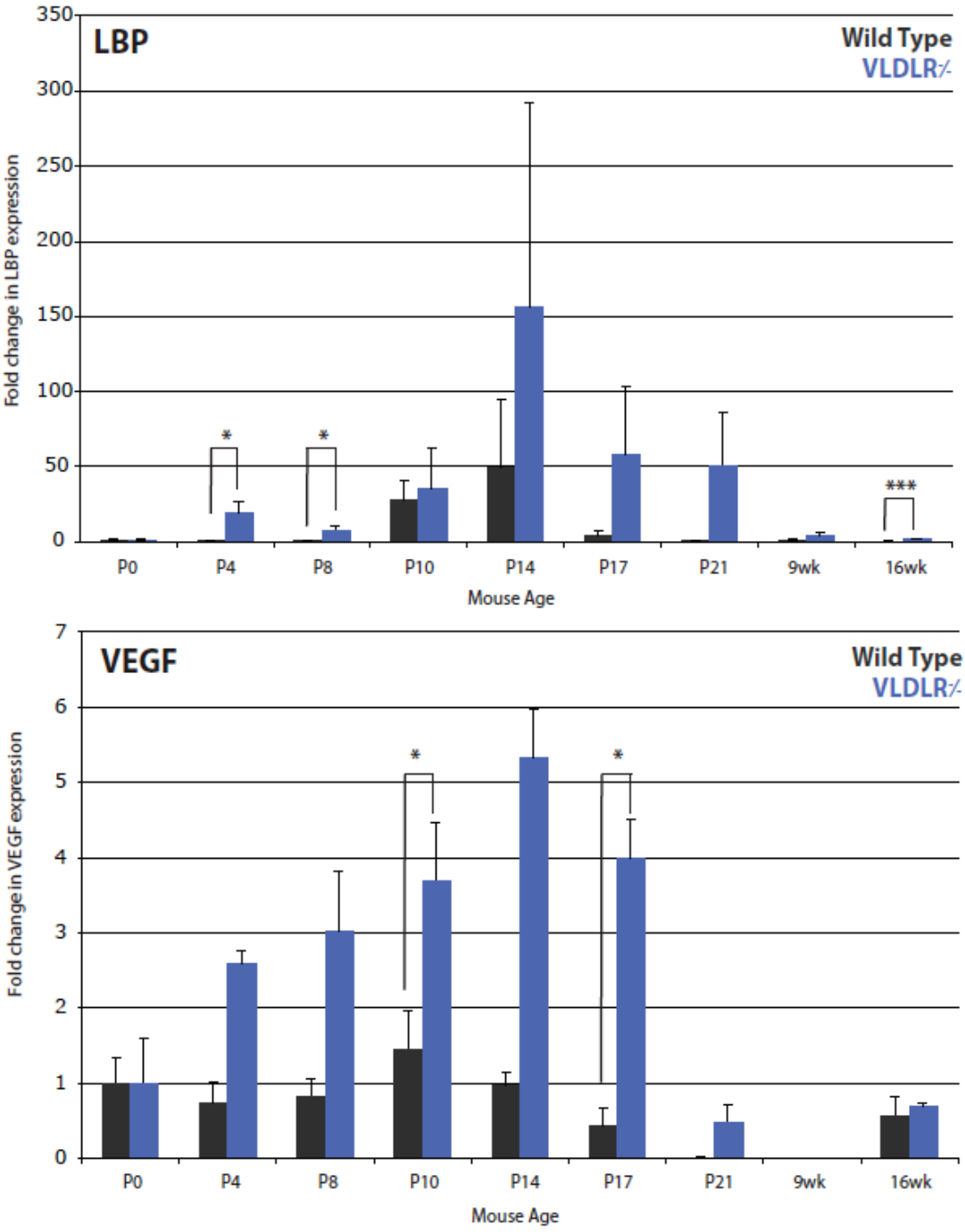

Figure 13: q-PCR Analysis of LBP and VEGF-A p0-16wk C57B6 wild type vs *VLDLR*$^{-/-}$ Mice. Neuroretina tissue was dissected from p0-16wk old Very-Low Density Lipoprotein Receptor Knock Out (*VLDLR*$^{-/-}$) mice. RNA was isolated and cDNA synthesised from the tissue samples. q-PCR analysis was then performed to determine *LBP* and *VEGF* expression compared to age-matched C57B6 wild type mice, and normalised to internal *ß-actin* expression. (n=3) p= <0.05* <0.01** <0.001***

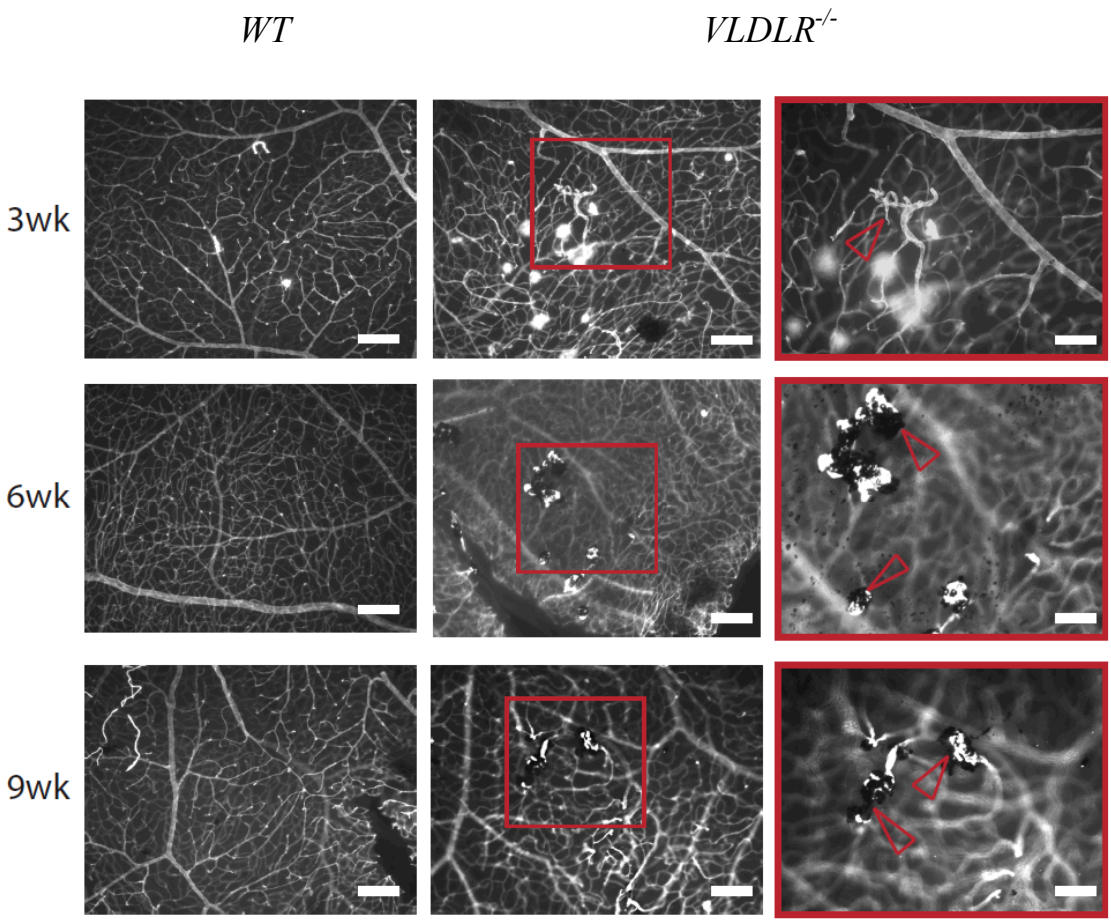

Figure 14: 3-9wk old C57B6 wild type and *VLDLR*$^{-/-}$ Mouse Retina Flatmounts stained with Antisere to Collagen-IV. Neuroretina tissue was dissected from 3-9wk old wild type (WT) and very-low density lipoprotein receptor knock out (*VLDLR*$^{-/-}$) mice. The tissue was flatmounted and incubated with a collagen-IV antibody to label the vessels. Images were taken using a Leica epifluorescent microscope to observe the vascular pathology (arrowed). (Scale bars 50µm, zoom 20µm)

In order to determine the site(s) of LBP expression in the retina, eyes were isolated from 16wk old C57B6 wild type and *VLDLR*$^{-/-}$ mice, the cornea, iris and lens were removed, and the 'eye cup' fixed in paraformaldehyde (PFA) before being embedded in optimal cutting temperature (OCT) compound and sectioned. To visualise LBP expression in the retina the tissue sections were immunostained with an antibody against LBP and then washed with diaminobenzidine (DAB), which yields a brown stain where the LBP antibody was bound.

The staining pattern suggests that LBP is expressed throughout the retina, with no obvious site of cellular enrichment, or differences between the C57B6 wild type and *VLDLR*$^{-/-}$ mice (figure 15). There was little staining on the photoreceptor layers, but most prominent staining in the retinal ganglion cell layers and a striated staining in outer nuclear layer (ONL), which could suggest some Müller cell enrichment.

3. Chapter Discussion

The up-regulation of LBP observed in the microarray was validated in the *VLDLR*$^{-/-}$ and CT models but not in the RD1 mouse. As previously mentioned, and as described recently by our group [152] the RD1 mouse has been shown to have limited new vessel formation, making it a model for vascular remodelling rather than angiogenesis [150], whereas the *VLDLR*$^{-/-}$ and CT mice are more representative models of angiogenesis [152]. Therefore for LBP to be validated only in the angiogenic models suggests it is most likely to have a hypothetical role in blood vessel production and growth, rather than remodelling.

This notion is further supported by the *LBP* and *VEGF-A* *VLDLR*$^{-/-}$ timecourse analysis, which showed that *LBP* is up-regulated in the retinas of C57B6 wild type mice during the physiological angiogenesis required for vascular development and in *VLDLR*$^{-/-}$ mice prior to the pathogenic vascular observations. Thus, the up-regulation of LBP in both normal and disease models is not a consequence of the vascular changes. There appears to be a similar pattern in *LBP* and *VEGF-A* expression in the developing retina, suggesting some co-ordination of regulation of the two genes. It could be that both genes are under the same transcriptional initiation signals / regulators, or as the increase in *LBP* expression slightly precedes an increase in

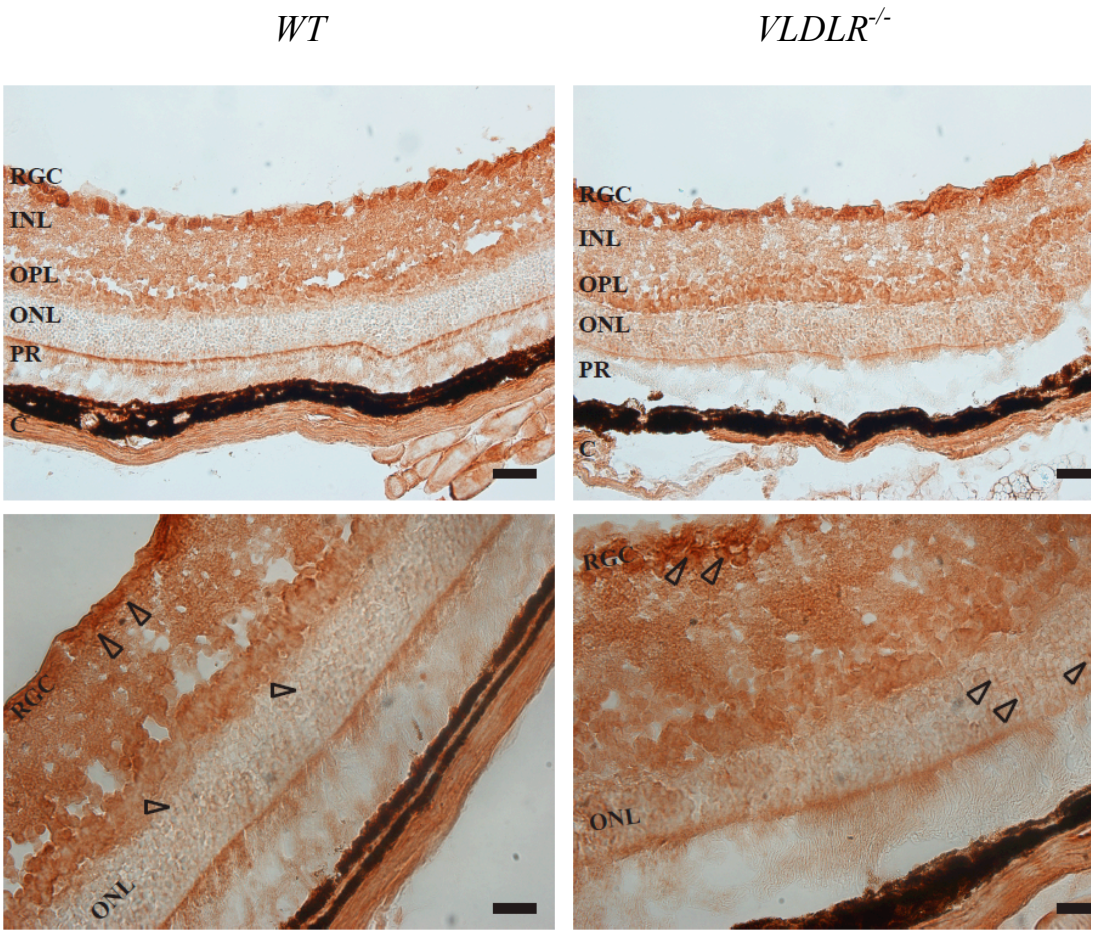

Figure 15: LBP Immunostaining of C57B6 wild type and VLDLR$^{-/-}$ Mouse Eye sections. Eyes were dissected from 16wk C57B6 wild type (WT) and very-low density lipoprotein receptor knock out (*VLDLR*$^{-/-}$) mice. The cornea and lens were removed and the 'eye cup' embedded in OCT for sectioning. The tissue sections were then incubated with an antibody for LBP and counter-stained with DAB to visualise LBP localisation as brown. The samples were then imaged using a light microscope to assess LBP staining enrichment. LBP appeared to be expressed throughout the retina with some enhanced staining observed in the retinal ganglion cell layer (RGC) and some striated staining in the outer nuclear layer (ONL), arrowed. There were no striking differences between the WT and *VLDLR*$^{-/}$ mice although there was some enrichment in visible retinal angiomatous proliferation (RAP) lesions. Negative antibody staining protocols confirmed the staining. Inner nuclear layer (INL), Outer plexiform layer (OPL), Photoreceptors (PR), Choroid (C). The dark stained layer represents the retinal pigment epithelium (RPE) and Bruch's membrane. (Scale 20µm, zoom 10µm).

VEGF-A expression it could be that *LBP* is required for the later induction of *VEGF-A*. LBP has been found to induce *VEGF* signalling under angiogenic switch conditions [130] (Introduction, section 3.3), however the mice used for this experimental analysis were notionally pathogen free and thus were free from LPS, suggesting that if LBP does induce *VEGF,* then it may not be via the angiogenic switch signalling pathway.

In newborn C57B6 wild type mice, levels of LBP expression in the developing and adult retina appear to be low, only increasing at P10-14. LBP expression is significantly higher in the *VLDLR*$^{-/-}$ mouse, with q-PCR analysis suggesting a dramatic fold increase (30-160) during development. This is in contrast to *VEGF-A*, which although increased in the *VLDLR*$^{-/-}$ mouse is elevated by a much smaller fold amount (2-4). This suggests that if LBP does have an effect on retinal neovasculaturisation it may not be as potent as VEGF-A. LBP is expressed constitutively at 2-5ng/ml in circulating plasma [160, 161], which is substantially higher then VEGF (approximately 30pg/ml) [94]. However, upon infection, LBP concentrations have been reported to increase up to 50µg/ml within 36h [161]. But during infection LBP will often be in complex with LPS and not circulating freely. LBP is mostly synthesised by the liver and macrophage cells, but local production by the eye during retinal vascular development (as revealed by the microarray and q-PCR analysis), suggests that in the absence of infection (and by association, LPS), LBP may have some angiogenic role. The fact that LBP is elevated in the *VLDLR*$^{-/-}$ mouse argues that it contributes to the onset of pathological angiogenesis in the retina of these animals, and is consistent with the increase in expression of other established angiogenic factors such as VEGF.

Retinal flatmount analysis comparing 3-9wk old C57B6 wild type and *VLDLR*$^{-/-}$ mice confirmed that vascular abnormalities are present and can be detected in p21 *VLDLR*$^{-/-}$ mice, supporting findings elsewhere [154, 155] and illustrating that the vascular changes occur alongside the alterations in gene expression we detected using q-PCR.

LBP was originally detected in our microarray analysis, which was performed on isolated retinal vessels. The vessels were isolated through neuroretina dissection and digestion with collagenase and dispase, the tissue was then incubated with rat antibodies for the vascular marker PECAM1 before being mixed with magnetic beads

coated with an anti-rat antibody [152]. The anti-rat antibody detected the rat-PECAM1 and upon positioning of the sample near to a magnet the PECAM1 positive cells (i.e. vessels) were separated. However, there is no mention in the literature of LBP being expressed by endothelial cells. Immunostaining of C57B6 wild type and *VLDLR*$^{-/-}$ retinal sections was inconclusive in this respect, revealing that LBP is expressed throughout the retina with no specific enrichment in the vasculature. However there did appear to be an enrichment of LBP in the ONL of the *VLDLR*$^{-/-}$ mouse, and the somewhat striated staining pattern could correspond to the extensive Müller cell projections known to reside in this layer. The notion that Müller cells in the vessel prep might explain the presence of LBP in the microarray study, is supported by cell culture q-PCR analysis showing that LBP was not expressed by a variety of endothelial cells (HUVEC, GPNT and RBE4), but was expressed by the MIO-M1 Müller cell line. Although the retinal vessel prep was clearly enriched for endothelial cells it is inevitable that there would be other vascular supportive cell types contaminating the preparation (e.g. pericytes, smooth muscle cells and Müller cells). Müller cells are known to be activated during retinal disease, changing their phenotype and secreting a range of angiogenic factors including VEGF, TGFß and PDGF, that may all contribute to pathological neovascularisation [162]. Should LBP prove to directly affect vascular behaviour, those Müller cells in close proximity to the retinal vessels would be ideally placed to influence angiogenesis, as a source of secreted LBP.

Results Chapter Two

Investigation of the Angiogenic Potential of LBP

Chapter Two
Investigation of the Angiogenic Potential of LBP

1.1 Background

LBP is an innate immune system glycoprotein, which binds to LPS, a component of gram-negative bacteria such as *E. coli* and presents it to CD14 antigen presenting cells to activate TLR4 signalling to induce an inflammatory response [106, 151]. In all of the experiments carried out investigating the role of LBP, none have reported it to have an effect on vascular growth.

LBP was the third most up regulated protein in the microarray analysis of three mouse models (*VLDLR*$^{-/-}$, RD1 and CT) of retinal vascular disease. Further characterisation of the angiogenic *VLDLR*$^{-/-}$ model confirmed LBP as being up-regulated prior to disease onset and around the same time as an increase in *VEGF* expression. RT-PCR analysis has also shown *LBP* to be expressed in Müller cells, which are known to be activated in pathogenic conditions in the retina [73, 162]. Our observations, alongside known associations between immunity and angiogenesis (see Introduction 6.3), suggests that LBP could have an as yet uncharacterised role, independent of LPS, affecting vascular behaviour.

1.2 Aim

The aim of work in this chapter was to identify whether LBP has another role outside of its function in inflammatory responses of the innate immune system. Specifically, does LBP exhibit any effects on vascular proliferation / angiogenic behaviour?

2. Results

2.1 Limulus Amebocyte Lysate (LAL) assay

All experimental systems needed to be demonstrably free of LPS in order to investigate whether LBP has biological activity, independent of LPS. In 1956 it was reported that horseshoe crab blood would turn into a semi-solid gel upon exposure to endotoxin (e.g. LPS) due to a coagulogen clotting factor within their amebocyte cells [165]. When infected with endotoxin the horseshoe crab ambeocytes release the

coagulogen in order to encase the bacteria and prevent it from spreading further into the animals circulatory system [165]. This biological mechanism forms the basis of the LAL assay [158] (figure 16). Studies have shown that a minimum of 10pg/ml LPS is required to induce a cellular response [165]. The LAL assay has a sensitivity of 3pg/ml endotoxin, therefore as all cell media samples collected from plates during the experiments as well as the treatment solutions, culture media and wash buffers tested negative using LAL, we can say with confidence that LPS was absent from all experiments or that it was below the threshold needed for signalling activation.

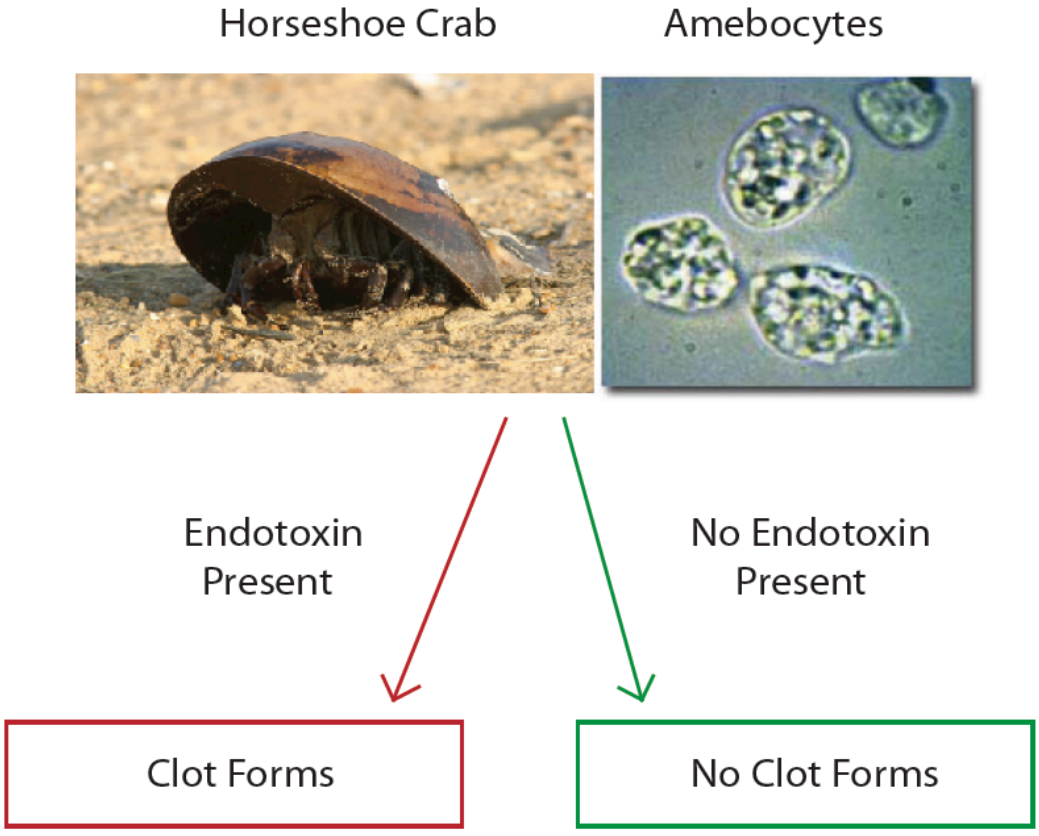

Figure 16: Limulus Amebocyte Lysate (LAL) Assay Schematic. A Schematic to illustrate the methodology of the Limulus Amebocyte Lysate (LAL) Assay approved by the American Food and Drug Administration (FDA) to test products for endotoxin contamination.

2.2 Matrigel assay

The Matrigel assay is a well-established *in vitro* angiogenesis assay using HUVEC in a semi-solid growth matrix (Matrigel) to assess whether a treatment has an effect on vessel sprouting, branching and network complexity [166, 167]. The HUVEC were seeded onto a growth factor reduced Matrigel support, treated as desired (PBS control, 10ng/ml LBP, 10ng/ml LBP + 1µg LPS or 1µg LPS), incubated for 12-16h, imaged

and analysed for number of sprouts, branch points and closed loops. HUVEC have been reported to alter their protein expression profiles as they are cultured (e.g. CD14 expression decreases dramatically past passage five) [168], therefore the Matrigel assays were performed using passage two HUVEC to ensure maximal *in vivo* 'like' protein expression.

The results showed that 10ng/ml LBP (bought as a recombinant protein from R&D Systems, with 10ng/ml chosen as it was reported by R&D systems to have maximal effect in an inflammatory assay) was able to increase sprouting, branch points and closed loop formations (figure 17). However, upon addition of 10ng/ml LBP + 1µg/ml LPS this increase appeared to be inhibited as we observed sprout, branch and loop numbers similar to basal condition numbers. If the HUVEC used in the assay expressed CD14, which is likely, the LBP + LPS treatment would be expected to induce an inflammatory response. Therefore LPS might have inhibited the pro-angiogenic effects of LBP in one of two ways – 1) by binding to LBP and promoting an inflammatory response and 2) by binding to and sequestering LBP, thereby preventing it from signalling independently to induce vascular growth.

Interestingly addition of 1µg/ml LPS alone appeared to decrease the observed sprouts, branches and closed loops suggesting that the LPS endotoxin is able to suppress HUVEC tubulation. However, 1µg/ml LPS would correspond to a severe infection and it may be that such high concentrations of LPS are toxic to HUVEC.

2.3 Aortic ring assay

The aortic ring assay is an *ex vivo* tissue based assay routinely used to assess the angiogenic activity of natural or synthetic molecules [169]. Aortic tissue was dissected from 2wk old C57B6 wild type mice and embedded in a collagen-I gel. The tissue was then incubated for 2 days and assessed for fibroblast sprouts, which indicated the tissue was alive and able to grow. The rings were then treated with the desired treatment (PBS, 10ng/ml LBP, 20ng/ml LBP, 50ng/ml LBP, 10ng/ml LBP + 1µg/ml LPS, 20ng/ml LBP + 1µg/ml LPS, 50ng/ml LBP + 1µg/ml LPS, 1µg/ml LPS, 20ng/ml LBP + 50ng/ml VEGF, 50ng/ml VEGF + 1µg/ml LPS and 50ng/ml VEGF) for 6 days (fresh media + treatment every 2 days). After 6 days the rings were stained with antibodies to detect isolectin-B4 and imaged. The image was inverted using ImageJ

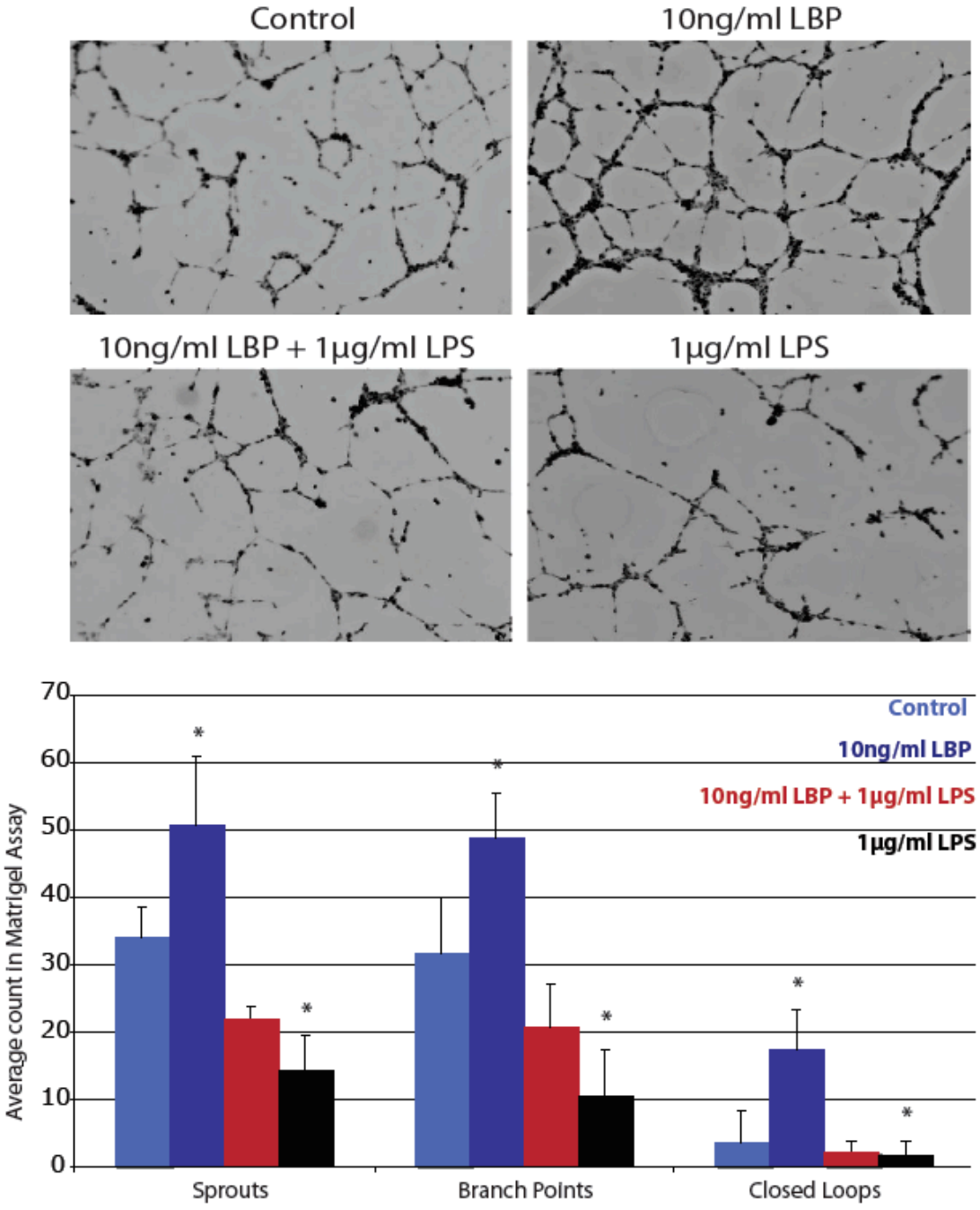

Figure 17: HUVEC (passage 2) Matrigel Angiogenesis Assay. HUVEC were seeded onto growth factor reduced Matrigel (BD) at $2x10^5$/ml cell density. Treatments were then added (PBS control, 10ng/ml LBP, 10ng/ml LBP + 1µg/ml LPS or 1µg/ml LPS and the gels incubated overnight at 37°C 5% CO_2. The gels were imaged using a Lecia epifluorescence microscope under brightfield conditions. Sprouts, branch points and closed loops were counted manually. Student's t-test was performed and standard error of the mean calculated p = <0.05 * <0.001 ** <0.0001 *** (n=4).

software and the sprouts traced to calculate any changes in the vascular area covered (figure 18).

The aortic ring results (figures 19 and 20) supported the previous Matrigel observations. Increasing the concentration of LBP increased the size of the vascular area in a dose dependent manner with the highest concentration of LBP we tested (50ng/ml) giving similar amounts of vascular growth to that observed with 50ng/ml VEGF.

The presence of LPS with any concentration of LBP markedly inhibited vascular growth induction, with mean vascular area size similar to control levels, and as before, addition of LPS alone appeared to inhibit basal vascular growth. Interestingly, LPS appeared at times to inhibit VEGF induced vessel growth, although this effect varied substantially and was not statistically significant. The observation that LPS inhibits both VEGF and LBP was unexpected. As previously mentioned LBP + LPS could induce an inflammatory response in the tissue, thus inhibiting vascular growth or LPS could be sequestering LBP, therefore preventing its independent activity. The VEGF inhibition by LPS is not so easy to explain. It could suggest a common modality between LBP and VEGF with some overlap in the signal cascades induced. Interestingly, we observed a significant number of unidentified cell types in the LBP + VEGF treated tissue that were not present in the cultures only treated only with VEGF. This shows that LBP, but not VEGF promotes migration of non-vascular cell type(s) from the aortic ring tissue (figure 21).

2.4 Metatarsal assay

The metatarsal assay is another *ex vivo* tissue-based angiogenesis assay [170]. This assay uses the metatarsal bones from embryonic E16.5 C57B6 wild-type mice. The dissected bones were plated onto 0.1% gelatin coated dishes and incubated for 2 days allowing the bones to settle. Any bones that failed to settle were disregarded as dead tissue. Desired treatments (PBS, 10ng/ml LBP, 20ng/ml LBP, 10ng/ml LBP + 1µg/ml LPS, 1µg/ml LPS) were then applied to the live samples for 7 days (fresh media + treatment every 3 days) before being stained with antibodies to detect PECAM-1, and imaging. This protocol has two advantages over the aortic ring assay; firstly the

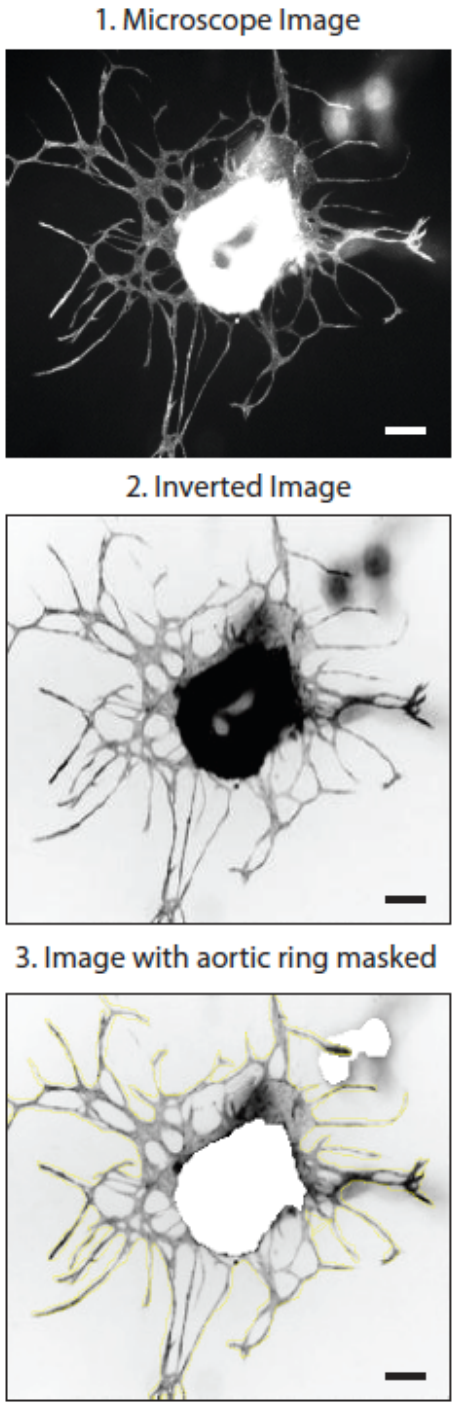

Figure 18: Aortic Ring Assay Analysis. The top fluorescent image shows an aortic ring stained with isolectin B4 and imaged using Lecia epifluorescence microscope. The image was exported into ImageJ software and inverted. The freehand selection tool was used to trace the vessel sprouts and the mean pixel reading recorded (VESSEL+RING). The freehand selection tool was then used to trace around the ring and the mean pixel reading recorded (RING). The RING pixel reading was then subtracted from the VESSEL+RING value in order to give the isolated VESSEL value. The values were then averaged for each treatment and compared to control conditions. (Scale = 100µm).

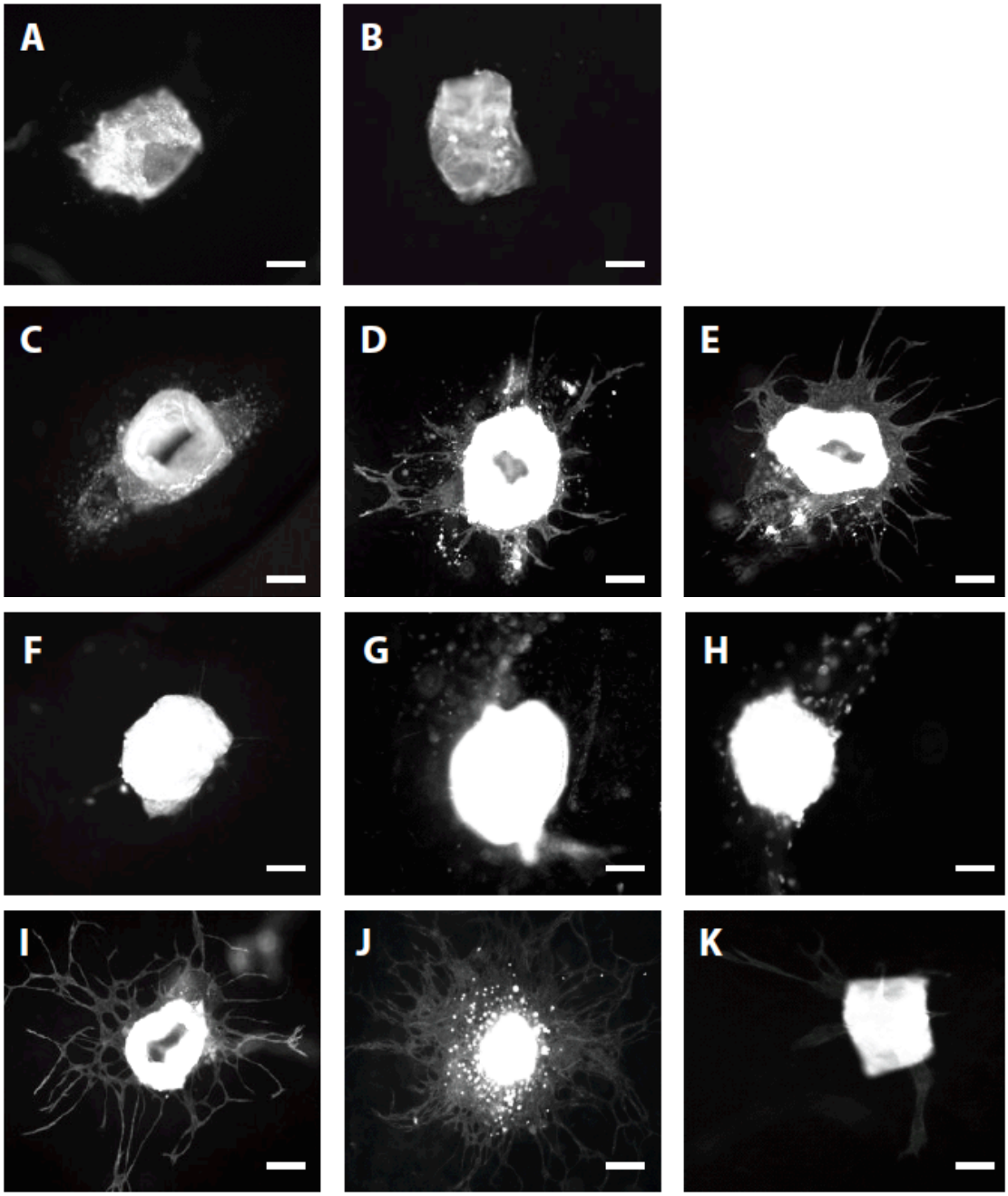

Figure 19: Mouse Aortic Ring Angiogenesis Assay. Thoracic aortas were dissected from 2wk old C57B6 wild type mice. The tissue was placed onto collage-I gels and cultured in DMEM with 10% FCS. After 2 days incubation at 37°C 5% CO_2 the rings were observed for fibroblast sprouting to indicate alive tissue. Fresh media + desired treatment was then added to the rings and they were reincubated. A) PBS Control B) 1µg/ml LPS C) 10ng/ml LBP D) 20ng/ml LBP E) 50ng/ml LBP F) 10ng/ml LBP + 1µg/ml LPS G) 20ng/ml LBP + 1µg/ml LPS H) 50ng/ml LBP + 1µg/ml LPS I) 100ng/ml VEGF J) 100ng/ml VEGF + 20ng/ml LBP K) 100ng/ml VEGF + 1µg/ml LPS. The treatment media was replenished every 2 days and after 8 days the tissue was fixed in 4% PFA, stained with 1:200 Isolectin B4 (VECTOR) and imaged using a Lecia epiflourecent microscope. 6 mice were used for each experiment to give 10 rings per treatment (n=4). (Scale = 100µm).

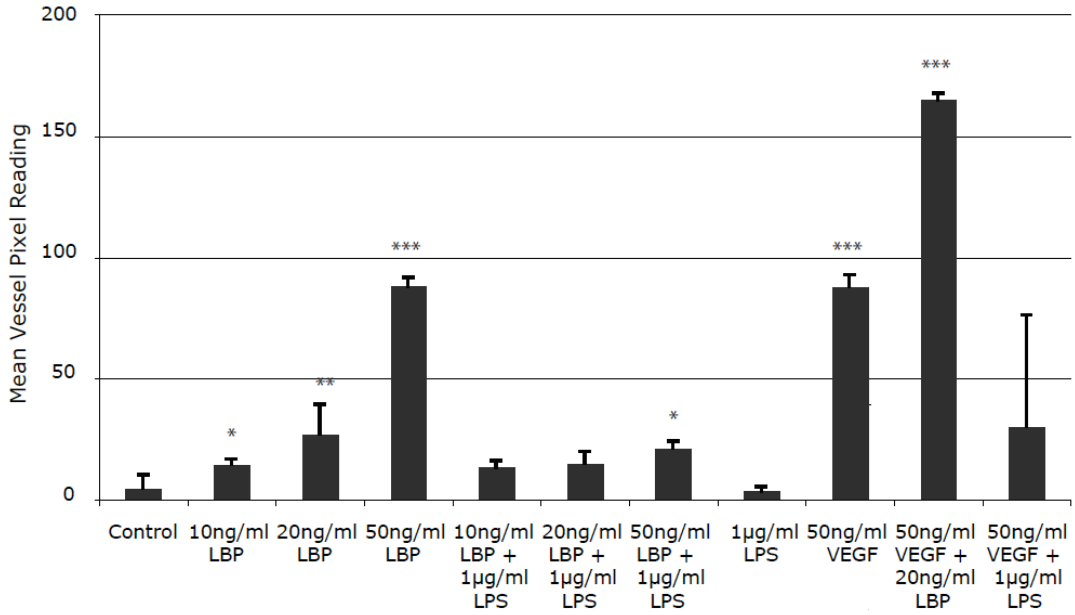

Figure 20: Mouse Aortic Ring Angiogenesis Assay Analysis. Thoracic aortas were dissected from 2wk old C57B6 wild type mice. The tissue was placed onto collage-I gels and cultured in DMEM with 10% FCS. After 2 days incubation at 37°C 5% CO_2 the rings were assessed for fibroblast sprouting to indicate alive tissue. Fresh media + desired treatment was then added to the rings and they were reincubated. A) PBS Control B) 1µg/ml LPS C) 10ng/ml LBP D) 20ng/ml LBP E) 50ng/ml LBP F) 10ng/ml LBP + 1µg/ml LPS G) 20ng/ml LBP + 1µg/ml LPS H) 50ng/ml LBP + 1µg/ml LPS I) 100ng/ml VEGF J) 100ng/ml VEGF + 20ng/ml LBP K) 100ng/ml VEGF + 1µg/ml LPS. The treatment media was replenished every 2 days and after 8 days the tissue was fixed in 4% PFA, stained with 1:200 Isolectin B4 (VECTOR) and imaged using a Lecia epiflourecent microscope. The image was then exported into ImageJ. The pixel readings for the total sprouts observed with each treatment were then averaged and compared to control conditions. 6 mice were used for each experiment to give 10 rings per treatment (n=4). Student t-test was performed and the standard error of the mean calculated for each treatment $p = <0.05$ * <0.001 ** <0.0001 ***

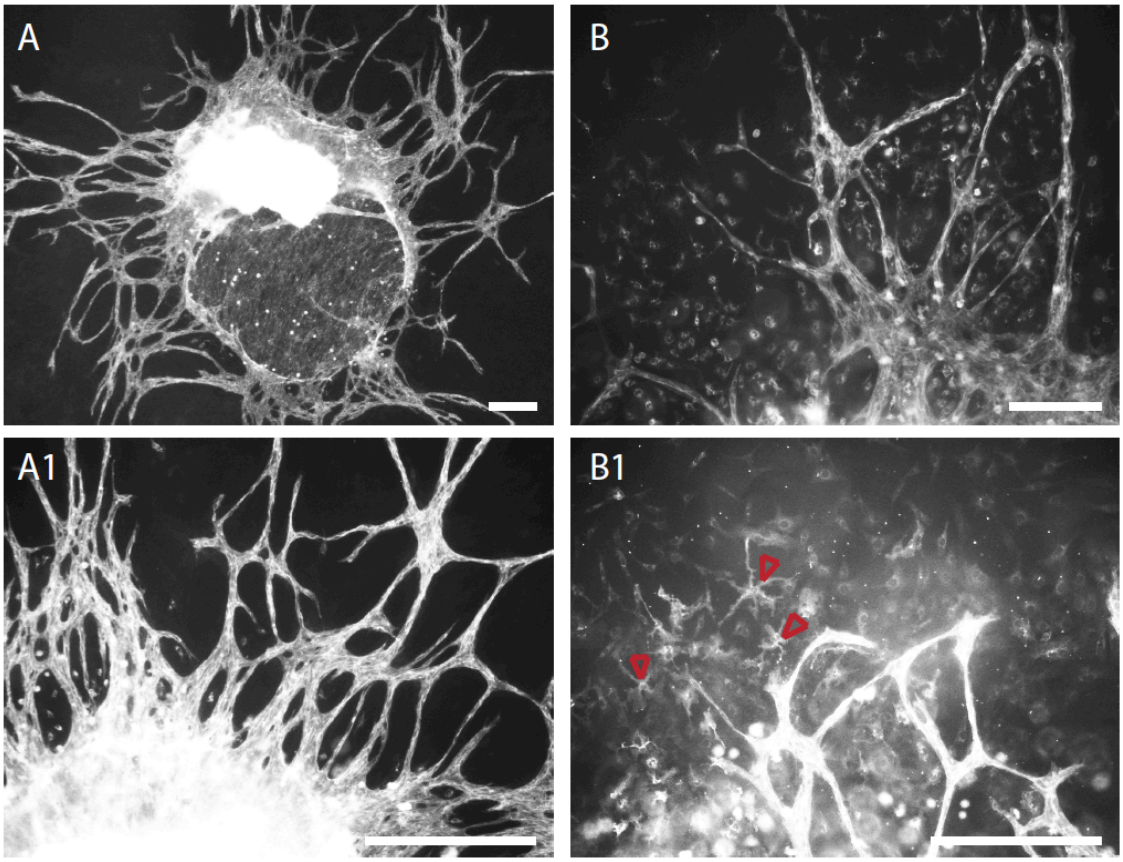

Figure 21: LBP Stimulates Non-Vascular Cell Growth in the Mouse Aortic Ring. Aortic rings were treated with A) VEGF, and B) 20ng/ml LBP + VEGF, and stained for Isolectin B4. Images were obtained using a Leica epiflourescent microscope. In the presence of LBP (B1), but not VEGF (A1), we observed a large number of non-vascular cell types, marked with arrow heads (B1). (Scale = 100µm).

metatarsal tissue always sprouts even under basal conditions, unlike the aortic ring, which can sometimes produce no sprouts even with VEGF treatment. This makes the effects of treatments much easier to detect in the metatarsal assay. Secondly the images obtained from the metatarsal assay are suitable for IMARIS analysis (figure 22). Imaris is a filament tracing software, which is able to trace vessel sprouts and analyse the volume, area and branch number in a network [171]. This makes the metatarsal assay analysis completely objective and removes any user experimental bias.

The results (figures 23 and 24) supported the previous observations in the Matrigel and aortic ring assays with 10-20ng/ml LBP having a dose-dependent effect on vascular growth. Addition of LPS prevented this LBP-induced increase, and LPS treatment alone appeared to inhibit basal growth. As previously discussed (see Introduction 2) tip cells are indicative of sprouting angiogenesis [172], therefore metatarsal samples were magnified in an attempt to observe whether there was a change in the number of tip cells when treated with LBP (figure 25). Unfortunately the image resolution was not sufficient for detailed analysis but the images do suggest the presence of stereotypical tip cell filipodia projections in the control conditions. Furthermore the number of filipodia appeared to be elevated upon treatment with LBP alone, but with co-addition of LPS there were fewer filipodia and the cell tips appeared smooth.

Data analysis showed that 20ng/ml LBP treatment was sufficient to increase overall vascular area as well as branch point number, and that LPS inhibited both of these effects. This suggests that LPS prevents LBP from inducing growth and remodelling of the vessel network (as is observed during intussusceptive angiogenesis, Introduction 2). The Imaris software enables separation of the results into macro and microvessel denominations. Interestingly, this analysis showed that 20ng/ml LBP increased the area, length and the number of segments of macro but not microvessels (figures 26 and 27). This could mean that a hypothetical LBP receptor is differentially expressed in the two vessel populations, or that only the larger vessels express the required proteins to exhibit an angiogenic response to LBP.

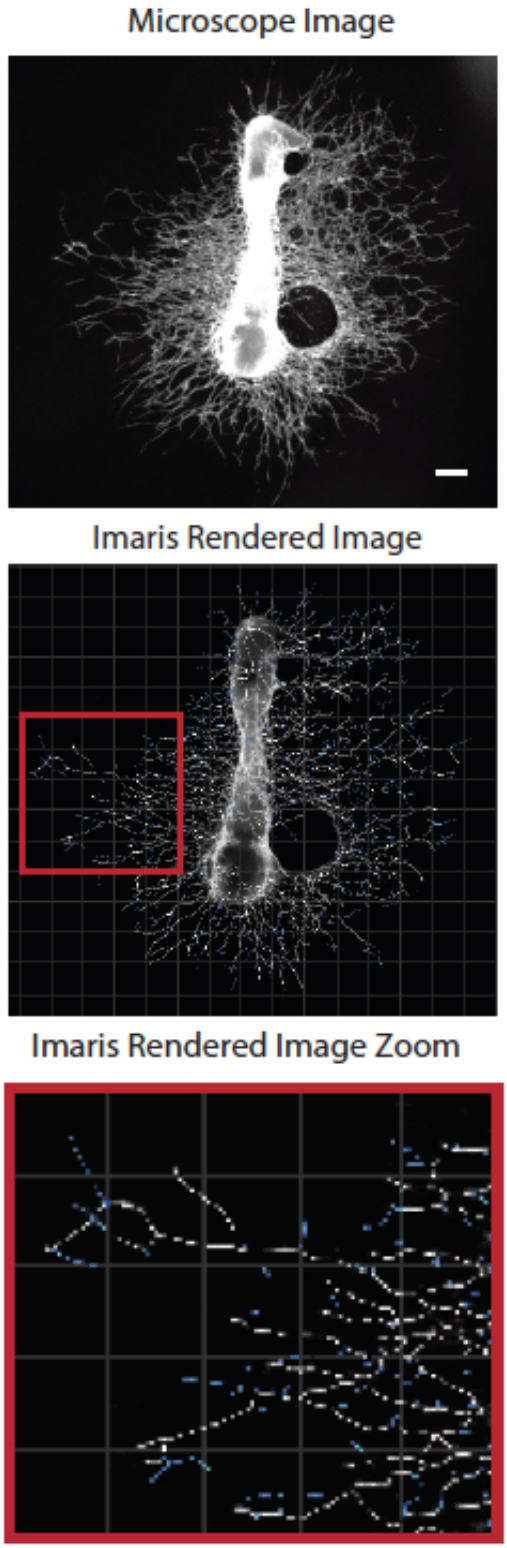

Figure 22: Mouse metatarsal angiogenesis assay with Imaris rendering. Magnified fluorescent metatarsal image was taken and inserted into the Imaris filament tracer software. The bone was set as a point of origin, macrovessels assessed by the programme and marked in white, microvessels assessed and marked as blue. (Scale = 100μm).

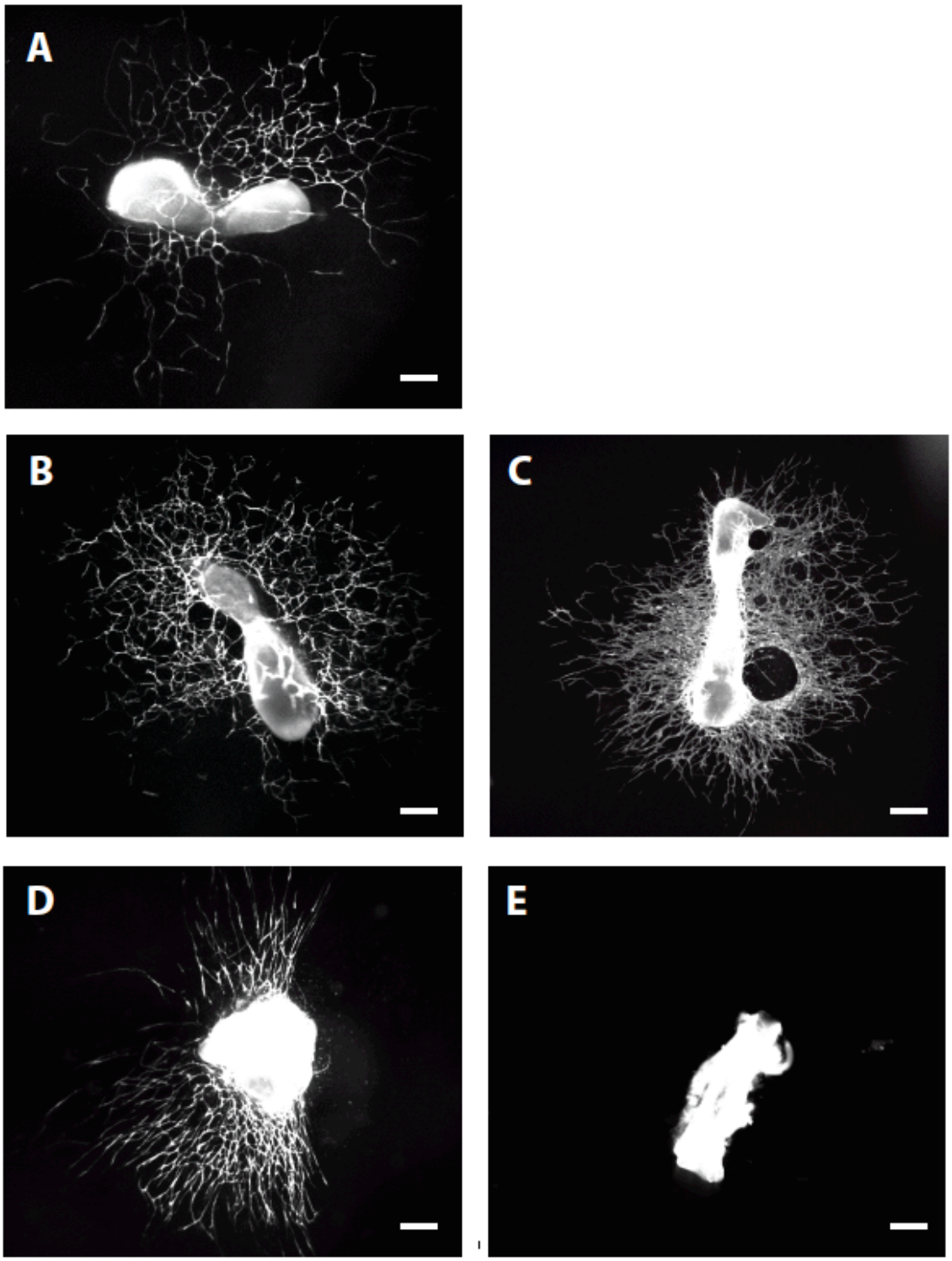

Figure 23: Mouse Metatarsal Angiogenesis Assay. Metatarsal bones were dissected from E16.5 C57B6 wild type mice embryos. The bones were placed onto a 0.1% gelatin coated dish and cultured with EGM2. After 2 days incubation at 37°C 5% CO_2 the bones were observed and any floating tissue disregarded. The settled bones then received desired treatment and were reincubated. A) PBS Control B) 10ng/ml LBP C) 20ng/ml LBP D) 10ng/ml LBP + 1µg/ml LPS E) 1µg/ml LPS. Every 3 days the treatment media was replenished and after 9 days the tissue was fixed in 4% PFA, stained with 1:200 PeCAM-1 and imaged using a Leica epiflourecent microscope. 8 embryos were used for each experiment, yielding 4-7 bones per treatment (n=4). (Scale = 100µm).

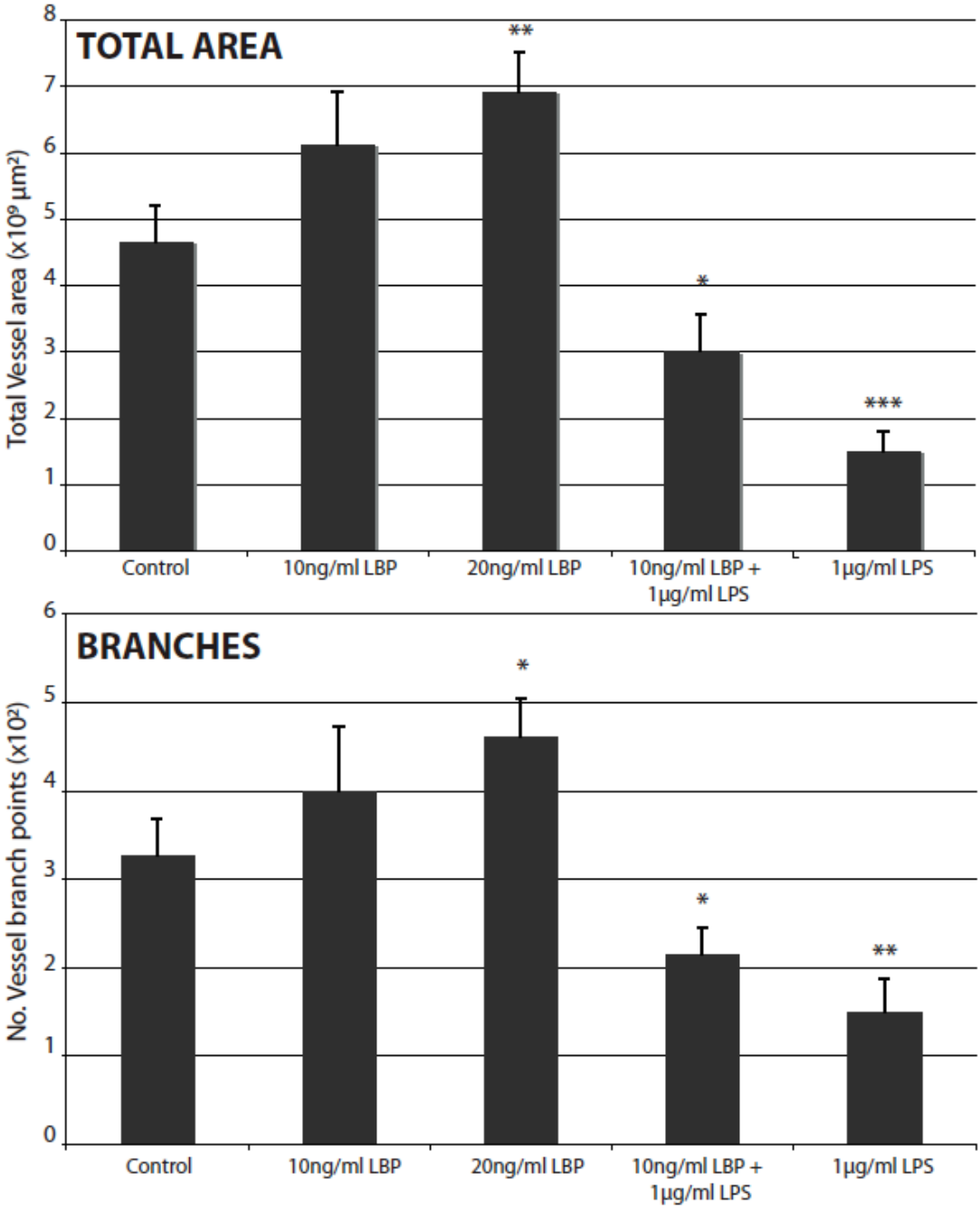

Figure 24: Mouse Metatarsal Angiogenesis Assay Total Area and Branching Analysis. Metatarsal bones were dissected from E16.5 C57B6 wild type mice embryos. The bones were placed onto a 0.1% gelatin coated dish and cultured in EGM2. After 2 days incubation at 37°C 5% CO_2 the bones were observed and floating samples disregarded. The settled bones then received desired treatment and were reincubated. A) PBS Control B) 10ng/ml LBP C) 20ng/ml LBP D) 10ng/ml LBP + 1µg/ml LPS E) 1µg/ml LPS. Every 3 days the treatment media was replenished and after 9 days the tissue was fixed in 4% PFA, stained with 1:200 PECAM-1 and imaged using a Lecia epiflourecent microscope. Images were exported into Imaris for analysis. 8 embryos were used for each experiment, yielding 4-7 bones per treatment. Student t-test was performed and the standard error of the mean calculated for each treatment p = <0.05 * <0.001 ** <0.0001 *** (n=4).

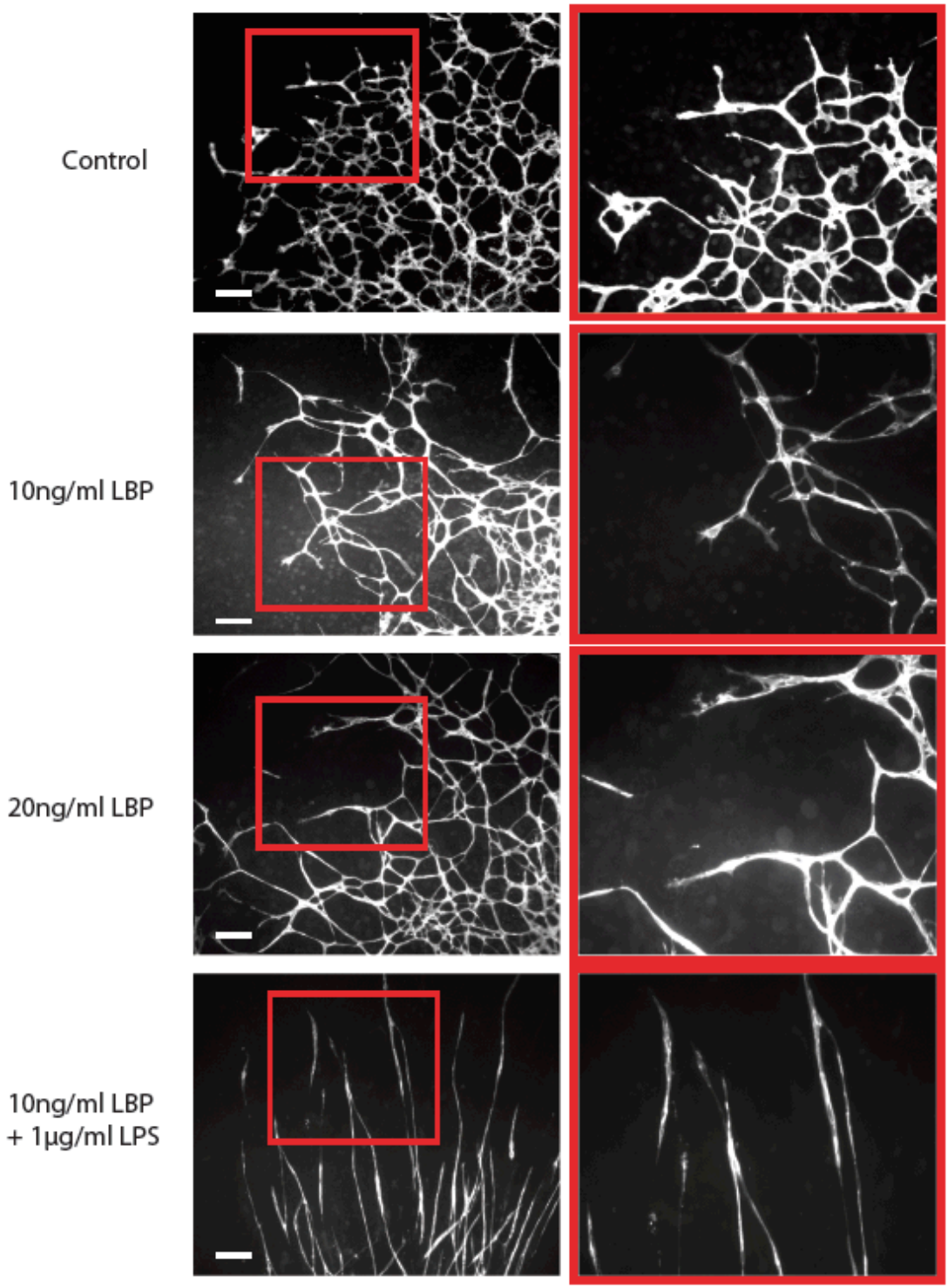

Figure 25: Mouse Metatarsal Tip Cell Analysis. Metatarsal bones were dissected from E16.5 C57B6 wild type mice embryos. The bones were placed onto a 0.1% gelatin coated dish and cultured in EGM2. After 2 days incubation at 37°C 5% CO_2 the bones were observed and floating samples disregarded. The settled bones then received desired treatment and were reincubated. A) PBS Control B) 10ng/ml LBP C) 20ng/ml LBP D) 10ng/ml LBP + 1µg/ml LPS E) 1µg/ml LPS. Every 3 days the treatment media was replenished and after 9 days the tissue was fixed in 4% PFA, stained with 1:200 PECAM-1 and imaged using a Leica epiflourecent microscope. Magnification ability of the microscope proved inadequate to visualise the sprouting tip cells. (Scale = 20µm)

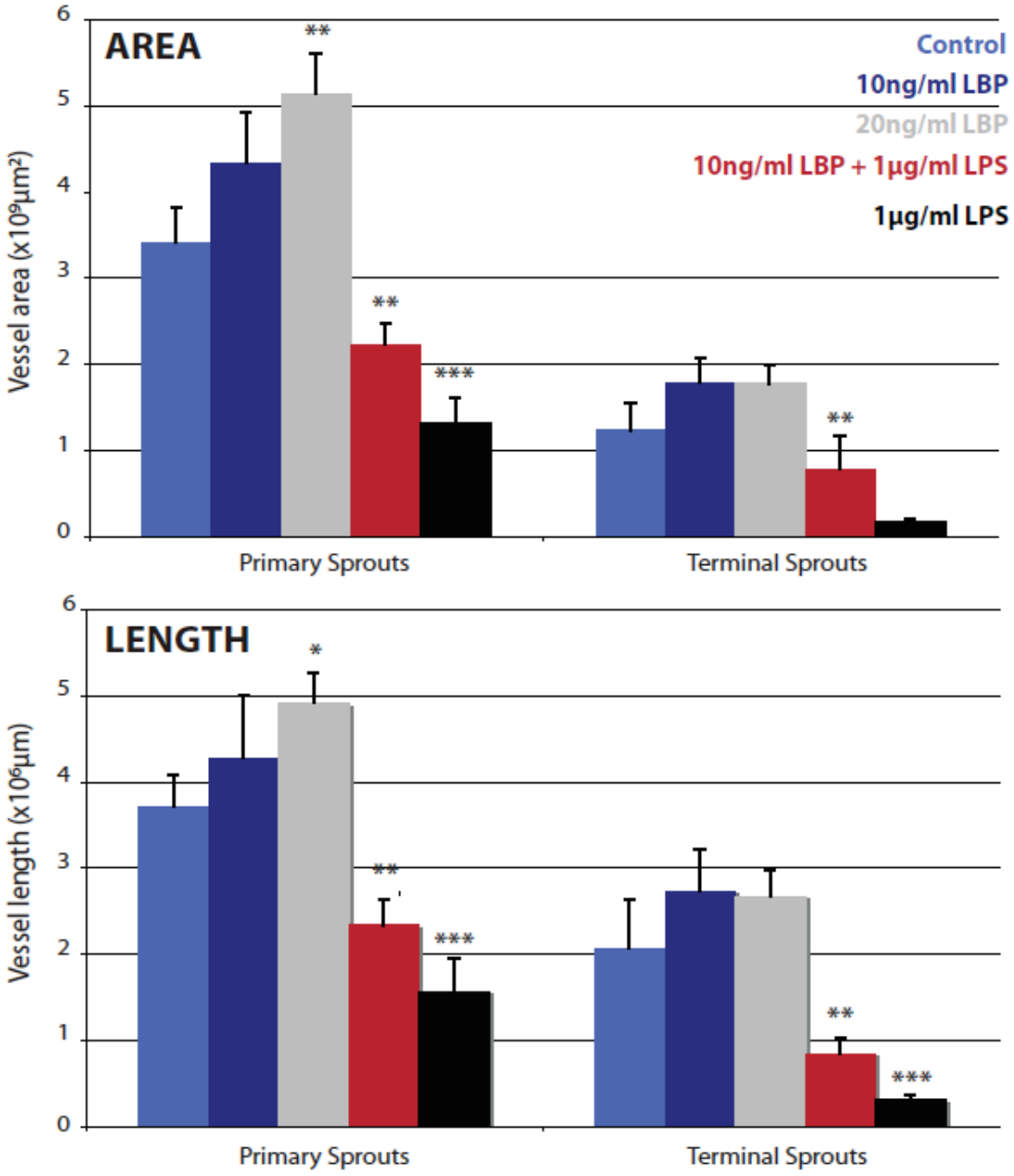

Figure 26: Mouse Metatarsal Angiogenesis Assay Area and Length Analysis. Metatarsal bones were dissected from E16.5 C57B6 wild type mice embryos. The bones were placed onto a 0.1% gelatin coated dish and cultured in EGM2. After 2 days incubation at 37°C 5% CO_2 the bones were observed and floating samples disregarded. The settled bones then received desired treatment and were reincubated. A) PBS Control B) 10ng/ml LBP C) 20ng/ml LBP D) 10ng/ml LBP + 1µg/ml LPS E) 1µg/ml LPS. Every 3 days the treatment media was replenished and after 9 days the tissue was fixed in 4% PFA, stained with 1:200 PECAM-1 and imaged using a Leica epiflourecent microscope. Images were exported into Imaris for analysis. 8 embryos were used for each experiment, yielding 4-7 bones per treatment. Student t-test was performed and the standard error of the mean calculated for each treatment p = <0.05 * <0.001 ** <0.0001 *** (n=4).

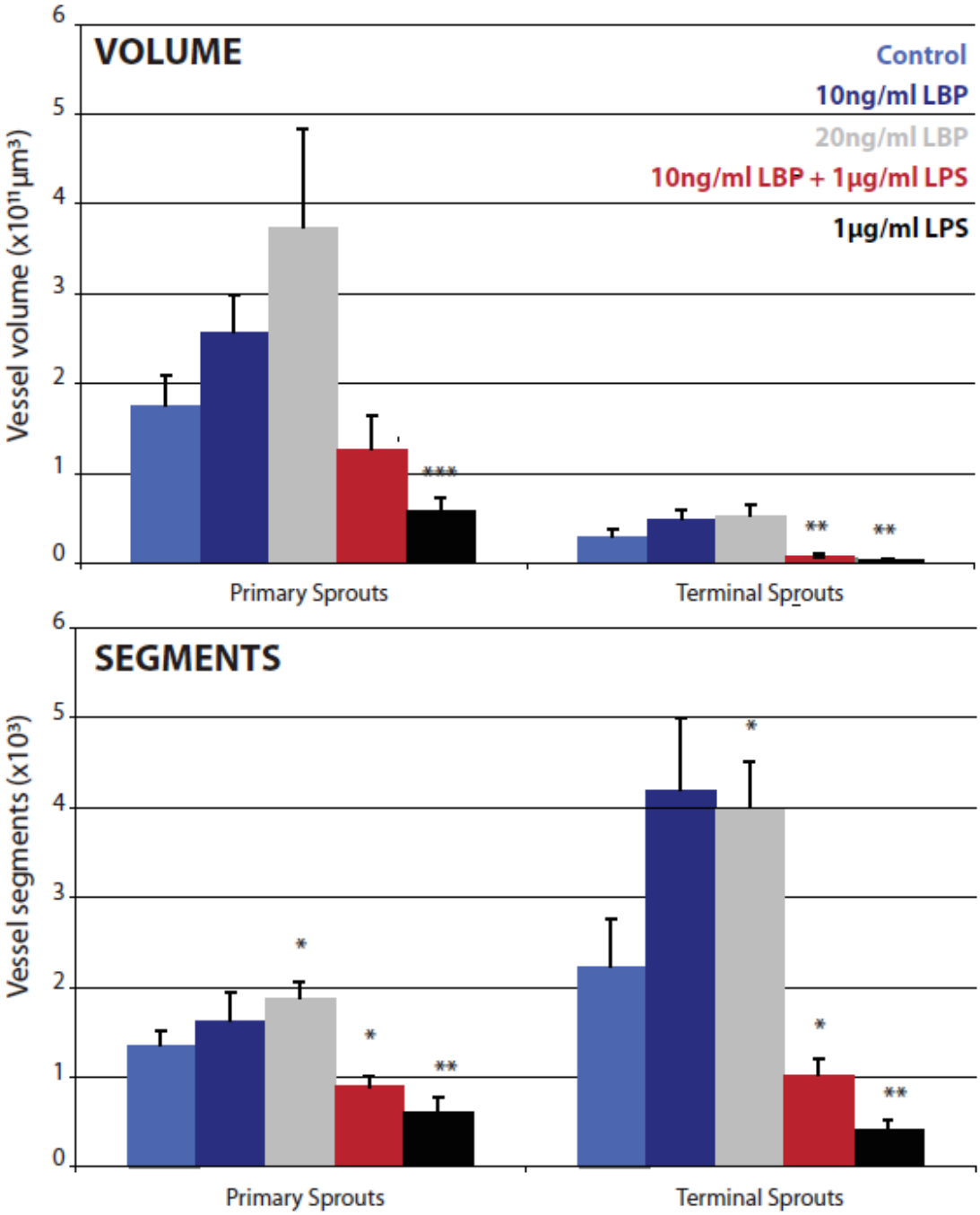

Figure 27: Mouse Metatarsal Angiogenesis Assay Volume and Segment Analysis. Metatarsal bones were dissected from E16.5 C57B6 wild type mice embryos. The bones were placed onto a 0.1% gelatin coated dish and cultured in EGM2. After 2 days incubation at 37°C 5% CO2 the bones were observed and floating samples disregarded. The settled bones then received desired treatment and were reincubated. A) PBS Control B) 10ng/ml LBP C) 20ng/ml LBP D) 10ng/ml LBP + 1µg/ml LPS E) 1µg/ml LPS. Every 3 days the treatment media was replenished and after 9 days the tissue was fixed in 4% PFA, stained with 1:200 PECAM-1 and imaged using a Leica epiflourecent microscope. Images were exported into Imaris for analysis. 8 embryos were used for each experiment, yielding 4-7 bones per treatment. Student t-test was performed and the standard error of the mean calculated for each treatment p = <0.05 * <0.001 ** <0.0001 *** (n=4).

Overall, the Imaris analysis of the metatarsal samples suggested that in contrast to the Matrigel and aortic ring assay, 10ng/ml LBP did not significantly increase angigogenesis, however 20ng/ml LBP promoted a statistically significant increase in vascular growth although the effect was smaller than that observed in the aortic ring assay. There are many possible reasons for the differences in response magnitude in these two experimental models. For example they could be due to the different cell types present within each culture and the age of the tissue. The Matrigel assay contains only cultured HUVEC (human macrovascular endothelium) and the aortic ring has adult rodent microvascular endothelia with supporting cells (e.g. smooth muscle cells), whereas the metatarsal assay uses embryonic tissue with developing endothelia, fibroblasts and supportive osteoblast cells. If one assumes the existence of a receptor for LBP, it could be that the osteoblasts, or other supporting cells express this molecule, and that modulation of those cells by LBP indirectly contributes to endothelial cell growth. Another possibility could be that embryonic endothelia lack the necessary receptor(s) or signalling molecules needed for a full LBP response, or that the activity of other angiogenic signalling pathways in this tissue makes LBP signalling at least partly redundant.

Staining the metatarsals with isolectin B4, PECAM1 and DAPI showed that alongside the expected PECAM1 positive vasculature there was a population of isolectin B4 positive cells. These unidentified cells are present in basal conditions but appeared to decrease upon LPS treatment (figure 28), suggesting that LPS is somehow detrimental to these cells.

2.5 Oxygen Induced Retinopathy (OIR)

Oxygen induced retinopathy (OIR) is a well-established model for investigating angiogenesis and has been in use in mice since 1994 [173]. Neonatal mice are exposed to hyperoxic (75%) conditions, usually from P7-P12. This abundance of oxygen causes retinal vessels to restrict and immature vessels to regress. This regression results in central vaso-obliteration and a delayed development of the deeper plexus. At P12-17 the mice are returned to normal oxygen (21%) conditions, which is sensed as hypoxic by the hyperoxic central retina, resulting in growth factor induction and vessel sprouting [173-175]. We used the OIR model to induce pathologic

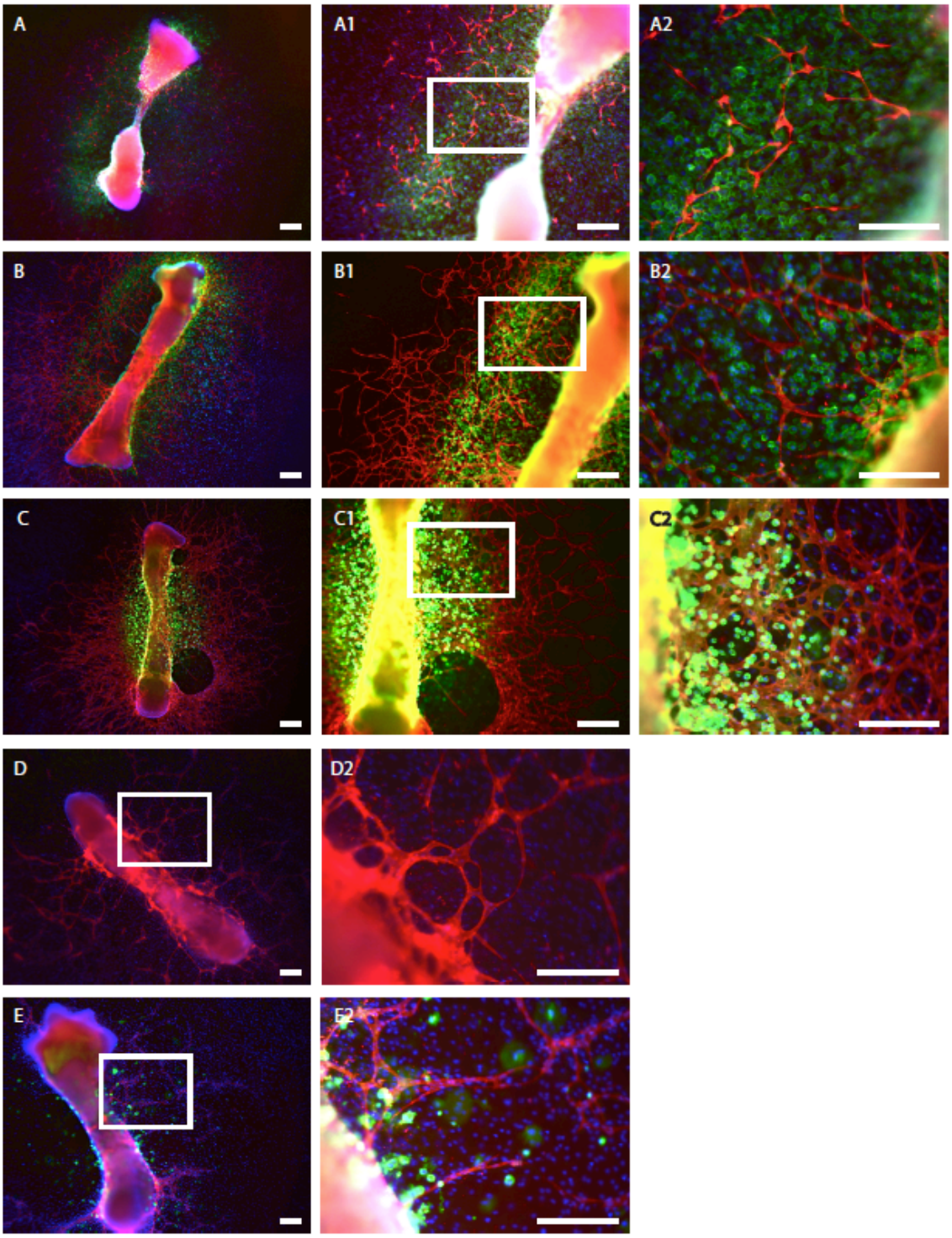

Figure 28: Non-Vascular Cell Types in the Mouse Metatarsal Assay. Metatarsals were treated as follows; A) Control, B) 10ng/ml LBP, C) 20ng/ml LBP, D) 10ng/ml LBP + 1µg/ml LPS, E) 1µg/ml LPS and stained with PECAM1 (red), isolectin B4 (green) and DAPI bisbenzimide (blue) and imaged using a Leica epiflourescent microscope. The middle and right hand panels show higher magnification images of the corresponding low power images on the left. In the presence of LBP we observed an increase in an unidentified isolectin B4 positive cell type. This cell type was much less evident in the presence of LPS. (Scale = 100µm).

angiogenesis in the mouse eye in order to find out how the changes in oxygen tension might affect LBP expression. Three C57B6 wild type mice were placed into the hyperoxic conditions until P12 when their eyes were removed, neuroretinas dissected, RNA isolated for cDNA synthesis and LBP expression analysed via q-PCR. At this stage the retina is oxygen-rich and there is little vascular growth.

The other set of three mice were also kept in hyperoxic conditions until P12 when they were placed into normal (hypoxic perceived) oxygen conditions until P17 when their eyes were removed, neuroretinas dissected, RNA isolated for cDNA synthesis and LBP mRNA expression analysed via q-PCR, with normalisation to ß-actin expression. At P17 the retina is depleted of oxygen and there is a sudden burst in vascular growth, therefore an increase in LBP expression at this time point would be consistent with a role in vascular proliferation *in vivo*. This may also indicate that the LBP promoter could contain a hypoxic response element (e.g. HIF) as in the case for certain established growth factors, such as VEGF [176].

The results showed that at P12 LBP expression was down regulated relative to *ß-actin*, whilst at P17 it was up regulated (figure 29). This pattern mirrored that of VEGF [177], and is similar to other known regulators of angiogenesis such PlGF [178] and provides correlative evidence of an angiogenic role for LBP in an *in vivo* model, that supports the findings described earlier using *ex vivo* tissue models.

3. Chapter Discussion

The picture that emerges from these studies is that LBP clearly has a biological activity independent of its established role as a partner for LPS. To elicit the effects observed in these experiments it must therefore be assumed that LBP either binds to a cell surface receptor on endothelial or associated cells, or that its binds to another soluble factor, which in turn associates with a cell receptor.

The Matrigel assay is the simplest model of angiogenesis used here, and has the advantage that using solely HUVEC removes the complication of multicellular interactions and the inevitable interplay between different cell types and their signalling activities

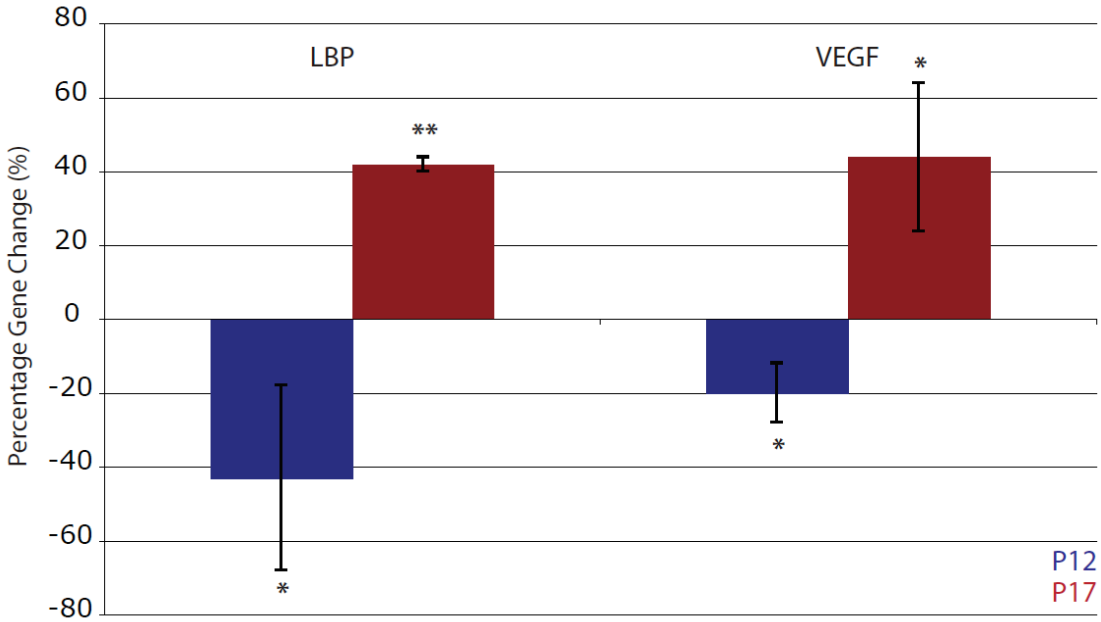

Figure 29: q-PCR Anlalysis of *LBP* expression after Mouse Oxygen-Induced Retinopathy (OIR). Neonatal C57B6 mice p9-12 were maintained in hyperoxic (75%) conditions and then place into standard oxygen conditions (21%) at p12-17. The eyes were removed at either p12 immediately after hyperoxia or at p17 after 5 days in perceived hypoxic conditions. The RNA was isolated (quality checked using Thermodynamic Nanodrop), cDNA synthesised and q-PCR analysis performed. *LBP* expression was normalised to *ß-actin, VEGF* expression was normalised to *GAPDH* (Dr. Xiaomeng Wang) and a percentage in gene expression calculated via comparison to mice without OIR (set as 0% change). Student t-test was performed and the standard error of the mean calculated for each treatment p = <0.05 * <0.001 ** <0.0001 *** (n=3).

[166, 167], LBP was found to increase sprout and branch number as well as the number of closed loop formations. The observed vessel sprouting enhancement reveals that LBP is able to promote HUVEC proliferation. Branching and loops are an indication of vascular network complexity and so suggest that LBP does more then just promote endothelial cell growth. If we consider sprout formation to approximate to sprouting angiogenesis, and complexity to provide a model of intussusceptive angiogenesis the data suggest that LBP may either potentiate VEGF signalling, which is known to be required for both angiogenic processes [11, 25, 26], or it could be inducing alternate pathways more specific to the type of growth alteration observed. Alternatively, LBP may have an activity similar to that of other angiogenic growth factors.

In the aortic ring assay there is little if any spontaneous sprouting in basal conditions so 50ng/ml VEGF is added as a supplement to provide a positive control. Surprisingly 50ng/ml LBP induced the same level of vascular sprouting as VEGF. It could be suggested from this observation that in this assay LBP is as potent an angiogenic factor as VEGF. However, it may be that the aortic ring tissue is relatively rich in the hypothetical LBP receptors and that the comparatively modest VEGF response indicates low levels or inaccessibility of VEGFR2'. Interestingly, with treatment using 20ng/ml LBP + VEGF we observed an additive growth effect, as well as the presence of other unidentified cell types. These cells did not stain with Iba or F4/80, suggesting that they are not macrophages (data not shown). Morphologically, the cells resemble dendritic cells, which are known to play a role in angiogenesis [178, 179] but further staining would be required to identify these cells and determine their role in the assay. There are several possible explanations LBP enhancing the vascular growth we observed with VEGF alone; LBP may induce vascular growth via an angiogenic signalling pathway distinct to that of VEGF, so when both pathways are active this leads to increased growth. A second possibility is that LBP induces VEGF or another angiogenic growth factor to stimulate vascular growth even further. Our observations in the VLDLR$^{-/-}$ mouse, in which a substantial increase in *LBP* expression occurred just prior to the burst in *VEGF* expression may support the latter suggestion.

Imaris rendered images of the metatarsal assay suggest that LBP may influence larger vessel growth more than small vessels, however the assignment of vascular sprouts

into macro and micro phenotypes by the filament tracer did not appear completely accurate with the programme often labelling the initial vessel sprout as a macro-vessel and the terminal peripheral sprouts as microvessels. It may be that the terminal sprouts are more microvascular in nature but when regarding the Imaris images it appears that the assignment of 'micro' appears to be more dependent on the position of the sprout as opposed to its morphology, that is to say that some of the initial sprouts appear just as thin as the terminal sprouts, but because they are located close to the metatarsal the programme labels them as macrovessels. However, if the Imaris assignments are correct, this might imply that the end micro-sprouts have not fully matured into vessel tubes and so may not express the requisite cell surface markers or hypothetical receptors necessary to elicit a response to LBP. It would be interesting to isolate RNA from samples taken from macro and micro sections to identify whether there are any differences in gene expression between the two Imaris designated vascular types.

Interestingly, as in the aortic ring assay, we observed that LBP treatment correlated with an increase in an isolectin B4 positive, unidentified cell type. Whether these are the same cell type in both arrays and whether they play a role in vascular growth is not known, but LPS treatment (where we observe a decrease or inhibition of angiogenesis) appeared to decrease the number of these cells, which suggests that they could indeed contribute to angiogenesis.

In each assay LBP significantly enhanced vessel formation when used alone, though with a dramatic inhibition of these effects upon coincident addition of LPS. In combination, LBP + LPS will almost certainly induce an inflammatory response (providing the target cells express the required CD14 and TLR4), which in itself did not appear to affect basal levels of vascular growth. This supports LBP-induced inflammation as not being inherently detrimental to endothelial cells and suggests that LBP is not required for basal/physiological levels of vascular growth. Indeed, the sole publication describing the LBP knock-out mouse reported the animals to be essentially normal, and made no mention of any vascular phenotype [174]. Independent LPS treatment appeared to inhibit vessel growth suggesting that LPS may be cytotoxic and supporting the idea that LBP functions as an LPS 'catcher', to prevent or protect against the possible cytotoxic effects of endotoxin.

The OIR model showed *LBP* expression to be down-regulated in hyperoxic conditions and up-regulated in hypoxic conditions, providing further indirect support for a role in pathogenic angiogenesis. Thus, consistent with *VEGF*, *LBP* expression in adult C57B6 wild type was suppressed in hyperoxia, but elevated during hypoxia.

Taken together, these three angiogenesis assays and one induced *in vivo* angiogenic model provide compelling evidence that LBP is able to induce vascular growth. These observations imply that LBP has a function, independent from LPS, and suggests that LBP possess a novel growth factor activity. However it is important to note that these assays do not identify whether it is LBP itself that drives the vascular effects, or whether LBP is in fact inducing another factor (e.g. VEGF) that then mediates the angiogenic effects observed. Either way, the data imply the existence of a receptor for LBP on endothelial cells, and initial attempts to identify this molecule form the next chapter.

Results Chapter Three

Investigation of the LBP Signalling Mechanism

Chapter Three
Investigation of the LBP Signalling Mechanism

1. Background

The current view of LBP is that it functions only when bound to LPS. During bacterial infection LBP binds to LPS and then either presents the endotoxin to CD14, inducing TLR4 signalling, activating NF-kß and inducing an inflammatory response [112, 151] or it promotes lipoprotein clearance of LPS from the circulation [181, 182]. Indeed, this was verified by the sole publication describing the LBP knock-out mouse, in which, the animals were shown to avoid septic shock upon endotoxin infection [181]. However, the observation reported in previous chapters suggest that LBP is capable of inducing an angiogenic response, and q-PCR analysis showed that LBP is expressed in Müller cells. These observations suggest that HUVEC and Müller cells would be appropriate cell types in which to investigate LBP signalling.

1.2. Aim

The aim of work in this chapter was therefore to use biological and biochemical techniques to explore the cellular responses to LBP, and to attempt to identify a candidate LBP receptor.

2. Results

2.1 Investigating the angiogenic switch

It has been shown that macrophages which are co-stimulated with LBP + LPS and an A2aR agonist (e.g. adenosine) undergo an alteration in intracellular signalling, switching off the normal LBP + LPS inflammatory response and instead inducing VEGF expression [136]. We wanted to investigate whether other cell types were able to make this signalling switch and whether LBP + adenosine, without LPS could still induce VEGF.

HUVEC and Müller cells were plated onto 35mm^2 culture dishes, and serum-starved overnight before being subjected to a variety of treatments (PBS control, 10ng/ml LBP + 1µg/ml LPS, 10ng/ml LBP + adenosine, 1µg/ml LPS, 1µM adenosine or 1µM

adenosine + 1µg/ml LPS + 10ng/ml LBP) for 12h. Cells were then lysed and analysed for VEGF expression using q-PCR.

The results of this one-off experiment showed a slight decrease in *VEGF* expression in HUVEC, and a small increase in Müller cells (figure 30). However as HUVEC are reported to express very low levels of VEGF [183] the decrease we observed with all treatment is unlikely to be physiologically meaningful. Müller cell *VEGF* expression was affected by all treatments, suggesting that the responses are probably non-specific. Taken together, these result suggest that the angiogenic switch does not occur in HUVEC or Müller cells and that LBP + adenosine alone do not induce VEGF in these cell lines. However it was noted that the cells were starved for 12h prior to a 12h treatment so it could be that the stress caused by 24h serum deprivation altered their signalling abilities or that different time points would have led to different outcomes.

2.2 LBP does not induce NF-kß signalling

LBP is known to induce NF-kß signalling when bound to LPS [115, 126]. We hypothesised that if LBP has an angiogenic activity independent of LPS, then it would be unlikely to stimulate the classic NF-kß pathway when applied on its own. To test this we utilised two read-outs of the NF-kß signalling pathway, ikßα phosphorylation on serines 32 and 36 [177], and p65 nuclear shuttling. As previously discussed (see Introduction 6.2) ikßα sequesters the NF-kß transcriptional elements (e.g. p65) in the cytoplasm in an inactive state. Upon cell activation ikßα is phosphorylated, releasing these transcriptional elements to translocate into the nucleus and drive gene transcription [184]. Therefore, if we observed ikßα phosphorylation and p65 nuclear staining after the cells are treated with LBP, this would suggest that LBP acts on its own much in the same way as it does with LPS.

Müller cells were plated onto 35mm^2 tissue culture dishes and serum-starved overnight before being treated as followed (PBS control, 10ng/ml LBP, 1µg/ml LPS or 10ng/ml LBP + 1µg/ml LPS) for 5min – 1h. The cells were then lysed and the samples resolved by SDS-PAGE with subsequent immunoblot detection of phosphorylated ikßα. The results showed (figure 31) that upon LBP + LPS treatment

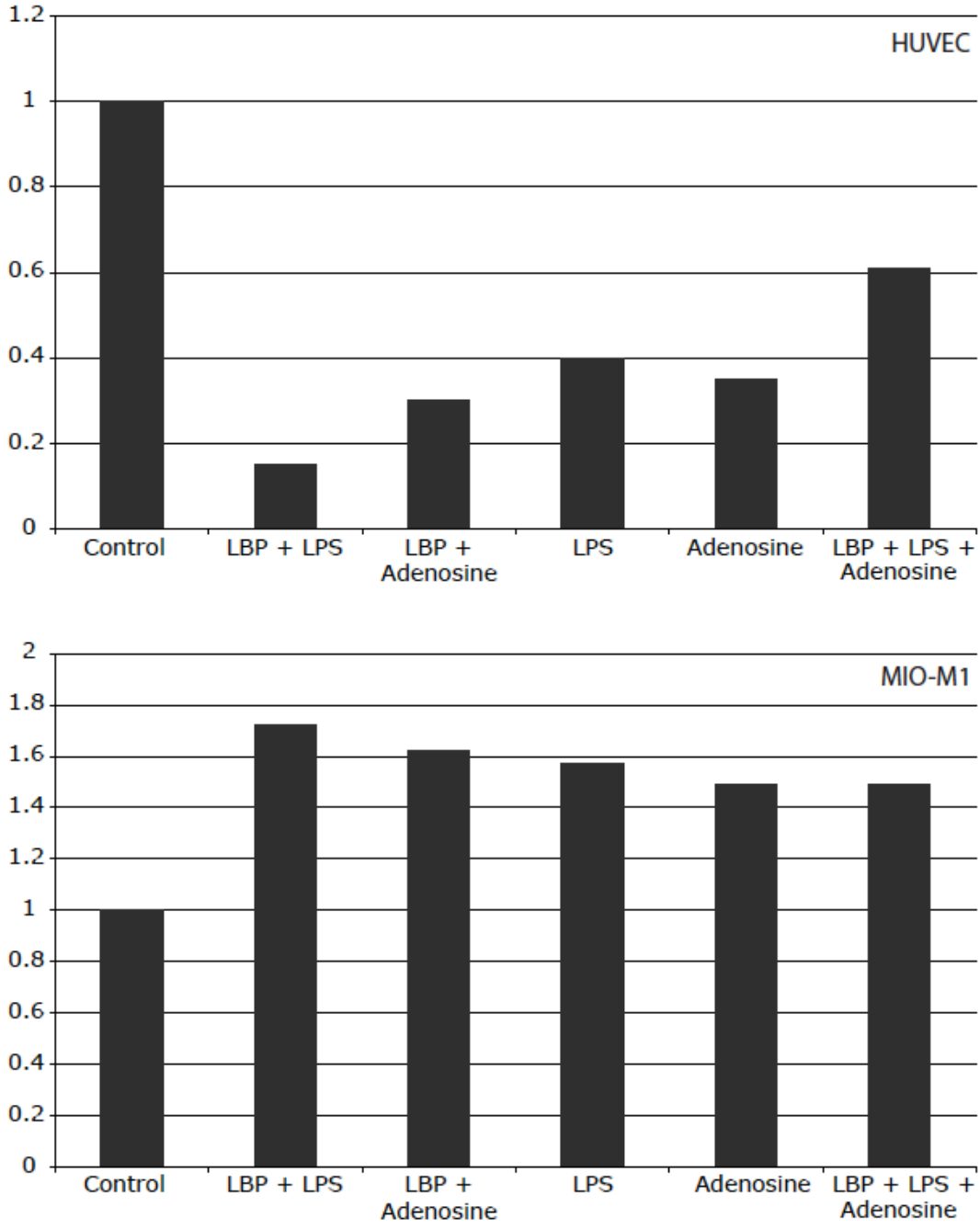

Figure 30: Angiogenic Switch Investigation in HUVEC and Müller cells. HUVEC and Müller cells were seeded onto 35mm^2 culture dishes and starved overnight before being treated with either PBS control, 10ng/ml LBP + 1µg/ml LPS, 10ng/ml LBP + 1µM adenosine, 1µg/ml LPS, 1µM adenosine or 1µM adenosine + 1µg/ml LPS + 10ng/ml LBP for 12h. Cells were then lysed, RNA isolated and cDNA synthesised. *VEGF* expression was analysed using q-PCR and the fold change in *VEGF* expression calculated by normalisation to cell matched *ß-actin* expression levels. (n=1)

ikßα was phosphorylated but that there was no response to LBP treatment alone. Thus, LBP treatment alone does not appear to activate NF-kß in Müller cells.

Next, HUVEC and Müller cells were plated onto 35mm^2 tissue culture dishes and starved overnight before being treated with the desired treatment (PBS control, 10ng/ml LBP or 10ng/ml LBP + 1µg/ml LPS) for 15 min, fixed with PFA, permeabilised with Triton-X 100 and stained with antibodies to detect p65. The results showed that again, whilst LBP + LPS treatment was sufficient to induce p65 nuclear translocation, LBP treatment alone was not (figures 32 and 33). These observations support the ikßα phosphorylation data and provide evidence that LBP is unable to induce NF-kß signalling independent of LPS.

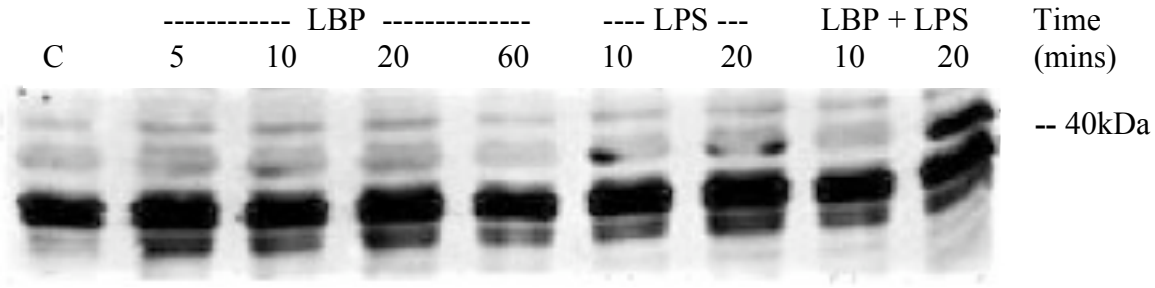

Figure 31: ikßα phosphorylation observed in Müller cells. MIO-M1 Müller cells were treated with 10ng/ml LBP, 1µg/ml LPS or 10ng/ml LBP + 1µg/ml LPS for 5min – 1h, lysed and samples ran on a 10% SDS gel before being immunoblotted with an antibody to detect serine 32/36 phosphorylated ikßα. Bands were visualised using ECL. The imaged gel was inverted in ImageJ. The line depicts the phospho- ikßα protein band.

2.3 LBP induces a phosphotyrosine response

Having established that LBP alone did not elicit the same response as LBP + LPS, we next used two non-specific read-outs of cell activation, namely ERK phosphorylation and global tyrosine phosphorylation, to gain insight into the cellular responses to LBP.

Two immortalised rat brain endothelial cell lines, GPNT [186] and RBE4 [187], and Müller cells were plated onto 35mm^2 tissue culture dishes and starved overnight before being treated with either PBS (control), 10ng/ml LBP or 10ng/ml LBP + 1µg/ml LPS for 0-8h. The cells were then lysed and the samples resolved by SDS-PAGE prior to western blotting and immuno-detection of phosphotyrosine. The results showed that LBP was able to induce protein tyrosine phosphorylation in all of

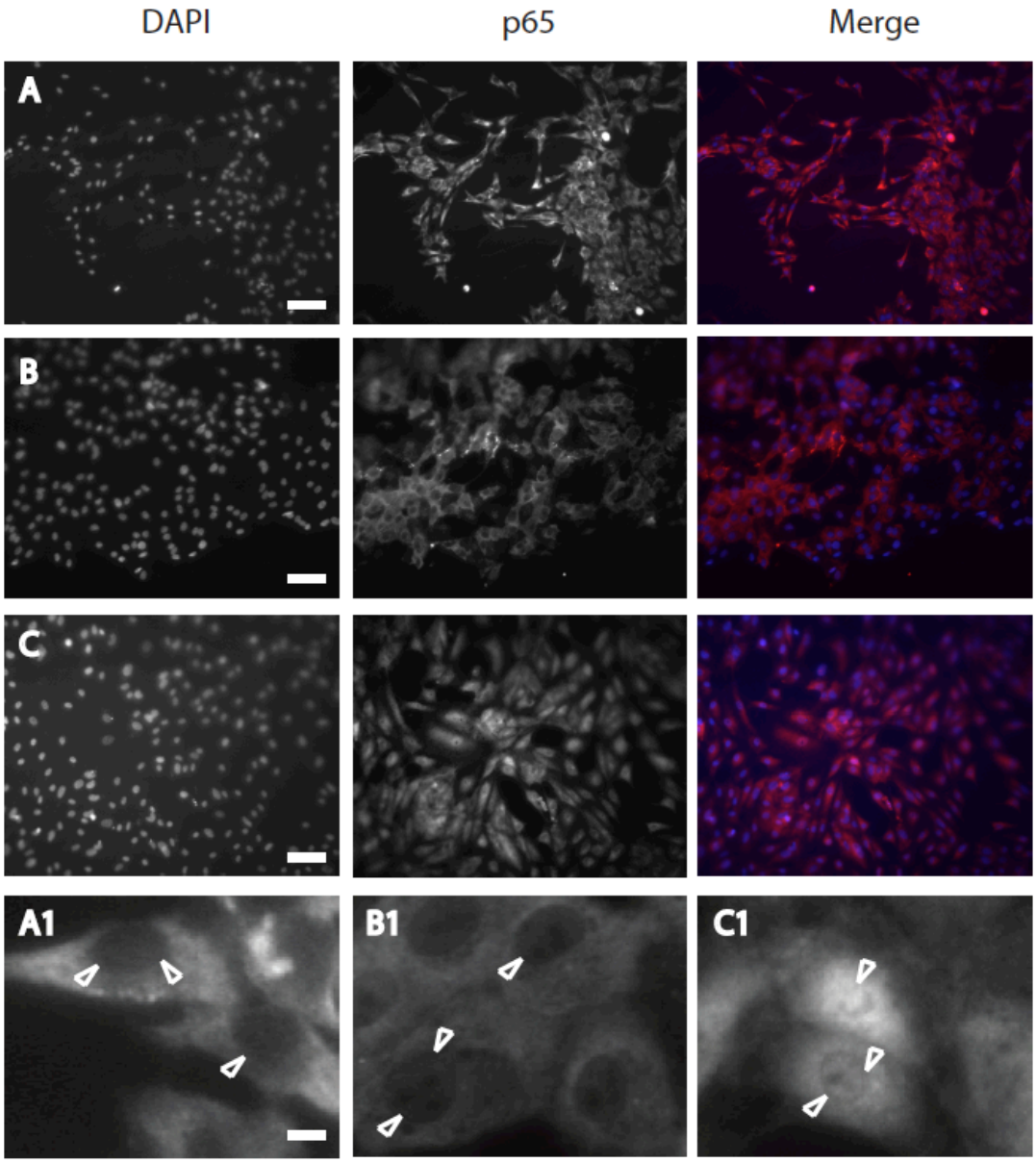

Figure 32: Nuclear Translocation of p65 in HUVEC. HUVEC (passage 2) were seeded onto 35mm^2 culture dishes, cultured in EGM2 and left to reach 70% confluence before being serum starved overnight and treated with either A) PBS control, B) 10ng/ml LBP or C) 10ng/ml LBP + 1µg/ml LPS for 15min. Cells were then fixed in 4% PFA and incubated with an antibody to detect p65 (Santa Cruz C20, 0.2µg/ml) and Dapi bisbenzimide (1µg/ml). Cells were then imaged using a Leica epifluorescent microscope. A1-C1 are magnifications with arrows showing the cell nucleus. (n=3) (Scale = 40µm, zoom = 5µm).

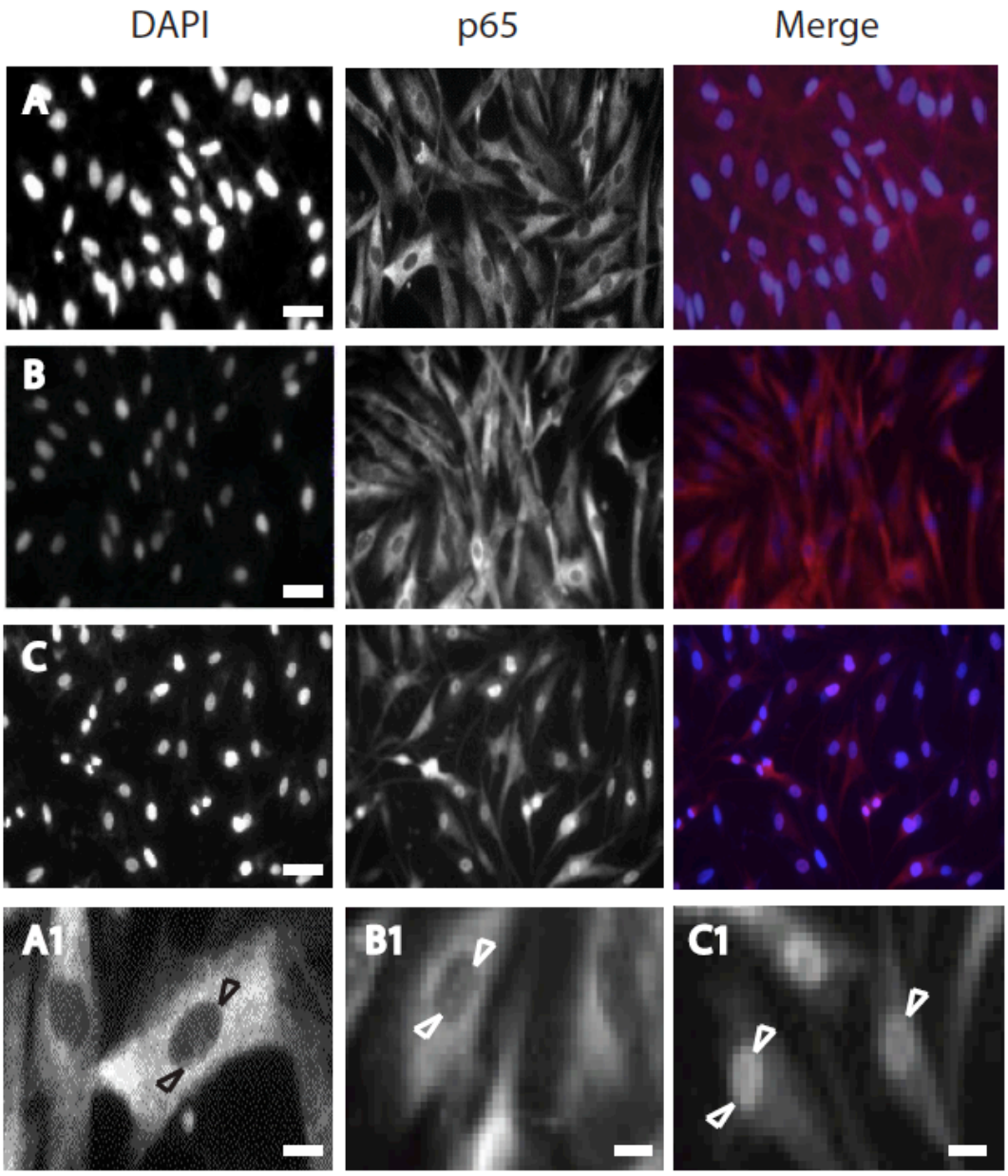

Figure 33: Nuclear Translocation of p65 in MIO-M1 Cells. MIO-M1 Müller cells were seeded onto 35mm^2 culture dishes, cultured in DMEM with 10% FCS and left to reach 70% confluence before being serum starved overnight and treated with either A) PBS control, B) 10ng/ml LBP or C) 10ng/ml LBP + 1µg/ml LPS for 15min. Cells were then fixed in 4% PFA and incubated with an antibody to detect p65 (Santa Cruz C20, 0.2µg/ml) and Dapi bisbenzimide (1µg/ml). Cells were then imaged using a Leica epifluorescent microscope. A1-C1 are magnifications with arrows showing the cell nucleus. (n=3) (Scale = 40µm, zoom = 5µm).

the cell lines tested (see figures 34, 35 and 36). There was some variation in the kinetics of the response, with GPNT taking the longest time to respond, however we noted that two phospho-bands of 60kDa and 150kDa appeared to be most intense in all three cell lines, suggesting that these two proteins could be important for LBP signal transduction.

In order to identify some of the tyrosine phosphorylated proteins we scaled up the process for mass spectroscopy. Müller cells were treated with either PBS or 10ng/ml LBP for 30min and then lysed in 250µl 2x lysis buffer (no SDS). The lysates were first incubated with empty agarose beads in order to clear the samples of sticky protein aggregates. They were then incubated with anti-phosphotyrosine agarose beads before being washed repeatedly to remove any non-specific bound protein. The samples were then heated to denature the antibody, therefore dissociating the proteins from the beads, before being resolved by 10% SDS-PAGE and visualised with Coomassie blue staining (figure 37). The 150-140kDa and 60kDa bands together with a few other prominent bands were then cut out of the gel, placed into Eppendorf tubes and despatched for Mass-Spectroscopy peptide fingerprint sequencing by Alphalyse pick'n'post (figure 38). Alphalyse analysis was unable to obtain sequence from the 140-150kDa protein band but did reveal that the 60kDa protein was vimentin and some other protein bands found to change upon LBP treatment were Myosin-9, heterogeneous nuclear ribonucleoprotein A1 (HNRPA1) and heterogeneous nuclear ribonucleoprotein U (hnRNPU).

The majority of LBP + LPS signalling occurs via TLR4 and has been shown to stimulate protein tyrosine phosphorylation [118], therefore to be sure that what we observed with LBP was different from LBP + LPS treatment, we compared the phosphotyrosine response of HUVEC treated with either LBP alone or LBP + LPS. The results showed that whilst LBP alone was able to induce tyrosine phosphorylation of bands at 150kDa and 60kDa within 30 min, LBP + LPS was not (figure 39). This shows that the phosphotyrosine responses observed in HUVEC and the other cell lines are specific to LBP activity alone. These observations also reaffirm that our experimental systems are absent of LPS, and reinforce the idea that LBP signalling is distinct from signalling by LBP + LPS.

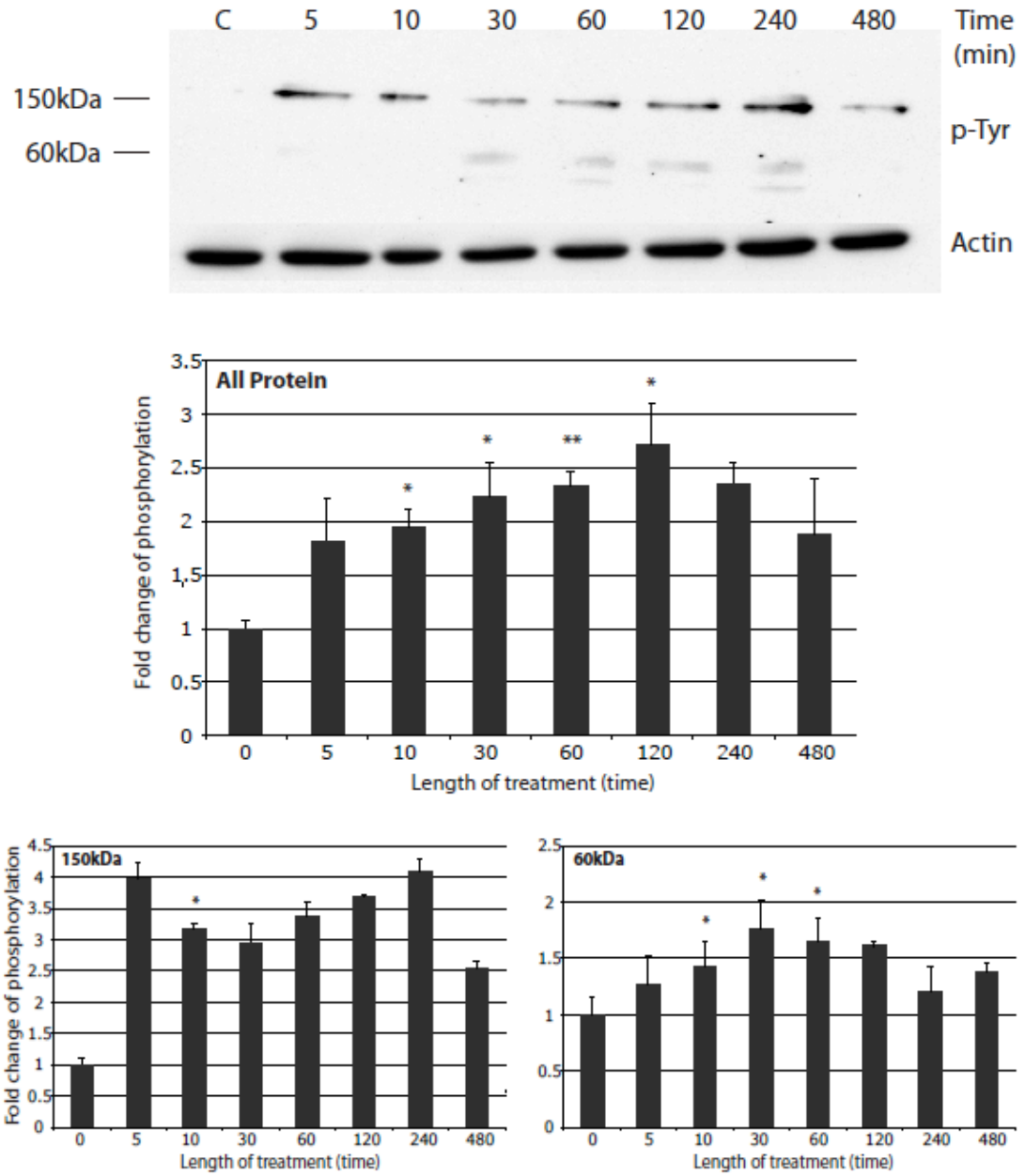

Figure 34: LBP Stimulates Tyrosine Phosphorylation in MIO-M1 Cells. MIO-M1 Müller cells were seeded onto 35mm^2 culture dishes cultured in DMEM with 10% FCS and left to reach 70% confluence before being serum starved overnight and treated with either PBS control or 10ng/ml LBP for 5min – 8h. The cells were then lysed in 200µl 2x lysis buffer and boiled at 95^{o}C for 5 min. 25µl of each sample was resolved via SDS-PAGE, transferred onto nitrocellulose membrane, blocked and incubated overnight at 4^{o}C with 4G10 anti-phosphotyrosine antibody (Millipore 1:3000). The membranes were then developed and films analysed for an increase in phosphotyrosine. Membranes were then stripped and reblocked before being reincubated with an antibody to detect actin (Millipore 1:5000) as a protein loading control. The film images were exported to ImageJ and inverted. A box was traced around the protein band of interest and a mean pixel reading recorded. The phosphotyrosine reading was then divided by the time-matched actin value. Average values for total phosphotyrosine, 150kDa protein band and 60kDa protein band was calculated from 3 experiment repeats. Student t-test was performed and standard error of the mean calculated (n=3) p = <0.05 * <0.001 ** <0.0001 ***

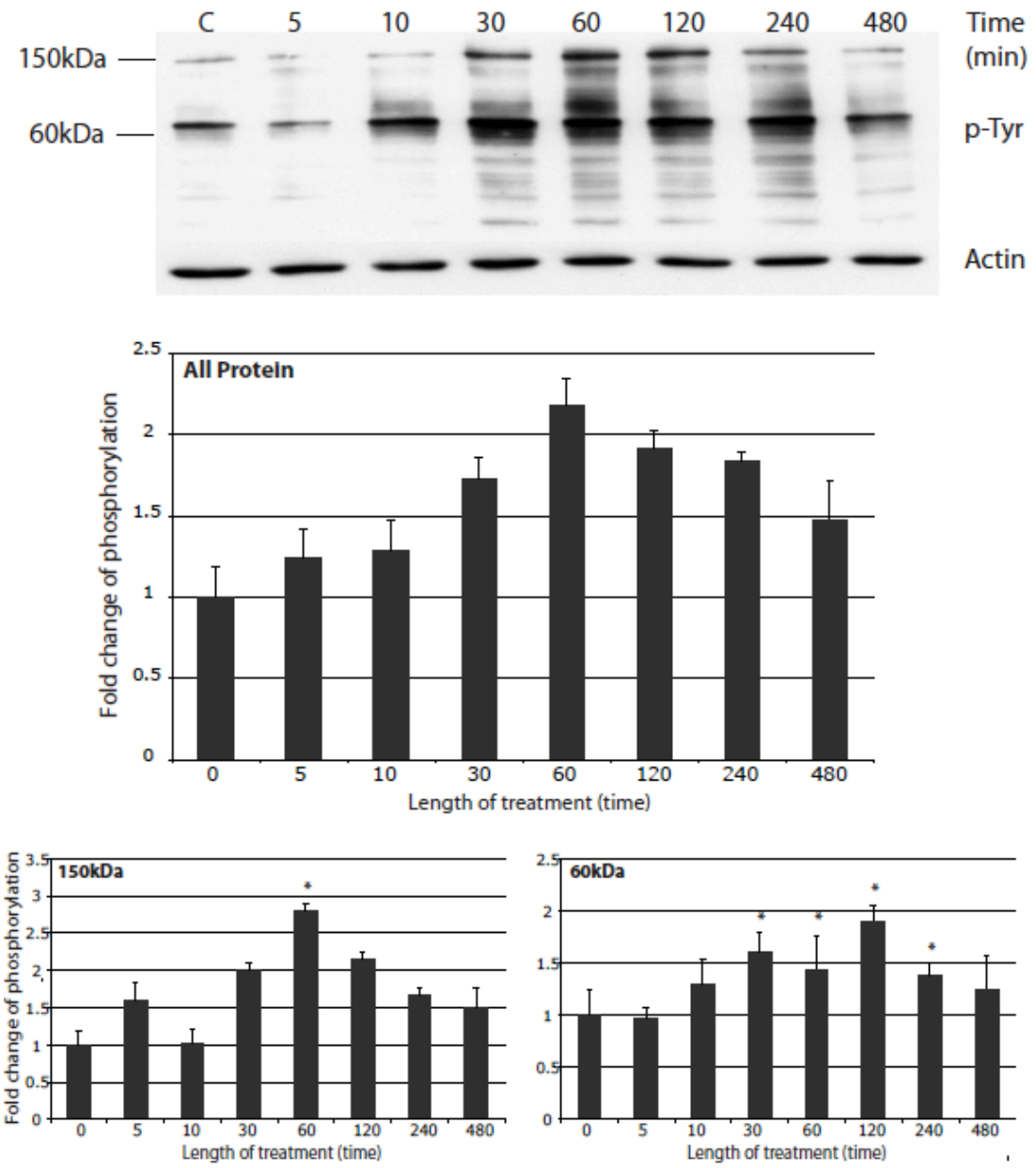

Figure 35: LBP Stimulates Tyrosine Phosphorylation in RBE4 Cells. RBE4 cells were seeded onto 35mm^2 culture dishes, cultured in 1:1 alpha-MEM, F-10 with 10% FCS and left to reach 70% confluence before being serum starved overnight and treated with either PBS control or 10ng/ml LBP for 5min – 8h. The cells were then lysed in 200µl 2x lysis buffer and boiled at 95^{o}C for 5 min. 25µl of each sample was resolved via SDS-PAGE, transferred onto nitrocellulose membrane, blocked and incubated overnight at 4^{o}C with 4G10 anti-phosphotyrosine antibody (Millipore 1:3000). The membranes were then developed and films analysed for an increase in phosphotyrosine. Membranes were then stripped and reblocked before being reincubated with an antibody to detect actin (Millipore 1:5000) as a protein loading control. The film images were exported to ImageJ and inverted. A box was traced around the protein band of interest and a mean pixel reading recorded. The phosphotyrosine reading was then divided by the time-matched actin value. Average values for total phosphotyrosine, 150kDa protein band and 60kDa protein band was calculated from 3 experiment repeats. Student t-test was performed and standard error of the mean calculated (n=3) p = <0.05 * <0.001 ** <0.0001

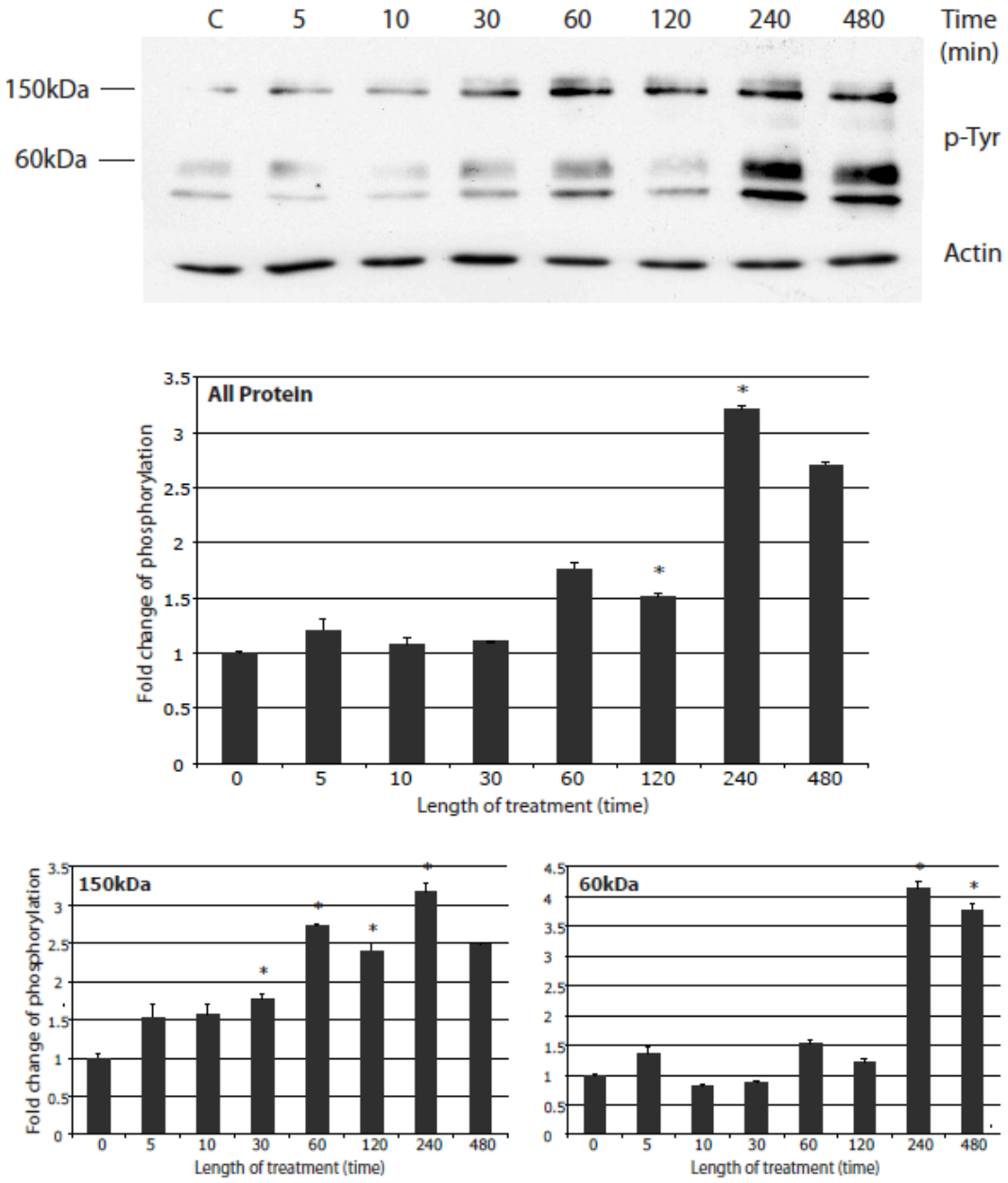

Figure 36: LBP Stimulates Tyrosine Phosphorylation in GPNT Cells. GPNT cells were seeded onto 35mm^2 culture dishes, cultured in 1:1 alpha-MEM, F-10 with 10% FCS and left to reach 70% confluence before being serum starved overnight and treated with either PBS control or 10ng/ml LBP for 5min – 8h. The cells were then lysed in 200µl 2x lysis buffer and boiled at 95^{o}C for 5 min. 25µl of each sample was resolved via SDS-PAGE, transferred onto nitrocellulose membrane, blocked and incubated overnight at 4^{o}C with 4G10 anti-phosphotyrosine antibody (Millipore 1:3000). The membranes were then developed and films analysed for an increase in phosphotyrosine. Membranes were then stripped and reblocked before being reincubated with an antibody to detect actin (Millipore 1:5000) as a protein loading control. The film images were exported to ImageJ and inverted. A box was traced around the protein band of interest and a mean pixel reading recorded. The phosphotyrosine reading was then divided by the time-matched actin value. Average values for total phosphotyrosine, 150kDa protein band and 60kDa protein band was calculated from 3 experiment repeats. Student t-test was performed and standard error of the mean calculated (n=3) p = <0.05 * <0.001 ** <0.0001 ***

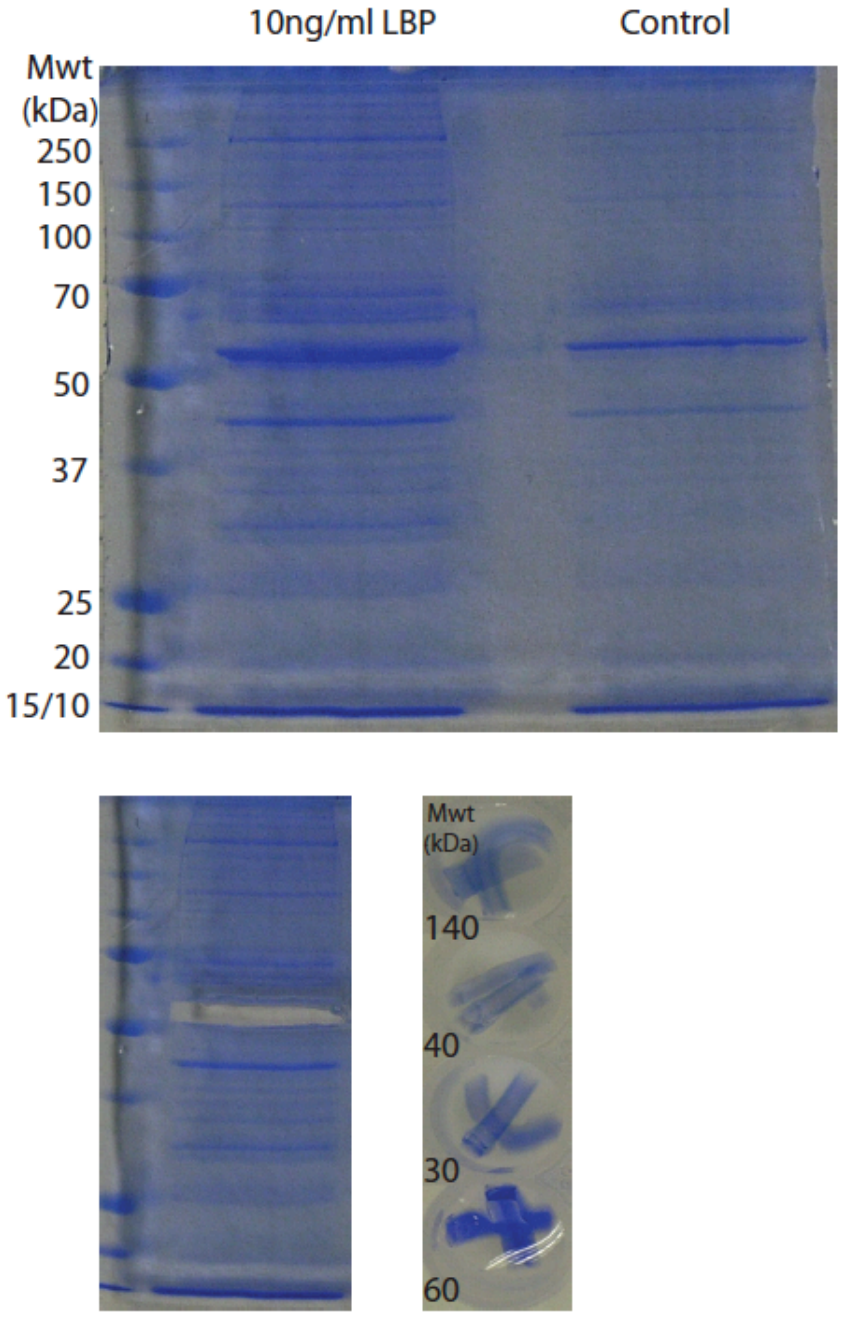

Figure 37: Phosphotyrosine Pull Down of MIO-M1 cells treated with LBP. MIO-M1 Müller cells were seeded onto 35mm^2 culture dishes, immersed in DMEM with 10% FCS and left to reach 70% confluence before being serum starved overnight and treated with either PBS control or 10ng/ml LBP for 30min. The cells were then lysed in 50µl 2x lysis buffer (-SDS) and incubated with agarose beads on a rotator for 1h before being washed in lysis buffer (-SDS) and incubated with anti-phospotyrosine agarose beads at 4^{o}C on a rotator for 2h. The beads were then washed extensively in ice cold PBS before being boiled at 95^{o}C for 5 min. The entire sample was resolved via SDS-PAGE and the gel incubated in comassie blue for 30min before being incubated in destain solution on a shaking plate >8h with frequent solution changes. The gel was then observed (n=2) and any protein bands of interest isolated to be sent to Alphalyse Pick'n'Post for peptide fingerprint mass spectroscopy sequencing.

Myosin-9

```
   1 MAQQAADKYL YVDKNFINNP LAQADWAAKK LVWVPSDKSG FEPASLKEEV
  51 GEEAIVELVE NGKKVKVNKD DIQKMNPPKF SKVEDMAELT CLNEASVLHN
 101 LKERYYSGLI YTYSGLFCVV INPYKNLPIY SEEIVEMYKG KKRHEMPPHI
 151 YAITDTAYRS MMQDREDQSI LCTGESGAGK TENTKKVIQY LAYVASSHKS
 201 KKDQGELEPQ LLQANPILEA FGNAKTVKND NSSRFGKFIR INFDVNGYIV
 251 GANIETYLLE KSRAIRQAKE ERTFHIFYYL LSGAGEHLKT DLLLEPYNKY
 301 RFLSNGHVTI PGQQDKDMFQ ETMEAMRIMG IPEEEQMGLL RVISGVLQLG
 351 NIVFKKERNT DQASMPDNTA AQKVSHLLGI NVTDFTRGIL TPRIKVGRDY
 401 VQKAQTKEQA DFAIEALAKA TYERMFRWLV LRINKALDKT KRQGASFIGI
 451 LDIAGFEIFD LNSFEQLCIN YTNEKLQQLF NHTMFILEQE EYQREGIEWN
 501 FIDFGLDLQP CIDLIEKPAG PPGILALLDE ECWFPKATDK SFVEKVMQEQ
 551 GTHPKFQKPK QLKDKADFCI IHYAGKVDYK ADEWLMKNMD PLNDNIATLL
 601 HQSSDKFVSE LWKDVDRIIG LDQVAGMSET ALPGAFKTRK GMFRTVGQLY
 651 KEQLAKLMAT LRNTNPNFVR CIIPNHEKKA GKLDPHLVLD QLRCNGVLEG
 701 IRICRQGFPN RVVFQEFRQR YEILTPNSIP KGFMDGKQAC VLMIKALELD
 751 SNLYRIGQSK VFFRAGVLAH LEEERDLKIT DVIIGFQACG RGYLARKAFA
 801 KRQQQLTAMK VLQRNCAAYL KLRNWQWWRL FTKVKPLLQV SRQEEEMMAK
 851 EELVKVREK QLAAENRLTE METLQSQLMA EKLQLQEQLQ AETELCAEAE
 901 ELRARLTAKK QELEEICHDL EARVEEEEER CQHLQAEKKK MQQNIQELEE
 951 QLEEEESAKQ KLQLEKVTTE AKLKKLEEEQ IILEDQNCKL AKEKKLLEDR
1001 IAEFTTNLTE EEEKSKSLAK LRNKHEAMIT DLEERLRREE KQRQELEKTR
1051 RKLEGDSTDL SDQIAELQAQ IAELKMQLAK KEEELQAALA RVEEEAAQKN
1101 MALKKIRELE SQISELQEDL ESERASRNKA EKQKRDLGEE LEALKTELED
1151 TLDSTAAQQE LRSKREQEVN ILKKTLEEEA KTHEAQIQEM KQKHSQAVEE
1201 LAEQLEQTKR VKANLEKAKQ TLENERGELA NEVKVLLQGK GDSEHKRKKV
1251 EAQLQELQVK FNEGERVRTE LADKVTKLQV ELDNVTGLLS QSDSKSSKLT
1301 KDFSALESQL QDTQELLQEE NRQKLSLSTK LKQVEDEKNS FREQLEEEEE
```

hnRNPU

```
   1 MSSSPVNVKK LKVSELKEEL KKRRLSDKGL KAELMERLQA ALDDEEAGGR
  51 PAMEPGNGSL DLGGDSAGRS GAGLEQEAAA GGDEEEEEEE EEEEGISALD
 101 GDQMELGEEN GAAGAADSGP MEEEEAASED ENGDDQGFQE GEDELGDEEE
 151 GAGDENGHGE QQPQPPATQQ QQPQQQRGAA KEAAGKSSGP TSLFAVTVAP
 201 PGARQGQQQA GGDGKTEQKG GDKKRGVKRP REDHGRGYFE YIEENKYSRA
 251 KSPQPPVEEE DEHFDDTVVC LDTYNCDLHF KISRDRLSAS SLTMESFAFL
 301 WAGGRASYGV SKGKVCFEMK VTEKIPVRHL YTKDIDIHEV RIGWSLTTSG
 351 MLLGEEEFSY GYSLKGIKTC NCETEDYGEK FDENDVITCF ANFESDEVEL
 401 SYAKNGQDLG VAFKISKEVL AGRPLFPHVL CHNCAVEFNF GQKEKPYFPI
 451 PEEYTFIQNV PLEDRVRGPK GPEEKKDCEV VMMIGLPGAG KTTWVTKHAA
 501 ENPGKYNILG TNTIMDKMMV AGFKKQMADT GKLNTLLQRA PQCLGKFIEI
 551 AARKKRNFIL DQTNVSAAAQ RRKMCLFAGF QRKAVVVCPK DEDYKQRTQK
 601 KAEVEGKDLP EHAVLKMKGN FTLPEVAECF DEITYVELQK EEAQKLLEQY
 651 KEESKKALPP EKKQNTGSKK SNKNKSGKNQ FNRGGGHRGR GGLNMRGGNF
 701 RGGAPGNRGG YNRRGNMPQR GGGGGGSGGI GYPYPRAPVF PGRGSYSNRG
 751 NYNRGGMPNR GNYNQNFRGR GNNRGYKNQS QGYNQWQQGQ FWGQKPWSQH
 801 YHQGYY
```

Vimentin

```
   1 MSTRSVSSSS YRRMFGGPGT ASRPSSSRSY VTTSTRTYSL GSALRPSTSR
  51 SLYASSPGGV YATRSSAVRL RSSVPGVRLL QDSVDFSLAD AINTEFKNTR
 101 TNEKVELQEL NDRFANYIDK VRFLEQQNKI LLAELEQLKG QGKSRLGDLY
 151 EEEMRELRRQ VDQLTNDKAR VEVERDNLAE DIMRLREKLQ EEMLQREEAE
 201 NTLQSFRQDV DNASLARLDL ERKVESLQEE IAFLKKLHEE EIQELQAQIQ
 251 EQHVQIDVDV SKPDLTAALR DVRQQYESVA AKNLQEAEEW YKSKFADLSE
 301 AANRNNDALR QAKQESTEYR RQVQSLTCEV DALKGTNESL ERQMREMEEN
 351 FAVEAANYQD TIGRLQDEIQ NMKEEMARHL REYQDLLNVK MALDIEIATY
 401 RKLLEGEESR ISLPLPNFSS LNLRETNLDS LPLVDTHSKR TLLIKTVETR
 451 DGQVINETSQ HHDDLE
```

HNRAP1

```
   1 MSKSESPKEP EQLRKLFIGG LSFETTDESL RSHFEQWGTL TDCVVMRDPN
  51 TKRSRGFGFV TYATVEEVDA AMNARPHKVD GRVVEPKRAV SREDSQRPGA
 101 HLTVKKIFVG GIKEDTEEHH LRDYFEQYGK IEVIEIMTDR GSGKKRGFAF
 151 VTFDDHDSVD KIVIQKYHTV NGHNCEVRKA LSKQEMASAS SSQRGRSGSG
 201 NFGGGSYNDF GNYNNQSSNF GPMKGGNFGG RSSGPYGGGG QYFAKPRNQG
 251 GYGGSSSSSS YGSGRRF
```

Figure 38: Phosphotyrosine Pull Down Protein Band Sequence Matches. The proteins isolated in figure 35 were subjected to peptide fingerprint mass spectroscopy, and identified as Myosin-9, hnRNPU, Vimentin and HNRAP1. The primary human amino-acid sequences are given for each protein, with the matching peptides highlighted in bold and underlined in each case.

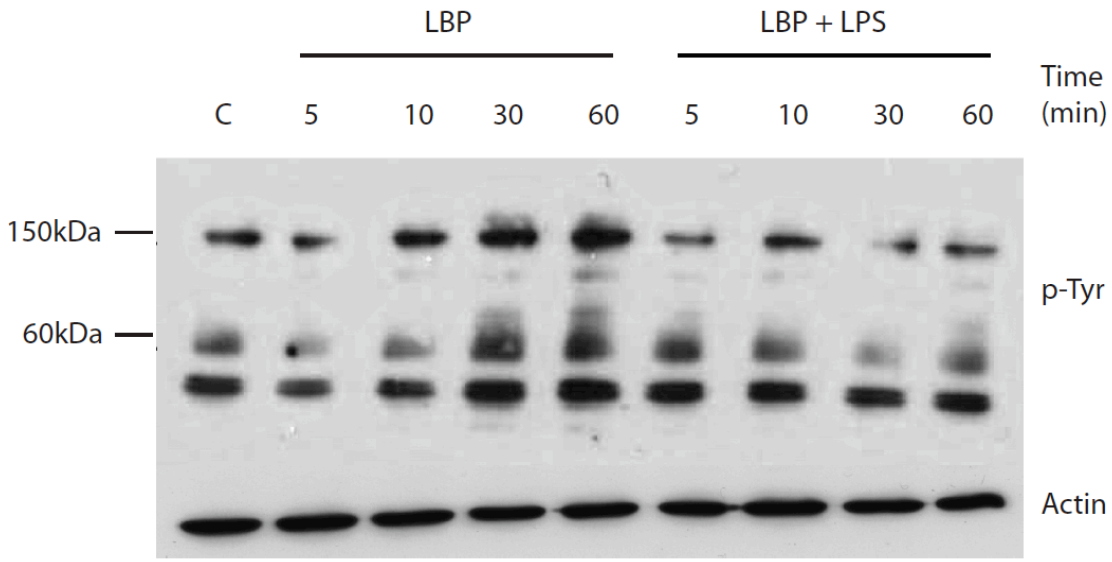

Figure 39: HUVEC protein tyrosine phosphorylation post-LBP treatment. HUVEC (passage 3) were seeded onto 35mm^2 culture dishes, EGM2 and left to reach 70% confluence before being serum starved overnight and treated with either PBS control, 10ng/ml LBP or 10ng/ml LBP + 1µg/ml LPS for 5min – 1h. The cells were then lysed in 200µl 2x lysis buffer and boiled at 95^{o}C for 5 min. 25µl of each sample was resolved via SDS-PAGE, transferred onto nitrocellulose membrane, blocked and incubated overnight at 4^{o}C with 4G10 anti-phosphotyrosine antibody (Millipore 1:3000). The membranes were then developed and films analysed for an increase in phosphotyrosine. Membranes were then stripped and reblocked before being reincubated with an antibody to detect actin (Millipore 1:5000) to use as a protein loading control. The film images were exported to ImageJ and inverted (n=2).

2.4 LBP induces ERK phosphorylation

Previous angiogenesis assays demonstrated that LBP increases vascular growth, and data in the previous section show that LBP promotes phosphotyrosine signalling independently of LPS, therefore we decided to focus our attention on signalling pathways that could influence cell proliferation and survival. As mentioned earlier (See Introduction 6.4) the ERKs are a family of serine/threonine kinases that are phosphorylated during cell activation and have roles in a wide range of cellular processes including survival, cell cycle and proliferation [139, 142]. We wanted to investigate whether LBP was able to induce ERK phosphorylation as this would be consistent with the angiogenic activity of LBP reported earlier.

HUVEC and Müller cells were plated onto 35mm^2 tissue culture dishes and starved overnight before being treated with PBS (control), 10ng/ml LBP or 10ng/ml LBP + 1μg/ml LPS for 5min – 1h. Cells were then lysed and the samples resolved by SDS-PAGE, followed by western transfer, and then immunoblot detection of phospho-ERK. The results showed that LBP was able to induce a phospho-ERK response in both HUVEC and Müller cells within 5 min (figure 40). The effect appeared stronger but transient in the Müller cells with basal levels of phospho-ERK re-established 30 min after treatment. HUVEC showed a smaller but prolonged response, with phospho-ERK still apparent 1h after treatment. This suggests some differences between the cell lines, consistent with the variations we had previously observed in phosphotyrosine responses. When the Müller cells were treated with LBP + LPS there appeared to be some phospho-ERK induction but this was not as marked as when cells were treated with LBP alone. HUVEC did not exhibit a phospho-ERK response when treated with LBP + LPS, indicating that their phospho-ERK response was specific to LBP.

2.5 Identification of a candidate LBP receptor

During the Matrigel assay experiments we had observed that once the HUVEC were beyond passage 10 they stopped being responsive to LBP treatment (figure 41). It is well known that as primary cells are passaged they alter their patterns of gene expression. This suggested to us that >p10 HUVEC no longer express the hypothetical 'LBP receptor' required for signal activation. As Müller cells had been

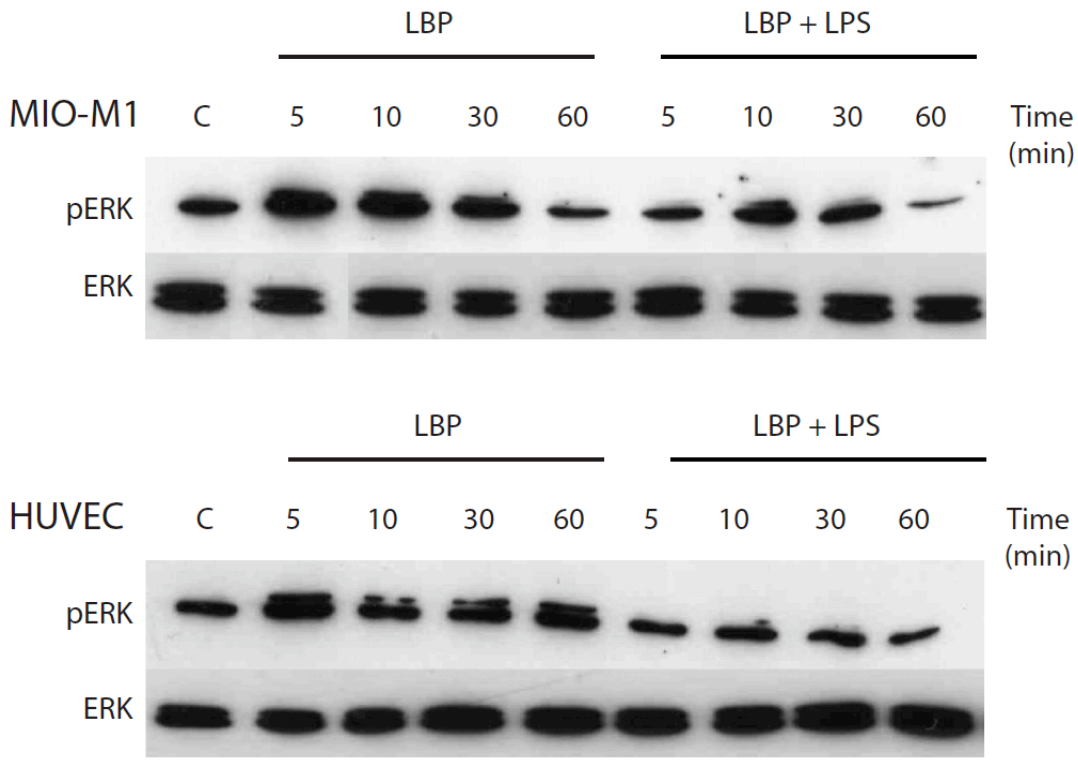

Figure 40: MIO-M1 and HUVEC phosphorylated ERK response post-LBP +/- LPS Treatment. MIO-M1 Müller cells and HUVEC (passage 3) were seeded onto 35mm^2 culture dishes and immersed in DMEM 10% FCS or EGM2 respectively. The cells were left to reach 70% confluence before being serum starved overnight and treated with either PBS control, 10ng/ml LBP or 10ng/ml LBP + 1µg/ml LPS for 5min – 1h. The cells were then lysed in 200µl 2x lysis buffer and boiled at 95^{o}C for 5 min. 25µl of each sample was resolved via SDS-PAGE, transferred onto nitrocellulose membrane, blocked and incubated overnight at 4^{o}C with an anti phospho-ERK antibody (Cell signalling 1:3000). The membranes were then developed and films analysed for an increase in phospho-ERK. Membranes were then stripped and reblocked before being reincubated with an antibody to detect ERK (Millipore 1:5000) to use as a protein loading control. The film images were exported to ImageJ and inverted (n=2).

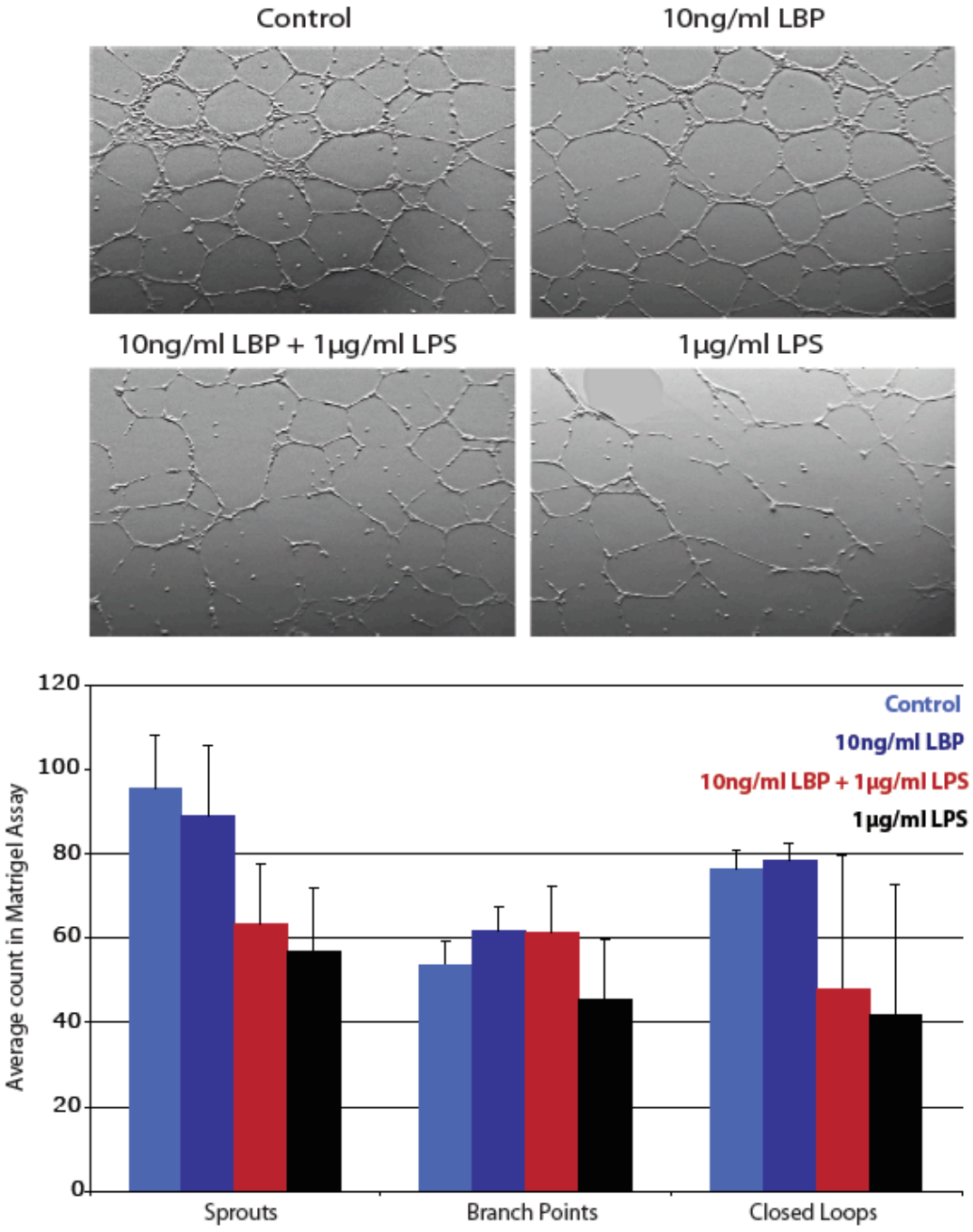

Figure 41: HUVEC (passage 10) Matrigel Angiogenesis Assay. HUVEC were seeded onto growth factor reduced Matrigel (BD) at $2x10^5$/ml cell density. Treatments were then added (PBS control, 10ng/ml LBP, 10ng/ml LBP + 1µg/ml LPS or 1µg/ml LPS and the gels incubated overnight at 37°C 5% CO_2. The gels were imaged using a Lecia epifluorescence microscope under brightfield conditions. Sprouts, branch points and closed loops were counted manually. Student's t-test was performed and standard error of the mean calculated p = <0.05 * <0.001 ** <0.0001 *** (n=3).

found to respond to LBP regardless of passage number we decided to compare old and young HUVEC to Müller cells with the assumption that commonalities could lead to the identification of a candidate LBP receptor. In an attempt to focus the search we decided to test three receptor families. These were the TLRs, since LBP + LPS signal via TLR4 [121], and the glypican and syndecan families because BPI, the protein with the highest sequence and structural homology to LBP, has been reported to signal through glypican-4 [112, 124].

RNA was isolated from old (passage 13) and young (passage 2) HUVEC and Müller cells. cDNA was synthesised and RT-PCR was used to check for TLR, glypican and syndecan expression. The results showed (figure 42) that the old and young HUVEC both express TLR4, suggesting that LBP does not elicit angiogenic responses via the receptor it binds with LPS. When passaged the HUVEC lose expression of TLR1, which would be consistent with a candidate LBP receptor, however Müller cells showed no TLR1 expression suggesting this is not the case. Old and young HUVEC did not express any of the glypicans unlike Müller cells, which express glypican-5. Interestingly the early passage HUVEC expressed one member of the syndecan family, namely syndecan-2, which was also expressed at high levels in the Müller cells and was lost in passage 13 HUVEC (figure 43). Therefore, among the three protein families, this singled out syndecan-2 as the sole candidate LBP receptor. Interestingly, syndecan-2 is the only member of these receptor families reported to play a role in angiogenesis, through potentiation of VEGF-A signalling [188].

2.6 siRNA knock down of syndecan-2 inhibits the LBP phospho-ERK response

Having identified syndecan-2 as a candidate LBP receptor the aim of the next experiment was to knock-down syndecan-2 expression and observe any changes in the LBP-induced phospho-ERK response. Ideally HUVEC would have been used for this experiment but due to time constraints and a requirement for an adenovirus-induced knockdown the protocol was instead attempted in Müller cells using oligofectamine. However, after numerous attempts at optimisation an effective knock-down was not achieved, and we were forced to consider other options. We found that Hela cells express syndecan-2, have a phospho-ERK response to LBP treatment and can achieve a reasonable syndecan-2 RNA knock-down within 2 days (figure 44). Therefore Hela cells were used for testing the requirement of syndecan-2

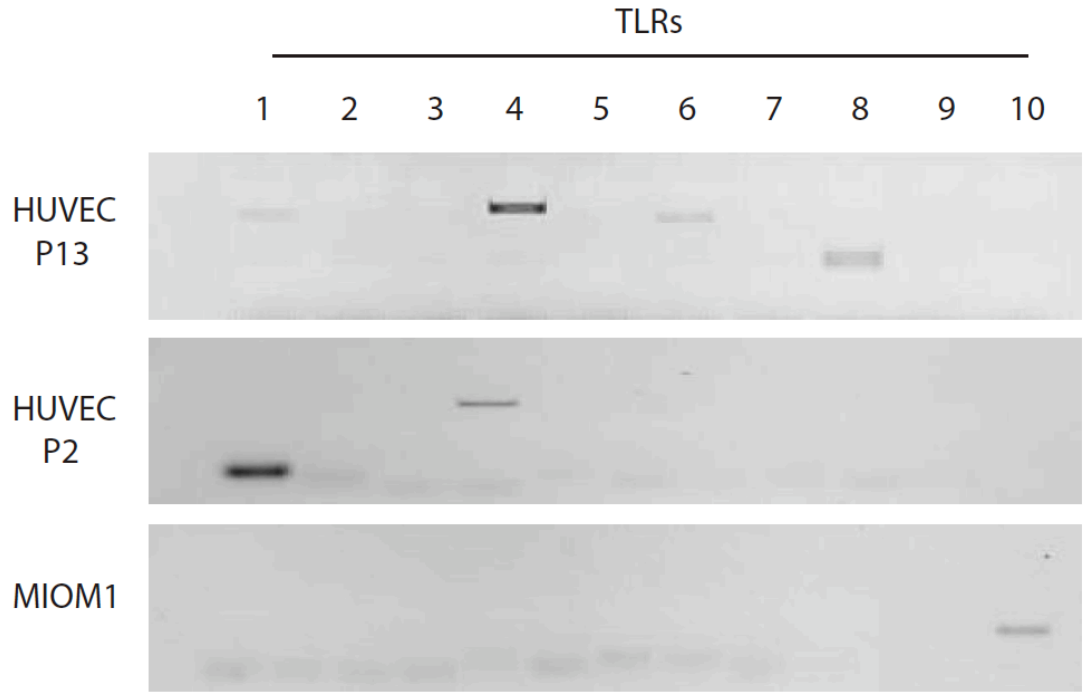

Figure 42: HUVEC and MIO-M1 Toll-Like Receptor RT-PCR Analysis. HUVEC (passage 2 and 13) and MIO-M1 Müller cells were seeded onto 35mm^2 culture dishes and immersed in EGM2 or DMEM 10% FCS respectively. RNA was isolated, cDNA synthesised and RT-PCR analysis performed to analyse TLR receptor expression.

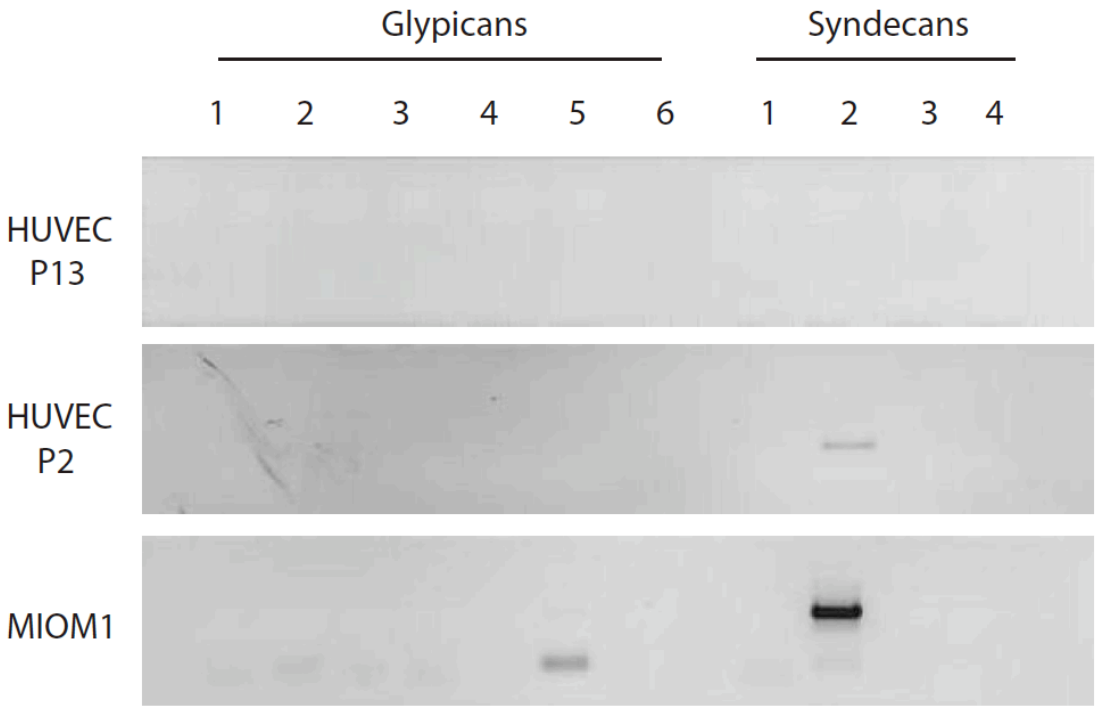

Figure 43: HUVEC and MIO-M1 Glypican and Syndecan RT-PCR Analysis. HUVEC (passage 2 and 13) and MIO-M1 Müller cells were seeded onto 35mm^2 culture dishes and immersed in EGM2 or DMEM 10% FCS respectively. RNA was isolated, cDNA synthesised and RT-PCR analysis performed to analyse GPC and SDC receptor expression.

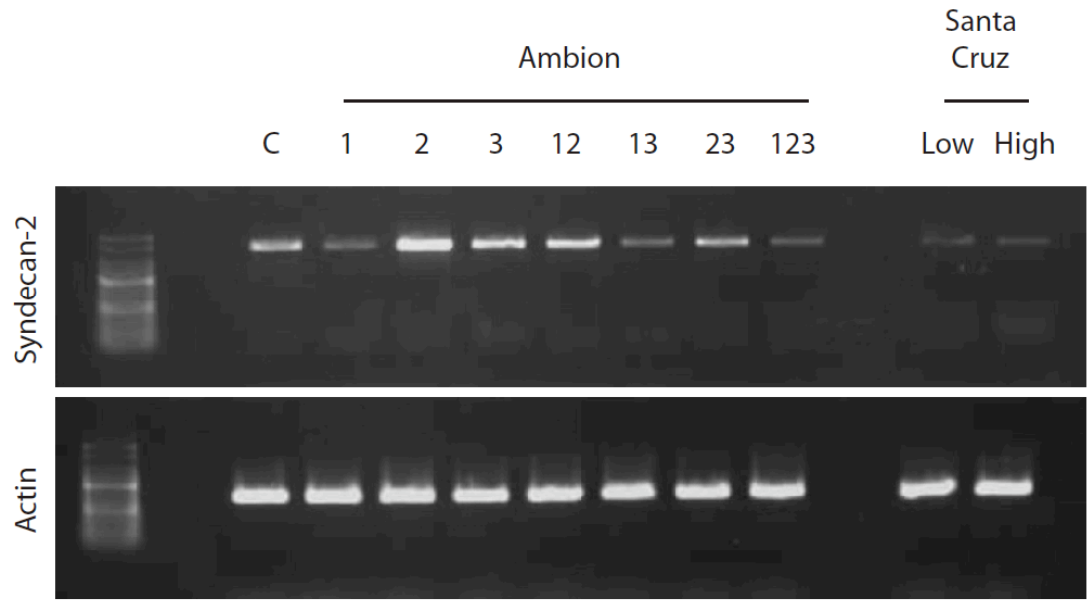

Figure 44: Hela Syndecan-2 Knock Down RT-PCR Analysis. Hela cells were transfected with human SDC2 siRNA using oligofectamine reagent. Ambion and Santa Cruz siRNA's were tested for efficiency. Ambion siRNA was supplied as three separate probes, each probe was tested alone (1, 2 and 3), in pair (1/2, 1/3 and 2/3) and in a pool together (1/2/3). They were delivered in 2x 100pmol transfections with cells harvested 2 days afterwards. Santa Cruz siRNA was delivered as a ready mixed pool of three probes and was given in a low dose of 2x 50pmol or high dose of 2x 100pmol transfections with cells harvested 2 days afterwards. RNA was isolated and quality checked using Thermodynamic Nanodrop. cDNA was synthesised and RT-PCR techniques used to analysis SDC2 expression.

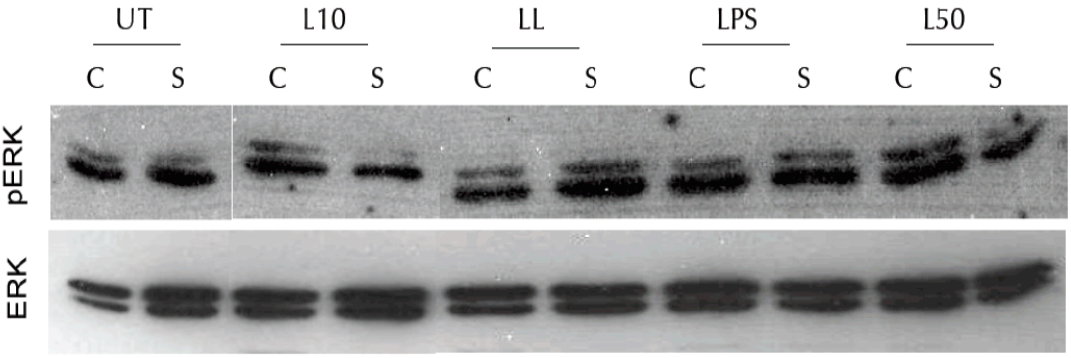

Figure 45: Phospho-ERK Response in Hela Cells Depleted in Syndecan-2. Hela cells were transfected with human SDC2 siRNA (50pmol Santa Cruz) using oligofectamine reagent to knock down SDC2 protein. The cells were then starved for 36h before being treated with PBS control, 10ng/ml LBP, 10ng/ml LBP + 1µg/ml LPS, 1µg/ml LPS or 50ng/ml LBP for 30min. The cells were lysed in 200µl 2x lysis buffer and resolved by 10% SDS-PAGE. Proteins were then transferred to a nitrocellulose membrane and the membrane immunoblotted for pERK. The blots were developed and imaged on film before being stripped and reprobed for total ERK protein. Gel images were exported to ImageJ and inverted (n=1).

for the LBP phospho-ERK response.

Hela cells were plated onto 24-well plate culture dishes at approximately 40% confluency and transfected with 100pmol syndecan-2 siRNA (Ambion) or control scrambled siRNA (Sigma) for 8h, the cells were then washed twice in fresh media and left overnight. The following morning the cells were trypsinized and split 1:2 before being transfected as before for a further 8h. The cells were then washed again in media and left overnight. On day three the cells were washed once and placed into fresh media for 24h. On day four the cells were washed and starved for 48h before being treated with 10-50ng/ml LBP, 10ng/ml LBP + 1µg/ml LPS or 1µg/ml LPS for 30min. The cells were then lysed and the samples resolved using SDS-PAGE, followed by immunoblot detection of phospho-ERK. Preliminary results showed that 10-50ng/ml LBP treatment was able to induce a phospho-ERK response in scrambled control siRNA treated Hela cells but not in the syndecan-2 knocked down cells (figure 45). In control Hela cells LBP+LPS and LPS alone were able to induce phospho-ERK, knocking down syndecan-2 did not appear to affect this response. These data support the idea that syndecan-2 is required for the LBP-independent effects, and suggest that in Hela cells syndecan-2 mediates the phospho-ERK response induced by LBP, but not that by LBP + LPS or LPS alone.

2.7 LBP induces *VEGF* in Müller cells and *TGFß1* in HUVEC

The angiogenesis assays had shown that LBP treatment enhanced vascular growth, with preliminary *in vitro* results suggesting LBP may mediate this effect through syndecan-2 and ERK signalling. VEGF and TGFß1 are potent growth factors able to induce endothelial proliferation [15, 111]. Other groups have shown syndecan-2 can potentiate VEGF-A [188] and TGFß1 [189] signalling so we next decided to investigate whether LBP was able to induce either, or both, of these growth factors in HUVEC or Müller cells.

HUVEC and Müller cells were plated onto 35mm^2 tissue culture dishes and starved overnight before being treated for 2-6h with either PBS or 10ng/ml LBP. Cells were then lysed, RNA isolated, cDNA synthesised and *VEGF* / *TGFß1* expression analysed using q-PCR. Fold changes were calculated via normalisation to cell matched *ß-actin* expression levels. The results showed that after 2h LBP treatment

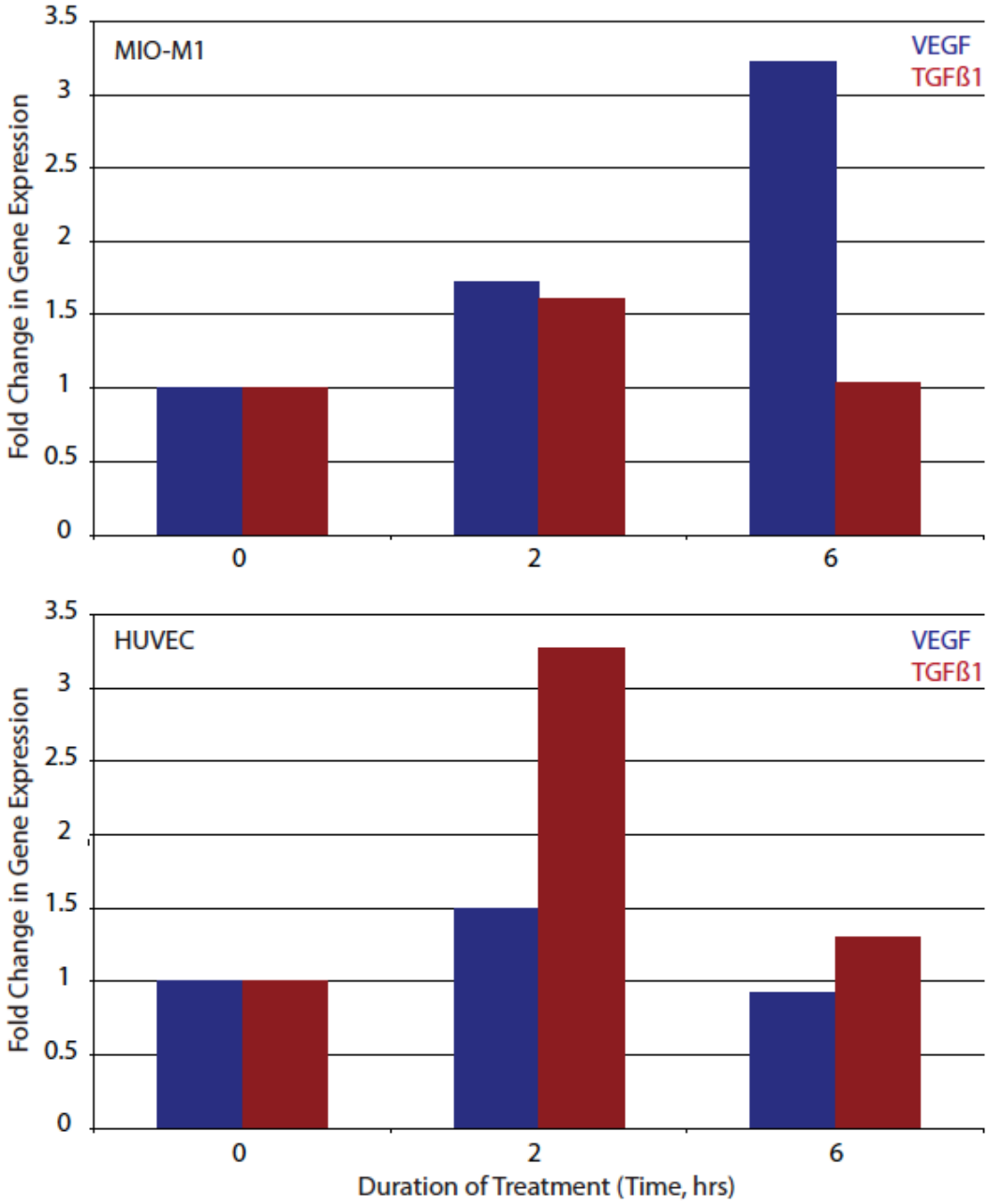

Figure 47: LBP induces *TGFβ1* and *VEGF* in a Cell Specific Manner. HUVEC (P2) and Müller cells were seeded onto 35mm^2 culture dishes and starved overnight before being treated with either PBS control or 10ng/ml LBP for 2-6h. Cells were then lysed, RNA isolated and cDNA synthesised. *VEGF* and *TGFβ1* expression was anaylsed using q-PCR and the fold change in gene expression was calculated by normalisation to cell matched ß-actin expression levels. (n=1).

HUVEC expressed >3x more *TGFβ1* but exhibited no increase in *VEGF* expression, whilst after 2-6h of LBP treatment, Müller cells expressed >3x more *VEGF* but exhibited no increase in the *TGFβ1* expression (figure 47). This suggests that LBP is able to modulate the expression of other angiogenic growth factors in a cell-type specific manner.

3. Chapter Discussion

There are two branches to the NF-kß signalling pathway, the canonical and non-canonical [121]. LBP + LPS signalling is known to activate the canonical pathway, inducing ikßα phosphorylation and p65 nuclear translocation [116]. Our experiments here indicate that LBP treatment alone is not sufficient to induce NF-kß. However it is important to note that these experiments examined cells at pre-determined timepoints (5min-1h) and we cannot completely rule out the possibility that LBP may induce ikßα phosphorylation and p65 nuclear shuttling outside of this time frame. Also, p65 is not the only activator of NF-kß gene transcription, c-Rel, RelB and p50 [122, 125] could also be activated to enter the nucleus and although LBP + LPS usually functions via p65 it could be that LBP alone induces a related factor.

LBP was shown to be able to induce phosphotyrosine responses in three endothelial cell lines (GPNT, RBE4 and HUVEC) and MIO-M1 Müller cells with two protein bands of 150kDa and 60kDa appearing to increase the most. Initially we attempted to identify the 60kDa band using the 'educated guess' approach. Several members of the Src family of tyrosine kinases have a molecular weight of approximately 60kDa, and these are commonly activated by tyrosine phosphorylation in multiple cell signalling pathways [190, 191]. However, probing blots with various phospho-specific Src antibodies led us to conclude this protein was probably not a member of this kinase family (data not shown).

In order to unequivocally identify the unknown protein bands we therefore performed mass spectroscopic analysis from a phosphotyrosine pull down using control vs. LBP stimulated Müller cell lysates. Five protein bands were selected for identification. No sequencing results were obtained for the 150kDa band, the 35kDa band was identified as myosin-9, which is a non-muscle myosin believed to associate with ALK in anaplastic large cell lymphoma [192]. A further two bands were identified as

heterogeneous nuclear ribonucleoprotein A1 (HNRPA1) and heterogeneous nuclear ribonucleoprotein U (hnRNPU), both of which bind to RNA to influence pre-mRNA processing and transport from the nucleus [193, 194]. Interestingly, the 60kDa protein was identified as vimentin.

Vimentin is an intermediate filament protein, which has been found to be important for cell integrity. It generally associates with the endoplasmic reticulum, nucleus and mitochondria and functions to anchor organelles in the cytoplasm [195]. It has been observed that an increase in vimentin serine phosphorylation is linked to epithelial cells taking on a mesenchymal state [196] and that cell surface expression of vimentin increases angiogenesis [197]. Phosphorylation of vimentin has also been reported to increase during cell mitosis and motility [198] which would be consistent with the observations that LBP enhances vessel growth in the angiogenesis assays. However, most reports of vimentin phosphorylation are in regard to serine phosphorylation, and to the best of our knowledge our findings here are the first identification of tyrosine phosphorylation of vimentin.

ERK is activated through phosphorylation by the upstream MAP kinases, MEK1/2 and has a long established role in regulating cell survival, differentiation and proliferation though induction of growth factors, such as VEGF [139, 199-202]. Here we show that LBP can induce phospho-ERK in HUVEC and Müller cells, which supports the increased growth we observed in the angiogenesis assays. It is interesting that LBP + LPS appeared to initially increase phospho-ERK in Müller cells and then inhibit it, this could suggest some kind of negative feedback loop for the phospho-ERK activation caused by LBP + LPS.

RT-PCR comparisons of old (passage 13) LBP unresponsive and young (passage 2) LBP-sensitive HUVEC showed that upon multiple passages the cells down-regulate expression of a heparan sulphate proteoglycan (HSPG) syndecan-2. Syndecan-2 belongs to a small HSPG sub-family, along with three further syndecans and six glypicans. Syndecans are type 1 transmembrane proteoglycans, which can vary greatly in size depending on their side chain attachments [202, 203]. They all share a conserved core protein and a short cytoplasmic tail and it is the divergence of their side chains that determines the ligands with which they can interact [203-205]. They

are present on the cell surface usually as homodimers, occasionally as multimers [203-205]. Syndecan-2 has been shown to have altered expression in cancer and to be involved in cell proliferation and migration [206-209]. Interestingly syndecan-2 is the only member of the syndecan family to be linked to vascular behaviour, with some groups reporting that it is vital for sprouting angiogenesis [210, 211]. Moreover zebra fish studies have found syndecan-2 to interact directly with VEGF-A and have shown that $VEGF_{165}$ induced angiogenic sprouting is compromised in syndecan-2 mutants [189]. Unfortunately, syndecan-2 is the only member of this HSPG family not to have been genetically targeted in mice, therefore we had to use siRNA to investigate the potential role of syndecan-2 as a receptor for LBP. siRNA knockdown in Hela cells showed that syndecan-2 is indeed required for LBP induction of phospho-ERK, supporting the notion that LBP promotes angiogenesis via syndecan-2. However these are preliminary data in need of further validation. In particular we have only been able to establish a knockdown of SDC2 at the RNA level due to the technical challenges of western blotting for the protein. It would be important to confirm that the syndecan-2 protein expression is correspondingly diminished by the knockdown protocol. Also, despite 48h of starvation the Hela cells still exhibited a relatively high basal level of phospho-ERK, so although it was still possible to observe an increase in phospho-ERK with LBP treatment, ideally one would want a cell line with a lower basal level of ERK phosphorylation in future experiments.

q-PCR analysis of gene expression in HUVEC and Müller cells post LBP treatment showed that LBP induces alternate growth factors in the different cell lines (*TGFβ1* in HUVEC and *VEGF* in Müller cells). This is interesting as both are angiogenic factors, and shows that LBP may stimulate cell type-specific gene expression. Futhermore, induction of TGFß1 activity by LBP may explain why we observed enhanced vascular sprouting with LBP + VEGF treatments in the aortic ring angiogenesis assay (Results chapter 2 figures, 19 and 20).

Previously it was thought LBP only had signalling effects when bound to LPS, however we have identified a novel function for this protein. LBP can in fact induce phosphotyrosine responses in Müller, HUVEC, GPNT and RBE4 cells and can induce phosphoERK responses in Müller, HUVEC and Hela cells. The experiments show that LBP-induced signalling is different from that of LBP + LPS in that LBP does not

appear to activate the NF-kß p65 regulated pathway. We have also shown, by inference, that LBP does not signal via TLR4, and in syndecan-2 we have identified a candidate receptor for LBP already implicated in angiogenesis.

Summary and Conclusions

Summary and Conclusions

Previous work investigating LBP has identified it as being an important protein of the innate immune system. Primarily synthesised and secreted by macrophages, LBP functions to bind to circulating LPS, which is shed from the cell walls of gram-negative bacteria such as *E. coli*. Once bound, LBP-LPS can initiate TLR4 signalling to induce NF-kß transcription, cytokine production and an inflammatory response. The CD14 antigen has been reported to enhance the efficiency of LBP-LPS signalling. There are two types of CD14, membrane bound (mCD14, which is expressed on cells such as endothelial cells) and secretory (sCD14, which allows non-CD14 expressing cells to respond to LBP-LPS) [118, 122, 123, 212].

Through microarray analysis our group identified *LBP* as being increased in mouse models that display abnormal retinal vasculature. Further characterisation of the *VLDLR*$^{-/-}$ mouse showed *LBP* to be up-regulated prior to the onset of vascular abnormalities and an associated increase in *VEGF*. This is important because a gene that is identified as being up-regulated in a microarray may be so either as a consequence of vascular remodelling / angiogenesis or because it has a causative pro-angiogenic activity.

These observations suggested a possible functional link between *VEGF* and *LBP*, this was an unexpected result but the links between immunity and angiogenesis have been implicated in many investigations, with LBP previously reported to have a role in the 'angiogenic switch' [136]. For these reasons LBP was judged to be a good candidate for further investigation.

Macrophages co-stimulated with a TLR agonist and an adenosine A2a receptor agonist (such as adenosine) have been found to switch off inflammatory signalling and instead activate VEGF production [136]. Although the retina is an immune-privileged tissue it does contain some resident macrophages [213], and clearly these could be a source of LBP in the context of vascular growth. However the microarray study was performed on isolated retinal vessels, which we assume to be essentially free of macrophages, so

we decided to investigate whether LBP could activate the angiogenic switch in endothelial cells. In our initial studies using cultured endothelial cell lines (HUVEC, GPNT and RBE4) we not only found that they failed to activate VEGF transcription upon LBP + adenosine treatment, but also that the cells themselves did not express LBP. This suggested that the presence of LBP transcripts in the microarray could have come from a non-endothelial cell type (e.g. smooth muscle cells or pericytes) and that possibly it was these cells that could be driving the vascular changes. Alternatively, it is possible that the microvascular endothelial cells of the retina do express LBP, and that in this respect the endothelial cell types tested represent inaccurate models. A further possibility is that Müller cells could have been present in the vessel preparation, as they express LBP and have specialised 'end-feet' connections with the vasculature [73, 162]. However when Müller cells were treated with LBP + adenosine we found there was no increase in VEGF expression. These observations suggested to us that LBP was not affecting vascular behaviour through induction of the TLR-A2aR angiogenic switch pathway.

The current literature reports LBP inducing physiological inflammatory effects only when in partnership with LPS, however our experimental approach provides evidence that LBP is able to elicit a change in vascular behaviour and signal independently of LPS, suggesting the existence of an alternate signalling mechanism. *In vitro* cell culture techniques have demonstrated that whilst LBP in complex with LPS is able to induce ikßα phosphorylation and p65 nuclear translocation, LBP treatment alone does not. However we have shown that exogenously added LBP is able to induce protein tyrosine phosphorylation and phospho-ERK signalling in cultured endothelial and Müller cells, and LPS appears to inhibit this activation. In three distinct angiogenesis assays; Matrigel, aortic ring and metatarsal we observed that exogenously added LBP was able to increase vascular growth. Again, we found that LPS inhibited this effect, and that when combined with VEGF, LBP had an additive effect. These observations support a novel angiogenic function for LBP and imply the activation of different signalling mechanisms being initiated by LBP when it is applied alone as opposed to being bound to LPS.

HUVEC have been reported to alter their protein expression profile as they are passaged in culture (e.g. CD14 expression is known to decrease dramatically beyond passage 5) [168], therefore our experiments employed HUVEC at a low passage (P2-4) number so that artefacts arising from loss of gene expression were minimised. However, when we used older (P12) HUVEC in the Matrigel assay we found they were no longer responsive to LBP, this was an interesting observation suggesting that a protein (or proteins) that had been down-regulated during passage were required for the LBP-induced effect. After RT-PCR analysis we identified SDC2 as being the only member of the TLR, Glypican and Syndecan families to be down-regulated in HUVEC as they aged. Thus HUVEC that express SDC2 respond to LBP whereas those that do not, don't. Although this is only circumstantial evidence that SDC2 is required for a response to LBP, this notion was supported by preliminary data in Hela cells, in which SDC2 knock down led to failure to generate a phospho-ERK response to LBP.

HSPGs have been reported to have a wide range of ligand types including growth factors and cytokines. SDCs and GPCs are transmembrane HSPG sub-families [203, 204]. BPI, like LBP, also binds to LPS and activates inflammatory signalling through TLRs. In 2007 BPI was found to be able to signal independently of LPS, inducing phospho-ERK responses in RPE through the HSPG, GPC6. LBP and BPI share 45% sequence homology and are predicted to have the same two-hinge structure [124, 138], therefore as HSPGs are known to mediate their ligand activity via the divergence in their heparan sulfate (HS) side chains, it is clearly plausible that two similar proteins such as LBP and BPI act via the same family of receptors, i.e. BPI through GPC6 and LBP possibly via SDC2.

SDC2 is a widely expressed HSPG, which has been shown to have altered expression in cancer [208, 209] and is involved in the promotion of sprouting angiogenesis in zebra fish [181]. SDC2 has been shown to interact with fibronectin, an extracellular matrix protein important for wound healing, migration and differentiation [209, 210]. This interaction occurs via the second heparin-binding domain within fibronectin and it has been reported that blocking this interaction via ligands such as tenascin-C (a large extracellular protein up-regulated in many cancers) enhances cell migration [217, 218]. If LBP was able to bind to SDC2 and perhaps inhibit its interaction with

fibronectin, thus un-anchoring endothelial cells from their basement attachment, this could be one way in which LBP induces vascular growth. Over expression of SDC2 has also been documented to enhance the migration and invasive nature of melanoma cells, with knock-down of SDC2 shown to inhibit this effect [214, 215, 224]. SDC2 has also been reported to enhance both VEGF and TGFß1 signalling, with some groups reporting an induction of intracellular ERK [216, 219] and co-immunoprecipitation experiments showing that Syndecan-2 associates with TGFß and its receptor [219].

As previously discussed in Results Chapter 3 section 4, LBP treatment appears to enhance the tyrosine phosphorylation of a 60kDa protein, which through investigation via mass spectroscopic analysis of a phosphotyrosine pull-down was identified as vimentin. Vimentin is an intermediate filament protein, regarded as a marker for mesenchymal transition of endothelial cells [223] and upon phosphorylation has been shown to promote cell migration (albeit through serine phosphorylation, although tyrosine phosphorylation may also regulate vimentin) [220, 221]. Targeting endothelial expressed vimentin in a mouse model of tumourgenesis was found to decrease both tumour growth and microvessel density [219] supporting a role for this protein in pathological endothelial behaviour.

SDC2 was identified late in this project so the data obtained on its potential interaction with LBP are limited. To irrefutably establish a functional link between LBP, SDC2 and phospho-ERK signalling will require extensive experimental studies, including knock-downs and possibly the generation and analysis of a SDC2 knock out mouse. However, from what is known about LBP, SDC2 signalling and the experiments undertaken in this thesis, it seems reasonable to hypothesise that an interaction between these two proteins may constitute a novel angiogenic signalling pathway.

To conclude, this work has demonstrated that LBP, a protein believed to function only as a binding partner for LPS, has a novel signalling role as an angiogenic factor. Although the mechanism remains elusive, observations here suggest that LBP mediates this effect through engagement of cell surface SDC2, cytoskeletal vimentin phosphorylation and downstream signalling via ERK (figure 47).

Further investigation would be required to elucidate the signalling mechanisms in more detail, unequivocal identification of the 60 and 150kDa phosphotyrosine protein bands might be informative, and confirmation of the LBP-SDC2 interaction would be essential. A luciferase reporter assay to analyse multiple gene promoters post LBP treatment would also be useful in order to link the observation of increased phospho-ERK to transcriptional activation. It would also be interesting to perform a microarray screen on cells and / or tissue samples untreated or treated with LBP to delineate the genes activated by LBP in an attempt to gain further insight into the signalling cascade behind the observations made in the angiogenic assays.

As with any angiogenic factor, it is interesting to consider the therapeutic potential of targeting LBP. In this case, blocking LBP function may be risky due to its fundamental role in bacterial recognition and innate immunity. Thus, systemic inhibition of LBP may not be viable, however due to the immune privileged nature of the eye local inhibition of LBP within the retina could be a possible treatment option. This would result in a narrow use for a hypothetical drug in treating only ophthalmic vascular disease but if, as this thesis work suggests, LBP is a major promoter of retinal pathogenesis then it could be beneficial. Alternatively, should future work clarify the signalling mechanism then it may be that accessory molecules are identified that may be targeted. In fact the syndecan HSPGs are starting to be considered as potential drug targets for disease [214]. It is interesting that we observed an increase in LBP expression in the *VLDLR*$^{-/-}$ mouse at P4 and P8, prior to onset of vascular abnormalities. This could suggest that LBP also has the potential to be used as a diagnostic marker, although it would prove difficult to separate an observed up regulation in LBP being due to the pre-angiogenic priming of a tissue as opposed to the up regulation of LBP observed during infection [225].

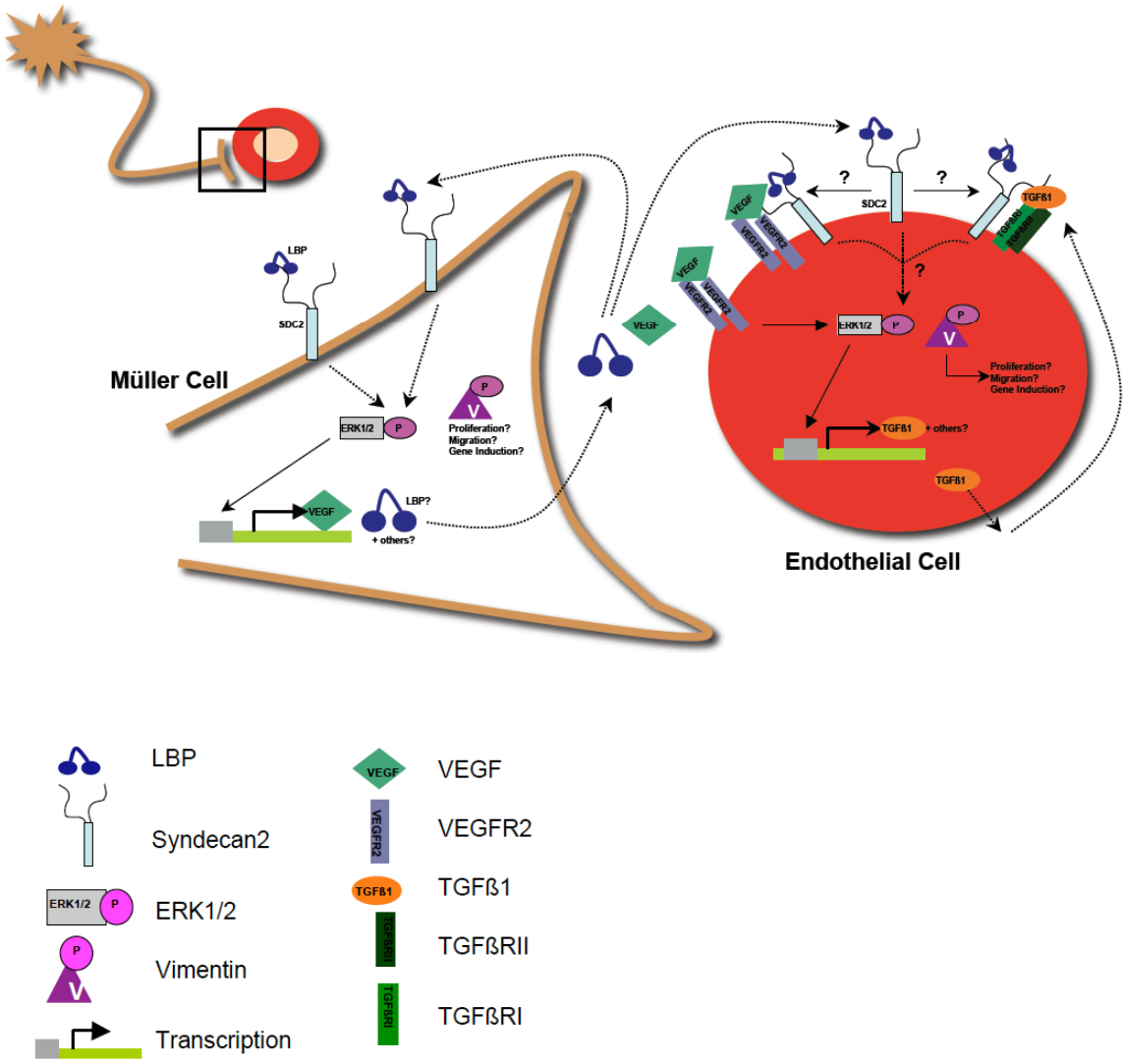

Figure 47: LBP Signalling Schematic. Our data have shown that LBP is able to activate signalling in HUVEC and MIO-M1 Muller cells to induce protein tyrosine phosphorylation (e.g. vimentin), phospho-ERK, TGFß1 and VEGF expression, with some speculation that the syndecan-2 HSPG is the LBP receptor. Syndecan-2 has been reported to interact with TGFß receptor 1 and 2 and has been shown to potentiate VEGF-A signalling. This schematic illustrates how LBP could mediate syndecan-2 activation to promote vascular growth.

References

1. Kolb, H, et al. *Webvision - The organization of the retina and visual system.* 2011.
2. Hecht, E., *Hecht Optics - Second Edition.* Addison Wesley, 1987.
3. Jorge Fischbarg, *The biology of the eye*, Elsevier. 2006.
4. Richard A. Bone, et al. *Preliminary identification of the human macular pigment.* Vision Research, 1985. **25**(11): p. 1531-1535.
5. Bartlett, H and Eperjesi, F. *Macular Pigment - The role of xanthophylls in preventing AMD.* Clinical Nutrition and The Eye, 2006.
6. Weinberg, R., *The Role of Oxidative Stress in the Pathogenesis of Age-Related Macular Degeneration.* Survey of Ophthalmology, 2000. **45**(2).
7. John T, et al. *A One Year Study of the Macular Pigment : The Effect of 140 Days of a Lutein Supplement* Experimental Eye Research, 1997. **65**(1): p. 57-62.
8. Funk, R. *Blood Supply of the Retina.* Ophthalmic Research - Journal for Research in Experimental and Clinical Ophthalmology, 1997. **29**(5): p. 320-5.
9. R.Muñoz-Chápuli, et al., *Angiogenesis and signal transduction in endothelial cells.* Cellular and Molecular Life Sciences, 2004(61): p. 2224-2243.
10. Gardner, R, et al. *Retinal angiogenesis in development and disease.* Nature Insight, 2005. **438**(7070): p.960-6.
11. Alitalo, R, et al. *Molecular regulation of angiogenesis and lymphangiogenesis.* Nature Reviews, 2007. **8**(6):464-78.
12. Ferguson, J, et al. *Mechanisms of Endothelial Differentiation in Embryonic Vasculogenesis.* Arterioscler. Thromb. Vasc. Biol., 2005. **25**(11): p. 2246-2254.
13. Shima, D et al. *VEGF function in vascular pathogenesis* Experimental Cell Research, 2006. **312**(5): p. 527-537.
14. Hideki Okazaki, S.T, et al. *Nuclear translocation of phosphorylated STAT3 regulates VEGF-A-induced lymphatic endothelial cell migration and tube formation.* Biochemical and Biophysical Research Communications, 2011. **412**(3): p. 441-445.
15. Montoro-García, S, et al. *Soluble vascular endothelial growth factor receptor (VEGFR)-2 in macular oedema—a mechanism for regulating angiogenesis?* British Journal of Ophthalmology, 2011. **95**(6): p. 757-758.
16. Nowak DG, et al. *Expression of pro- and anti- angiogenic isoforms of VEGF is differentiately expressed by splicing and growth factors.* J Cell Sci. 2008; **121**(4): p. 3487-95
17. Giacca, M. et al. *Non-redundant functions of the protein isoforms arising from alternative splicing of the VEGF-A pre-mRNA.* Transcription, 2010. **1**(3): p. 149-153.
18. Janet Rossant, L.C, et al. *Endothelial cells and VEGF in vascular development.* Nature Insight, 2005. **438**(7070): p. 937-45.
19. Ramanathan, M, et al. *Synergistic Up-regulation of Vascular Endothelial Growth Factor (VEGF) Expression in Macrophages by Adenosine A2A Receptor Agonists and Endotoxin Involves Transcriptional Regulation via the*

Hypoxia Response Element (HRE) in the VEGF Promoter, Mol Biol Cell, 2007; **18**(1): p. 14-23.
20. Rechka, A, et al. *Identification of VEGF receptor-2 tyrosine phosphorylation sites involved in VEGF-mediated endothelial platelet-activating factor synthesis.* Canadian journal of physiology and pharmacology, 2010. **88**(10): p. 968-976.
21. Chung, B, et al. *Promotion of direct angiogenesis in vitro and in vivo by Puerariae flos extract via activation of MEK/ERK-, PI3K/Akt/eNOS-, and Src/FAK-dependent pathways.* Phytotherapy research, 2010. **24**(6): p. 934-940.
22. Curtis, B, et al. *KLF2/KLF4 Double Knock-out Mouse Embryos Show Cranial Bleeding with Endothelial Disruption of the Primary Head Vein.* VCU Digital Archives, 2010 **8**(2).
23. Griffioen, F, et al. *Tumour vascularization: sprouting angiogenesis and beyond.* Cancer Metastasis, 2007. **26**(3): p. 489-502.
24. Wiley, D, et al. *Distinct signalling pathways regulate sprouting angiogenesis from the dorsal aorta and the axial vein.* Nature Cell Biology, 2011. **13**(6): p. 20-24
25. Peter H. Burri, V.D., *Intussusceptive angiogenesis—the alternative to capillary sprouting.* Molecular aspects of medicine, 2002. **23**(16): p. 113-117
26. Haymo Kurz, P, et al. *Angiogenesis and Vascular Remodeling by Intussusception: From Form to Function.* News Physiology Science 2003. **18**(1): p. 65-70.
27. Senior, K., *Causes of Blindness Worldwide: Facts and Figures.* 2010.
28. Anderson, D, et al. *A role for local inflammation in the formation of drusen in the aging eye.* American Journal of Ophthalmology, 2002. **134**(3): p. 411-431.
29. Lianga, F-Q, et al. *Oxidative stress-induced mitochondrial DNA damage in human retinal pigment epithelial cells: a possible mechanism for RPE aging and age-related macular degeneration.* Experimental Eye Research, 2003. **76**(4): p. 397-403.
30. Espinosa-Heidmann, D, et al. *Basal Laminar Deposit Formation in APO B100 Transgenic Mice: Complex Interactions between Dietary Fat, Blue Light, and Vitamin E* IOVS, 2004. **45**(1): p. 260-266.
31. Green, W, et al. *Pathologic features of senile macular degeneration.* ophthalmology, 1985. **92**(5): p. 615-627.
32. Fine, N, et al. *Age-Related Macular Degeneration.* Survey of Ophthalmology, 1988. **32**(6): p. 333-338.
33. Owen, C, et al. *How big is the burden of visual loss caused by age related macular degeneration in the United Kingdom?* British Journal of Ophthalmology, 2002. **14**(87): p. 312-317.
34. Fine, S.L., *Advising Patients About Age-Related Macular Degeneration.* Arch Ophthalmology, 1993. **111**(9): p. 1186-1188.
35. Marticorena, J et al. *Retinal Angiomatous Proliferation.* Curr Drug Targets. 2011. **12**(2): p.199-205.
36. Yannuzzi LA, et al. *Retinal angiomatous proliferation in age-related macular degeneration.* Retina, 2001. **21**(5): p.416-34.
37. Zarbin, M.A., *Current Concepts in the Pathogenesis of Age-Related Macular Degeneration.* Arch Ophthalmology, 2004. **42**(122): p. 598-614.

38. Renwick Beattie, J, et al. *Multiplex analysis of age-related protein and lipid modifications in human Bruch's membrane.* The FASEB Journal, 2010. **24**(12): p. 4816-4824.
39. Gold, B, et al. *Variation in factor B (BF) and complement component 2 (C2) genes is associated with age-related macular degeneration* Nature Genetics, 2006. **38**(4): p. 15-17.
40. Goverdhan, S, et al. *An analysis of the CFH Y402H genotype in AMD patients and controls from the UK, and response to PDT treatment.* Eye, 2008. **10**(22): p. 849-854.
41. Heinen, S, et al. *Factor H–related protein 1 (CFHR-1) inhibits complement C5 convertase activity and terminal complex formation.* Blood, 2009. **114**(12): p. 2439-2447.
42. Haines, J, et al. *Complement Factor H Variant Increases the Risk of Age-Related Macular Degeneration* Science, 2005. **15**(3): p. 419-421.
43. Klein, R, et al. *Complement Factor H Polymorphism in Age-Related Macular Degeneration* Science, 2005. **15**(1): p. 385-389.
44. Edwards, A, et al. *Complement Factor H Polymorphism and Age-Related Macular Degeneration.* Science, 2005. **15**(1): p. 421-424.
45. Johnson, P, et al. *Individuals homozygous for the age-related macular degeneration risk-conferring variant of complement factor H have elevated levels of CRP in the choroid.* PNAS, 2006. **103**(46): p. 17456-17461.
46. Mooijaart, S, et al. *Complement Factor H polymorphism Y402H associates with inflammation, visual acuity, and cardiovascular mortality in the elderly population at large.* experimental gerontology, 2007. **42**(11): p. 1116-1122.
47. Heurich, M, et al. *Common polymorphisms in C3, factor B, and factor H collaborate to determine systemic complement activity and disease risk* PNAS, 2011. **108**(21): p. 8761-8766.
48. Gotoh, N. *No association between complement factor H gene polymorphism and exudative age-related macular degeneration in Japanese* Human Genetics, 2005. **120**(1): p. 139-143.
49. Cao, X, et al. *Macrophage polarization in the maculae of age-related macular degeneration: A pilot study.* Pathology International, 2011. **61**(2): p. 528-535.
50. Retina-International-Organisation, *Mutation Database.* 2011.
51. Klevering, BJ, et al. *Microarray-based mutation analysis of the ABCA4 (ABCR) gene in autosomal recessive cone-rod dystrophy and retinitis pigmentosa.* Eur J Human Genetics, 2004. **12**(12): p. 1024-32.
52. Klevering, B.J., *Microarray-based mutation analysis of the ABCA4 (ABCR) gene in autosomal recessive cone-rod dystrophy and retinitis pigmentosa.* Eur J Human Genetics, 2004. **12**(12): p. 1024-32.
53. Inderjeet Kaur, S.R, and Subhabrata Chakrabarti, *Variations in TIMP3 are associated with age-related macular degeneration.* PNAS, 2010. **107**(28): E112-3
54. Carney, R, et al. *Free Radical Damage to Protein and DNA: Mechanisms Involved and Relevant Observations on Brain Undergoing Oxidative Stress.* Annals of Neurology, 1992. **32**: S22-7
55. Yang, Z, et al. *A Variant of the HTRA1 Gene Increases Susceptibility to Age-Related Macular Degeneration.* Science, 2006. **13**(10): p. 992-993.
56. DeWan, A, et al. *HTRA1 Promoter Polymorphism in Wet Age-Related Macular Degeneration.* Science, 2006. **314**(2): p, 323-25.

57. Barbara, E, et al. *The Prevalence of Age-Related Macular Degeneration and Associated Risk Factors: The Beaver Dam Offspring Study* Arch Ophthalmology, 2010. **128**(6): p. 575-82.
58. Knudtson, M, et al. *Physical activity and the 15-year cumulative incidence of age-related macular degeneration:the Beaver Dam Eye Study.* British Journal of Ophthalmology, 2006. **90**: p. 1461-1463.
59. NHS, *Diabetes Statistics UK.* 2010.
60. Klein, R, et al. *The Wisconsin Epidemiologic Study of Diabetic Retinopathy III.* Arch Ophthalmology, 1984. **102**(4): p. 527-532.
61. Klein, R et al. *The Wisconsin Epidemiologic Study of Diabetic Retinopathy II.* Arch Ophthalmology, 1984. **102**(4): p. 520-526.
62. Barber, G, et al. *Visual Dysfunction Associated with Diabetic Retinopathy* current diabetes reports, 2010. **10**(5): p. 380-384.
63. Ciulla, T, et al. *Diabetic Retinopathy and Diabetic Macular Edema.* Diabetes Care, 2003. **26**(2654-2664).
64. Duh, E., *Diabetic Retinopathy.* 2008.
65. Miyamoto, K, et al. *Prevention of leukostasis and vascular leakage in streptozotocin-induced diabetic retinopathy via intracellular adhesion molecule-1 inhibition.* proc. Natl. Acad. Sci USA, 1999. **96**: p. 10836-10841.
66. Stitt, A.W., *The role of advanced glycation in the pathogenesis of diabetic retinopathy.* Experimental and Molecular Pathology, 2003. **75**: p. 95-108.
67. Jax, T, et al. *Metabolic memory: a vascular perspective* cardiovascular dibetology, 2010. **9**(1): p. 1475-77.
68. Ihnat, MA et al. *Hypothesis: the 'metabolic memory', the new challenge of diabtetes.* Diabetic Medicine, 2007. **24**(1) p. 582-586
69. Stitt, AW, et al. *Advanced glycation end products (AGEs) co-localize with AGE receptors in the retinal vasculature of diabetic and of AGE-infused rats.* The American Journal of Pathology, 1997. **150**(2): p. 523-531.
70. Sato, TI, et al. *TAGE (Toxic AGEs) Theory in Diabetic Complications.* Current molecular medicine, 2006. **6**(3): p. 351-358.
71. Cooper, ME, et al. *The Role of Advanced Glycation End Products in Progression and Complications of Diabetes.* the journal of clinical endocrinology and metabolism, 2008. **98**(4): p. 1143-1152.
72. Cooper, ME, et al. *The Role of Advanced Glycation End Products in Progression and Complications of Diabetes.* the journal of clinical endocrinology and metabolism, 2008. **98**(4): p. 1143-1152.
73. Curtis, TM, et al. *Müller glial dysfunction during diabetic retinopathy in rats is linked to accumulation of advanced glycation end-products and advanced lipoxidation end-products.* Diabetologia, 2011. **54**(3): p. 690-698.
74. Swenarchuk, LE, et al. *The Role of Inflammation in the Pathophysiology of Diabetic Retinopathy* Contemporary Diabetes 2008. **2**(1): p. 303-331.
75. Baynes, JW, et al. *Role of Oxidative Stress in Diabetic Complications - A New Perspective on an Old Paradigm.* American Diabetes Association, 1999. **48**(1): p. 1-9.
76. Iwashima, Y, et al. *Advanced Glycation End Products-Induced Gene Expression of Scavenger Receptors in Cultured Human Monocyte-Derived Macrophages.* Biochemical and Biophysical Research Communications, 2000. **277**(2): p. 368-380.

77. Yamagishi, S, et al. *Advanced glycation end products inhibit de novo protein synthesis and induce TGF-bold beta overexpression in proximal tubular cells.* Kidney International, 2003. **14**(63): p. 464-473.
78. Vlassara, H., *Pathogenesis of diabetic nephropathy, advanced glcation and new therapy* Medicine, 1997. **92**(1): p. 29-34.
79. Sethi, N, et al. *The regulation of inflammation by galectin-3.* Immunology Reviews, 2009. **230**(1): p. 160-171.
80. Yonekura, H, et al. *Novel splice variants of the receptor for advanced glycation end-products expressed in human vascular endothelial cells and pericytes, and their putative roles in diabetes-induced vascular injury.* Biochem. J, 2003. **370**(3): p. 1097-1109.
81. Hudson, B, et al. *Effects of Novel Polymorphisms in the RAGE Gene on Transcriptional Regulation and Their Association With Diabetic Retinopathy.* Diabetes, 2001. **50**(6): p. 1505-1511.
82. Hudson, B, et al. *Identification of Polymorphisms in the Receptor for Advanced Glycation End Products (RAGE) Gene Prevalence in Type 2 Diabetes and Ethnic Groups.* Diabetes, 1998. **47**(7): p. 1155-1157.
83. Yamagishi, S, et al. *Role of advanced glycation end products (ages) and their receptor (RAGE) in the pathogenesis of diabetic microangiopathy.* International journal of clinical pharamcology research 2003. **23**(4): p. 129-134.
84. Lamoureux EL, et al. *The longitudinal impact of Macular Telangiectasia (MacTel) Type 2 on vision-related quality of life.* . IOVS, 2011. **2**(10): p. 6568-71.
85. Lawrence A, et al. *Idiopathic Macular Telangiectasia* Archives of Ophthalmology, 2006. **124**(4): p.15-19.
86. Charbel, PI, et al. *Idiopathic Macular Telangiectasia* Medical Retina, 2007. **12**(3): p. 183-197.
87. Charbel PI, et al. *Quantification of reduced macular pigment optical density in the central retina in macular telangiectasia type 2.* Experimental Eye Research, 2009. **89**(1): p. 25-31.
88. Helb, MH, et al. *Abnormal Macular Pigment Distribution in Type 2 Idiopathic Macular Telangiectasia.* Retina, 2008. **28**(6): p. 808-816.
89. Clemons, TE, et al. *The National Eye Institute Visual Function Questionnaire in the Macular Telangiectasia (MacTel) Project* IOVS, 2008. **49**(10): p. 4340.
90. Skorin, L.O. *Retinal vein occlusion – Diagnosis and management.* Optometry, 2002.
91. Tarkkanen, A, et al. *Coats's disease: clinical, angiographic, histopathological findings and clinical management.* British Journal of Ophthalmology, 1983. **67**(2): p. 766-776.
92. Manschot, A, et al. *Coats' Disease: Definition and Pathogenesis* British Journal of Ophthalmology, 1967. **51**(145).
93. Black, GC, et al. *Coat's disease of the retina caused by somatic mutation in the NDP gene: a role for norrin in retinal angiogenesis.* Human molecular genetics, 1999. **8**(11): p. 2031-2035.
94. Das, T et al. Eales'disease. Current Ophthalmology. 1994; 42(1) p.3-18
95. http://www.medicinenet.com/uveitis/article.htm#tocb (accessed 10/03/12)
96. Schlötzer-Schrehardt, U, et al. *Dose-related structural effects of photodynamic therapy on choroidal and retinal structures of human eyes*

Graefe's Archive for Clinical and Experimental Ophthalmology, 2002. **240**(9): p. 748-757.
97. Pieramici, DJ, et al. *Anti-VEGF therapy: comparison of current and future agents* Nature Eye, 2008. **6**(1): p. 1-7.
98. Sakai, K, et al. *Plasma VEGF as a marker for the diagnosis and treatment of vasculitic neuropathy.* Journal of Neurology, Neurosurgery and Psychiatry with practical Neurology, 2005. **76**(2): 50-52.
99. Smith, A.F., *The growing importance of pharmacoeconomics: the case of age-related macular degeneration.* British Journal of Ophthalmology, 2010. **94**(9): 71-74.
100. Saint-Geniez, M et al. *Endogenous VEGF is required for visual function: evidence for survival role on muller cells and photoreceptors,* PLoS One, 2008. **3**(11)
101. El-Mollayess, GM, et al. *Bevacizumab and Neovascular Age Related Macular Degeneration: Pathogenesis and Treatment.* Seminars in Ophthalmology, 2011. **26**(3): p. 69-76.
102. Shima, C, et al. *Complications in patients after intravitreal injection of bevacizumab.* Acta Ophthalmologica, 2008. **86**(4): p. 372-376.
103. Lockhart, AC, et al. *Phase I Study of Intravenous Vascular Endothelial Growth Factor Trap, Aflibercept, in Patients With Advanced Solid Tumors.* Journal of clinical oncology, 2010. **28**(2): p. 207-214.
104. Fischer, C, et al. *Anti-PlGF Inhibits Growth of VEGF(R)-Inhibitor-Resistant Tumors without Affecting Healthy Vessels.* Cell, 2007. **131**: p. 463-475.
105. Daud, J, et al. *Spectrum of Activity and Mechanism of Action of VEGF/PDGF Inhibitors.* Cancer Control, 2007. **14**(11): p.40-44.
106. Motzer, RJ, et al. *Sunitinib in Patients With Metastatic Renal Cell Carcinoma.* JAMA, 2006. **4**(21): p. 2516-2524.
107. Llovet, OM, et al. *Sorafenib in Advanced Hepatocellular Carcinoma.* The New England Journal of Medicine, 2008. **11**(359): p. 378-390.
108. Kerbel, N, et al. *Angiogenesis as a therapeutic target.* Nature Insight, 2005. **438**(4): p.32-37.
109. Fischer, C, et al. *FLT1 and its ligands VEGFB and PlGF: drug targets for anti-angiogenic therapy?* Nature, 2008. **8**(1): p.14-19.
110. Autiero, M, et al. *Role of PlGF in the intra- and intermolecular cross talk between the VEGF receptors Flt1 and Flk1.* Nature Medicine, 2003. **8**(9): p. 936-943.
111. Loges, S, et al. *Development of targeted angiogenic medicine.* Journal of Thrombosis and Haemostasis, 2009. **7**(1): p. 21-33.
112. Hailman, E, et al. *Lipopolysaccharide (LPS)-binding Protein Accelerates the Binding of LPS to CD14* J. Exp. Med, 1994. **179**(4): p. 269-277.
113. Nicolas, WJ, et al. *Lipopolysaccharide Binding Protein Binds to Triacylated and Diacylated Lipopeptides and Mediates Innate Immune Responses.* The Journal of immunology, 2004. **17**(3): p.44-47
114. Elsbach, P, et al. *The bactericidal/permeability-increasing protein (BPI) in antibacterial host defense,* Journal of Leukocyte Biology, 1998. **64**(11): p.54-57.
115. Gallay, P, et al. *Lipopolysaccharide-binding protein as a major plasma protein responsible for endotoxemic shock.* proc. Natl. Acad. Sci USA, 1993. **90**: p. 9935-9938.

116. Takeshige, TM, et al. *Essential roles of CD14 and lipopolysaccharide-binding protein for activation of toll-like receptor (TLR)2 as well as TLR4 - Reconstitution of TLR2- and TLR4-activation by distinguishable ligands in LPS preparations* FEBS, 2001. **22**(3): p. 4580-4589.
117. Mizanur R, et al. *Lipopolysaccharide-binding protein: Local expression in bovine extrahepatic tissues* Veterinary Immunology and Immunopathology, 2010. **137**: p. 28-35.
118. Hiroki T, et al. *Lipopolysaccharide-binding protein-mediated Toll-like receptor 4 dimerization enables rapid signal transduction against lipopolysaccharide stimulation on membrane-associated CD14-expressing cells.* International Immunology, 2010. **22**(4): p. 271-280.
119. Sullivan, C, et al. *Predictive of Their Divergent Functions Is tlr4b and tlr4a The Gene History of Zebrafish* The Journal of immunology, 2009. **183**(12): p. 5896-5908.
120. Dunzendorfer, S, et al. *TLR4 Is the Signaling but Not the Lipopolysaccharide Uptake Receptor.* The Journal of immunology, 2004. **12**(1): p.44-49
121. Takeuchi, O, et al. *Differential Roles of TLR2 and TLR4 in Recognition of Gram-Negative and Gram-Positive Bacterial Cell Wall Components* immunity, 1999. **11**: p. 443-451.
122. Nishikori, M, et al. *Classical and Alternative NF-kB Activation Pathways and Their Roles in Lymphoid Malignancies* Journal clinical experimental hematopathology, 2005. **45**(1): p. 111-119.
123. Finberg, RW, et al. *Cell activation by Toll-like receptors: role of LBP and CD14.* Journal od Endotoxin Research, 2004. **6**(10).
124. Kaltschmidt, L. et al. *NF-kB:a crucial transcription factor for glial and neuronal cell function* TINS, 1997. **20**(6): p 302-308.
125. Grosjean, J, et al. *The NfkB Pathway is Involved in VEGF-Induced survival in Human Endothelial Cells.* Cardiovascular Pathology, 2004. **4**(13): p.31-35.
126. Didier LR, *Monoclonal Antibodies to Murine Lipopolysaccharide (LPS)-Binding Protein (LBP) Protect Mice from Lethal Endotoxemia by Blocking Either the Binding of LPS to LBP or the Presentation of LPS/LBP Complexes to CD141.* The Journal of immunology, 1999. **162**: p. 7454-7460.
127. Xiong, H, et al. *NF-kß activity blockade impairs the angiogenic potential of human pancreatic cancer cells* Int. J. Cancer, 2004. **108**(3): p. 181-188.
128. Bannerman, D, et al. *Endotoxin induces endothelial barrier dysfunction through protein tyrosine phosphorylation.* AJP - Lung cellular and molecular physiology, 1997. **67**(5):p. 11-13
129. Grivennikov, SI, et al. *Immunity, Inflammation, and Cancer.* Cell, 2010. **140**(12): p. 883-899.
130. Beckner, M.E., *Factors Promoting Tumor Angiogenesis.* Cancer Investigation, 1999. **17**(8): p. 594-623.
131. Udaya K. et al. *Prevalence of Regulatory T Cells Is Increased in Peripheral Blood and Tumor Microenvironment of Patients with Pancreas or Breast Adenocarcinoma.* The Journal of immunology, 2002. **169(**4): p. 2756-2761.
132. Sunderkotter, C, et al. *Macrophages and angiogenesis* J. Leukoc. Biol, 1994. **55**: p. 410-422.
133. Sunderkotter, C, et al. Macrophage-derived angiogenic factors Pharmac. Ther. 1991. **51**: p. 195-216.
134. Pollard, C, et al. *Distinct Role of Macrophages in Different Tumor Microenvironments.* cancer research, 2005. **66**.

135. Mantovani, A, et al. *Tumour-associated macrophages as a prototypic type II polarised phagocyte population: role in tumour progression.* European Journal of Cancer, 2004. **72**(3): p.44-48
136. Pinhal-Enfield, G, et al. *An Angiogenic Switch in Macrophages Involving Synergy between Toll-Like Receptors 2, 4, 7, and 9 and Adenosine A2a Receptors.* American Journal of Pathology, 2003. **163**(2): p.3-8
137. Park, DW, et al. *Activation of toll-like receptor 4 modulates vascular endothelial growth factor synthesis through prostacyclin-IP signaling.* Biochemical and Biophysical Research Communications, 2007. **45**(362): p. 1090-1095.
138. Yamagata et al. *Bactericidal/permeability-increasing protein's signaling pathways and its retinal trophic and anti-angiogenic effects* FASEB J. 2006 **20**(12): p.2058-67.
139. Geraldes, P, et al. *Glypican 4, a Membrane Binding Protein for Bactericidal/Permeability-Increasing Protein Signaling Pathways in Retinal Pigment Epithelial Cells.* Invest Ophthalmol Vis Sci, 2007. **30**(2): p. 5750-5755.
140. Ling-Zhi L, et al. *MiR-21 Induced Angiogenesis through AKT and ERK Activation and HIF-1a Expression.* PLoS ONE, 2011. **6**(4).
141. Walsh, I. *Role of Akt Signaling in Vascular Homeostasis and Angiogenesis.* Circulation Research, 2002. **23(**6); p.21-25
142. Nakamura, S, et al. *Ruboxistaurin, a PKCb inhibitor, inhibits retinal neovascularization via suppression of phosphorylation of ERK1/2 and Akt* Experimental Eye Research, 2010. **90**: p. 137-145.
143. Xiufeng P, et al. *Morelloflavone, a biflavonoid, inhibits tumor angiogenesis by targeting Rho GTPases and ERK signaling pathways.* cancer research, 2009. **69**(2): p. 518-525.
144. Rizzo, M.T., *ERK and Smads: Getting together for angiogenic sprouting.* Cardiovascular Research, 2007. **76**: p. 375-376.
145. Astrid L, et al. *In Vitro Characterization of a Spontaneously Immortalized Human Muller Cell Line (MIO-M1).* Investigative Ophthalmology & Visual Science, 2002. **43**(3): p.231-235
146. Patterson, Am, et al. *Differential expression of syndecans and glypicans in chronically inflamed synovium.* Annals of the Rheumatic Diseases, 2008. **67**(5): p. 592-601.
147. Wittmaack, FM, et al. *Localization and regulation of the human very low density lipoprotein/apolipoprotein-E receptor: trophoblast expression predicts a role for the receptor in placental lipid transport.* Endocrinology, 1995. **136**(1): p. 340-348.
148. Oka, K, et al. *Mouse Very-Low-Density-Lipoprotein Receptor (VLDLR) cDNA Cloning, Tissue-specific Expression and Evolutionary Relationship with the Low-density-lipoprotein Receptor.* The FEBS Journal, 1994. **224**(3): p. 975-982.
149. Larouche, M, et al. *The Reelin Receptors Apoer2 and Vldlr Coordinate the Patterning of Purkinje Cell Topography in the Developing Mouse Cerebellum.* PLoS One, 2008. **3**(2): p13-17.
150. Sakai, K, et al. *A neuronal VLDLR variant lacking the third complement-type repeat exhibits high capacity binding of apoE containing lipoproteins.* Brain Research, 2009. **18**(1276): p. 11-21.

151. Boycott, KM, et al. *Mutations in VLDLR as a Cause for Autosomal Recessive Cerebellar Ataxia with Mental Retardation (Dysequilibrium Syndrome).* J Child Neurol, 2010. **24**(10): p. 1310–1315.
152. Heckenlively, J, et al. *Mouse Model of Subretinal Neovascularization With Choroidal Anastomosis.* Retina, 2003. **22**(4): p. 114-118.
153. Haines, J, et al. *Functional Candidate Genes in Age-Related Macular Degeneration: Significant Association with VEGF, VLDLR, and LRP6.* IOVS, 2006. **47**(1): p. 329-335.
154. Li, C., *Biochemical Alterations in the Retinas of Very Low-Density Lipoprotein Receptor Knockout Mice.* Arch Ophthalmology, 2007. **125**(3): p. 795-803.
155. Chun-hong, X., *The Role of VLDLR in Intraretinal Angiogenesis in Mice.* IOVS, 2011. **10**(4): p.10-14
156. Chen, Y., *Very Low Density Lipoprotein Receptor, a Negative Regulator of the wnt Signaling Pathway and Choroidal Neovascularization.* The journal of biological chemistry, 2007. **282**(47): p. 34420-34428.
157. Ahuja, S, et al. *rd1 Mouse Retina Shows an Imbalance in the Activity of Cysteine Protease Cathepsins and Their Endogenous Inhibitor Cystatin C.* IOVS, 2008. **49**(3): p. 1089-1096.
158. MizanurRahman, M., *Lipopolysaccharide-binding protein: Local expression in bovine extra hepatic tissues.* Veterinary Immunology and Immunopathology, 2010. **34**(2): p.102-105
159. McKenzie, J, et al. *Apelin is required for non-neovascular remodelling in the retina.* American Journal of Pathology, 2011 - In Press.
160. Heuman, D, et al. *Radioimmunoassay versus flow cytometric assay to quantify LPS-binding protein (LBP) concentrations in human plasma.* Journal of Immunological Methods, 1994. **171**: p. 169-176.
161. Meynaar, I, et al. *In Critically Ill Patients, Serum Procalcitonin Is More Useful in Differentiating between Sepsis and SIRS than CRP, Il-6, or LBP.* Critical care research and practice, 2011. **2011**(2): p.213-119.
162. Bai, Y, et al. *Muller cell-derived VEGF is a significant contributor to retinal neovascularization.* Journal of Pathology, 2009. **219**: p. 446-454.
163. Bang, F., *A bacterial disease of Limulus Polyphemus.* John Hopkins Medical School, 1955.
164. Nachum, R, et al. *Antimicrobial defense mechanisms in the horseshoe crab, Limulus polyphemus: Preliminary observations with heat-derived extracts of Limulus amoebocyte lysate.* Journal of Invertebrate Pathology, 1979. **33**(3): p. 290-299.
165. McCartney, A, et al. *Limulus amoebocyte lysate (LAL) assay and rapid detection of gram negative bacterial peritonitis in patients receiving CAPD.* Journal of Clinical Pathology, 1989. **42**(10): p. 112-117
166. Skovseth, D, et al. *The HUVEC/Matrigel assay: an in vivo assay of human angiogenesis suitable for drug validation.* Methods Molecular Biology, 2007. **7**(360): p. 253-268.
167. Guidolin, D, et al. *A new image analysis method based on topological and fractal parameters to evaluate the angiostatic activity of docetaxel by using the Matrigel assay in vitro.* Microvascular Research, 2004. **67**(2): p. 117-124.
168. Hubertus, P.A., *Synthesis and Surface Expression of CD14 by Human Endothelial Cells.* Infection and Immunity, 2001: p. 479-485.

169. Masson, V, et al. *Mouse aortic ring assay: A new approach of the molecular genetics of angiogenesis.* Biological Procedures Online, 2002. **4**(1): p. 24-31.
170. Cackowski, F, et al. *Osteoclasts are important for bone angiogenesis.* Blood, 2010. **115**(1): p. 140-149.
171. Bitplane, *Imaris 3D and 4D Real-Time Interactive Data Visualization.* http://www.bitplane.com/go/products/imaris, 2011.
172. Gerhardt, H, et al. *VEGF guides angiogenic sprouting utilizing endothelial tip cell filopodia.* Journal of Cell Biology, 2003. **161**(6): p. 1163-1177.
173. Smith, LE, et al. *Oxygen-induced retinopathy in the mouse.* Invest Ophthalmol Vis Sci, 1994. **35**(1): p. 101-111.
174. Stahl, A, et al. *The Mouse Retina as an Angiogenesis Model.* Investigative Ophthalmology & Visual Science, 2010. **51**(6): p.56-59.
175. Chikaraishi, Y, et al. *New quantitative analysis, using high-resolution images, of oxygen-induced retinal neovascularization in mice.* Experimental Eye Research, 2007. **84**: p. 529-536.
176. Gray, M, et al. *HIF-1alpha, STAT3, CBP/p300 and Ref-1/APE are components of a transcriptional complex that regulates Src-dependent hypoxia-induced expression of VEGF in pancreatic and prostate carcinomas.* Oncogene, 2005. **24**: p. 3110-3120.
177. Gao, G, et al. *Unbalanced expression of VEGF and PEDF in ischemia-induced retinal neovascularization.* FEBS Letters, 2001. **489**(2): p. 270-279.
178. Yao, Y, et al. *Upregulation of placental growth factor by vascular endothelial growth factor via a post-transcriptional mechanism.* FEBS Letters, 2005. **579**(5): p. 1227-1243.
179. Dong, D, et al. *Regulation of angiogenesis by macrophages, dendritic cells, and circulating myelomonocytic cells.* Curr Pharm Des, 2009. **15**(4): p. 365-79.
180. Sozzani, S, et al. *Dendritic cell-endothelial cell cross-talk in angiogenesis.* PMID, 2007. **223(**4): p.213-217.
181. Wurfel, M, et al. *Targeted Deletion of the Lipopolysaccharide (LPS)-binding Protein Gene Leads to Profound Suppression of LPS Responses Ex Vivo, whereas In Vivo Responses Remain Intact* J. Exp. Med, 1997. **186**(12): p. 2051-2056.
182. Vesy, CJ, et al. *Lipopolysaccharide-Binding Protein and Phospholipid Transfer Protein Release Lipopolysaccharides from Gram-Negative Bacterial Membranes* Infection and Immunity, 2000. **68**(5): p. 2410-2417.
183. Masood, R, et al. *Vascular endothelial growth factor/vascular permeability factor is an autocrine growth factor for AIDS–Kaposi□sarcoma.* PNAS, 1997. **94**(3): p. 979-984.
184. Ghosh, M. *Rel/NF-kB and IKB proteins: an overview.* Seminars in Cancer Biology, 1997(8): p. 63-73.
185. Brown, K, et al. *Control of I kappa B-alpha proteolysis by site-specific, signal-induced phosphorylation.* Science, 1995. **267**(5203): p. 1485-1488.
186. Régina A, *Dexamethasone regulation of P-glycoprotein activity in an immortalized rat brain endothelial cell line, GPNT.* J Neurochem, 1999. **73**(5): p. 1954-63.
187. Reichel A et al. *Evaluation of the RBE4 cell line to explore carrier-mediated drug delivery to the CNS via the L-system amino acid transporter at the blood-brain barrier.* J Drug Target, 2002. **10**(4): p. 277-83.

188. Chen, E, et al. *Syndecan-2 is essential for angiogenic sprouting during zebrafish development.* Blood, 2003(103): p. 1710-1719.
189. Tkachenko, E, et al. *Syndecans: New Kids on the Signaling Block.* Circulation Research, 2005(96): p. 488-500.
190. Klinghoffer, RA, et al. *Src family kinases are required for integrin but not PDGFR signal transduction.* The EMBO Journal, 1999. **18**: p. 2459-2471.
191. Okada, M, et al. *CSK: a protein-tyrosine kinase involved in regulation of src family kinases.* The journal of biological chemistry, 1991(266): p. 24249-24252.
192. Lamant L, *Non-muscle myosin heavy chain (MYH9): a new partner fused to ALK in anaplastic large cell lymphoma.* genes chromosomes cancer, 2003. **37**(4): p. 427-32.
193. *HNRNPA1 heterogeneous nuclear ribonucleoprotein A1 [Homo sapiens]* NCBI Gene http://www.ncbi.nlm.nih.gov/gene/3178.
194. *heterogeneous nuclear ribonucleoprotein U.* Gene Cards http://www.genecards.org/cgi-bin/carddisp.pl?gene=HNRNPU.
195. Katsumoto, T, et al. *The role of the vimentin intermediate filaments in rat 3Y1 cells elucidated by immunoelectron microscopy and computer-graphic reconstruction.* Biology of the Cell, 2004. **68**(1-3): p. 139-146.
196. Mendez, M, et al. *Vimentin induces changes in cell shape, motility, and adhesion during the epithelial to mesenchymal transition.* The FASEB Journal, 2010. **24**(6): p. 1838-1851.
197. Glaser-Gabay L, et al. *Endothelial cell surface vimentin binding peptide induces angiogenesis under hypoxic ischemic conditions.* Microvascular Research, 2011.
198. Evans, RM, et al. *An alteration in the phosphorylation of vimentin-type intermediate filaments is associated with mitosis in cultured mammalian cells.* Cell, 1982. **29**(1): p. 43-52.
199. Allan, L, et al. *Inhibition of caspase-9 through phosphorylation at Thr 125 by ERK MAPK.* Nature Cell Biology, 2003. **5**(7).
200. Zhang, Z, et al. *Phosphorylated ERK is a potential predictor of sensitivity to sorafenib when treating hepatocellular carcinoma: evidence from an in vitro study.* BMC Medicine, 2009. **7**(41): p. 1741.
201. J. Xu, et al. *MAPK/ERK signalling mediates VEGF-induced bone marrow stem cell differentiation into endothelial cell.* Journal of molecular and cellular medicine, 2008. **12**(6a): p. 2395-2406.
202. David, G, et al. *Developmental Changes in Heparan Sulfate Expression: In Situ Detection with mAbs* The Journal of Cell Biology, 1992. **119**(4): p. 961-975.
203. Sampaio, L.O., *Heparins and heparan sulfates. Structure, distribution and protein interactions.* Insights into Carbohydrate Structure and Biologcal Function, 2006.
204. Rapraeger, A.C., *Molecular interactions of the syndecan core proteins.* Current Opinion in Cell Biology, 1998(10): p. 620-628.
205. Lopes, C, et al. *Specific structural features of syndecans and heparan sulfate chains are needed for cell signaling.* Brazilian Journal of Medical Biology Research, 2006. **39**(2): p. 157-167.
206. Rapraeger, A., *Transforming growth factor (type beta) promotes the addition of chondroitin sulfate chains to the cell surface proteoglycan (syndecan) of mouse mammary epithelia.* JCB, 1989. **109**(5): p. 2509-2518.

207. Hoek, K, et al. *Expression Profiling Reveals Novel Pathways in the Transformation of Melanocytes to Melanomas.* Cancer Research, 2004(64): p. 5270.
208. Popović, D.A, et al. *Expression and prognostic role of syndecan-2 in prostate cancer.* Prostate Cancer Prostatic Dis, 2010. **13**(1): p. 78-82.
209. Park, H., *Syndecan-2 Mediates Adhesion and Proliferation of Colon Carcinoma Cells.* The journal of biological chemistry, 2002. **277**(3): p. 29730-29736.
210. Ligong C, et al. *Syndecan-2 Regulates Transforming Growth Factor-B Signaling.* The journal of biological chemistry, 2004. **279**(16): p. 15715-15718.
211. Fears, CY, et al. *Syndecan-2 Is Expressed in the Microvasculature of Gliomas and Regulates Angiogenic Processes in Microvascular Endothelial Cells.* The journal of biological chemistry, 2006. **281**(21): p. 14533-14536.
212. Ying L, et al. *The Lipopolysaccharide-activated Toll-like Receptor (TLR)-Induces Synthesis of the Closely Related Receptor TLR-2 in Adipocytes.* The journal of biological chemistry, 2000. **275**(32): p. 24255-24263.
213. Streilein, J.W., *Immune privilege as the result of local tissue barriers and immunosuppressive microenvironments* Current Opinion in Immunology, 1993. **5**: p. 428-432.
214. A Rek, et al. *Therapeutically targeting protein–glycan interactions.* British Journal of Pharmacology, 2009(157): p. 686-694.
215. Antonio, R, et al. *Heparan sulfate proteoglycans: heavy hitters in the angiogenesis arena.* The Journal of Clinical Investigation, 2001. **108**(3): p. 349-355.
216. Carmen M, et al. *Control of extracellular matrix assembly by syndecan-2 proteoglycan.* Journal of Cell Science, 2000. **113**: p. 493-506.
217. Chiquet-Ehrismann, G, et al. *Tenascin-C induced signaling in cancer.* Cancer Letters, 2006.
218. Lee, J, et al. *Syndecan-2 Regulates the Migratory Potential of Melanoma Cells.* The journal of biological chemistry, 2009. **284**(40): p. 27167-27175.
219. Ashikari-Hada, S, et al. *Heparin Regulates Vascular Endothelial Growth Factor165-dependent Mitogenic Activity, Tube Formation, and Its Receptor Phosphorylation of Human Endothelial Cells.* The journal of biological chemistry, 2005. **280**(36): p. 31508-31515.
220. Chi, F, et al. *Vimentin-mediated signalling is required for IbeA+ E.coli K1 invasion of human brain microvascular endothelial cells.* Biochem. J, 2010(427): p. 79-90.
222. Meriane, M, et al. *Cdc42Hs and Rac1 GTPases Induce the Collapse of the Vimentin Intermediate Filament Network.* The journal of biological chemistry, 2000. **275**(42): p. 33046-33052.
223. Goldman, L. *Intermediate filaments mediate cytoskeletal crosstalk* Nature Reviews, 2004. **5**.
224. Ramaekers, K, et al. *Gene expression of tumor angiogenesis dissected: specific targeting of colon cancer angiogenic vasculature.* Blood, 2006(108): p. 2339-2348.
225. Kubo, Y, et al. *Bacterial components regulate the expression of Toll-like receptor 4 on human mast cells* Inflammation Research, 2006. **56**(7): p. 70-75.